



MARMARA UNIVERSITY  
FACULTY OF ENGINEERING



**STRENGTHENING AND ANALYZING ASPHALT  
STRUCTURES WITH GEOGRID REINFORCEMENT WITH  
DIFFERENT GEOMETRIES, MATERIALS AND LOCATIONS**

---

Ahmet Arif AKMAN, Ömer Faruk ÖZDEN, Salih GÖKÇE

**GRADUATION PROJECT REPORT**

Department of Mechanical Engineering

**Supervisor**

Asst. Prof. Dr. Aybala YILDIRIM

ISTANBUL, 2024

---



MARMARA UNIVERSITY  
FACULTY OF ENGINEERING



**STRENGTHENING AND ANALYZING ASPHALT STRUCTURES WITH  
GEOGRID REINFORCEMENT WITH DIFFERENT GEOMETRIES,  
MATERIALS AND LOCATIONS**

**By**

**Ahmet Arif AKMAN, Ömer Faruk ÖZDEN, Salih GÖKÇE**

**JUNE 07, 2024, ISTANBUL**

**SUBMITTED TO THE DEPARTMENT OF MECHANICAL ENGINEERING IN  
PARTIAL FULFILLMENT OF THE REQUIREMENTS FOR THE DEGREE**

**OF**

**BACHELOR OF SCIENCE**

**AT**

**MARMARA UNIVERSITY**

The author(s) hereby grant(s) to Marmara University permission to reproduce and to distribute publicly paper and electronic copies of this document in whole or in part and declare that the prepared document does not in anyway include copying of previous work on the subject or the use of ideas, concepts, words, or structures regarding the subject without appropriate acknowledgement of the source material.

Signature of Author(s) .....

Department of Mechanical Engineering

Certified By .....

Project Supervisor, Department of Mechanical Engineering

Accepted By .....

Head of the Department of Mechanical Engineering

## **ACKNOWLEDGEMENT**

First, we would like to thank our valuable supervisor Asst. Prof. Dr. Aybala Yıldırım, who guided us throughout this project, shared all her knowledge, experience, and help with us, and encouraged us both materially and spiritually to prepare this thesis.

Also, we would also like to thank our valuable colleagues who spared their valuable time for us, helped us with their ideas at some points, and enlightened our path.

June 2024

Ahmet Arif AKMAN

Ömer Faruk ÖZDEN

Salih GÖKÇE

# CONTENTS

<b>ACKNOWLEDGEMENT .....</b>	<b>iii</b>
<b>CONTENTS.....</b>	<b>iv</b>
<b>ABSTRACT.....</b>	<b>vi</b>
<b>SYMBOLS.....</b>	<b>vii</b>
<b>ABREVIATIONS.....</b>	<b>ix</b>
<b>LIST OF FIGURES .....</b>	<b>x</b>
<b>LIST OF TABLES.....</b>	<b>xii</b>
<b>1. Introduction.....</b>	<b>1</b>
1.1 Deteriorations in Asphalt .....	1
1.2 Asphalt Pavement.....	3
1.2.1 Asphalt Pavement Types and Layers .....	3
1.3 Deformations in asphalt .....	5
1.3.1 Distortions .....	5
1.3.2 Cracks .....	5
1.3.3 Separations .....	6
1.3.4 Distortion by Shape Change .....	6
1.4 Rut Distortion .....	7
1.5 Geogrids.....	10
<b>2. Modelling.....</b>	<b>12</b>
2.1 Introduction to Modeling .....	12
2.2 Design Traffic Loading .....	13
2.3 Modeling procedures on ANSYS and SOLIDWORKS.....	14
2.4 Determination of Materials .....	15
2.5 Geometry in simulation.....	16
<b>3. Experiment and Analysis .....</b>	<b>19</b>

3.1 Geogrid Types .....	19
3.2 Model Analysis without Geogrid .....	20
3.2.1 Total Deformation .....	20
3.2.2 Von Misses Stress.....	20
3.3 Analysis of the Rectangular Geogrid Model.....	23
3.4 Analysis of Rhombus Geogrid Model.....	28
3.5 Analysis of Hexagonal Geogrid Model.....	32
3.6 Analysis of Rectangular Geogrid Model with Recycle Materials.....	35
3.7 Analysis of Rhombus Geogrid Model with Recycle Materials.....	37
3.8 Analysis of Hexagonal Geogrid Model with Recycle Materials.....	39
3.9 Analyzes in which the Geogrid Changes Position .....	41
3.10 Model Analysis without Geogrid with Increased Asphalt .....	50
<b>4. Analysis Results and Comparisons.....</b>	<b>51</b>
4.1 Deformation of PET Geogrid Under 60 mm Asphalt .....	51
4.2 Deformation of PA6 Geogrid Under 60 mm Asphalt .....	53
4.3 Deformation of PP Geogrid Under 60 mm Asphalt.....	54
4.4 Collection and Comparison of Data .....	55
4.5 Collection and Comparison of Max. Equivalent Stress Data.....	57
4.6 Geogrid Type and Material Selection .....	59
4.7 Determining Location for Hexagonal PP Geogrid .....	61
4.8 Effect of Geogrid Reinforcement on Service Life of Road .....	62
<b>5. Cost Analysis.....</b>	<b>66</b>
<b>6. Conclusion.....</b>	<b>69</b>
<b>7. References.....</b>	<b>70</b>

## **ABSTRACT**

Ground structures constitute an important issue in transportation and our daily lives. When we look around the world, it can be seen that road transportation is highly preferred. In our country, road transportation is one of the most preferred modes of transportation for both passenger and freight transportation. Asphalt pavements are the most preferred type of superstructure in road transportation. At this point, working on flexible coatings and extending the life of the structure reduces possible maintenance costs. One of the main forms of deterioration seen in pavement layers is rutting. In the study, finite element analysis was performed using the ANSYS program. This article examines the effects of geogrids made of different materials, recycled versions of these materials, and geogrids with different geometric structures on the formation of ruts on asphalt ground. Additionally, the effect of placing geogrid materials on asphalt in reducing ruts is being investigated. As a result of examination and research, the optimum choice is obtained by making a cost analysis for the geogrid with the optimum material and structure. The aim is to find out the advantages of reinforced asphalt as well as where and which geogrid gives better results.

## SYMBOLS

<b>mm</b>	Millimeter
<b><math>mm^2</math></b>	Square millimeter
<b>m</b>	Meter
<b><math>m^2</math></b>	Square meter
<b>N</b>	Newton
<b>kg</b>	Kilogram
<b>kgf</b>	Kilogram-force
<b><math>kg/m^3</math></b>	Kilogram per cubic meter
<b>GPa</b>	Gigapascal
<b>MPa</b>	Megapascal
<b>Pa</b>	Pascal
<b><math>X^2</math></b>	X Squared
<b><math>Y^2</math></b>	Y Squared
<b><math>Z^2</math></b>	Z Squared
<b><math>\sigma_r</math></b>	Total Stress
<b><math>\sigma_x</math></b>	Stress in x Direction
<b><math>\sigma_y</math></b>	Stress in y Direction
<b><math>\sigma_z</math></b>	Stress in z Direction
<b><math>\tau_{xy}</math></b>	Shear Stress on xy Plane
<b><math>\tau_{yz}</math></b>	Shear Stress on yz Plane
<b><math>\tau_{zx}</math></b>	Shear Stress on zx Plane
<b>Max</b>	Maximum
<b>E</b>	Young's Modulus
<b><math>\varepsilon_c</math></b>	Vertical compressive strains at the top of the subgrade layer
<b><math>N_r</math></b>	Number of load repetitions to limit rutting

$\Delta_L$	Change
$L_0$	Original Length
$N_{r1}$	First Number of load repetitions to limit rutting
$N_{r2}$	Second Number of load repetitions to limit rutting
$N_{r3}$	Third Number of load repetitions to limit rutting
$\%$	Percentage
<b>T</b>	Tons
<b>TL</b>	Turkish liras

## **ABREVIATIONS**

<b>2D</b>	Two Dimensional
<b>3D</b>	Three Dimensional
<b>AASHTO</b>	American Association of State Highway and Transportation Officials
<b>ANSYS</b>	Swanson Analysis Systems
<b>APA</b>	Asphalt Pavement Analyzer
<b>FE</b>	Finite Element
<b>LCPC</b>	Licensed Clinical Professional Counselor
<b>PA6</b>	Polyamide 6
<b>PET</b>	Polyethylene Terephthalate
<b>PLAXIS</b>	Finite Element for Soil and Rock Analysis
<b>PP</b>	Polypropylene
<b>RPA6</b>	Recycled Polyamide 6
<b>RPET</b>	Recycled Polyethylene Terephthalate
<b>RPP</b>	Recycled Polypropylene

## LIST OF FIGURES

<b>Figure 1</b> Deformation on asphalt [1] .....	1
<b>Figure 2</b> Potholes in asphalt [2].....	2
<b>Figure 3</b> Asphalt Layers [7].....	4
<b>Figure 4</b> Schematic view of asphalt.....	5
<b>Figure 5</b> Alligator Type Crack Formation [8].....	5
<b>Figure 6</b> Example of Separation Deformation [9].....	6
<b>Figure 7</b> Deterioration Caused by Insufficient Stability of Asphalt Pavement and Pavement Layers [10].	6
<b>Figure 8</b> Modeling the rut [12].....	7
<b>Figure 9</b> Wheel pressing area .....	8
<b>Figure 10</b> Meshing of the experimental setup.....	8
<b>Figure 11</b> Location of the wheel pressing area on the experimental setup. ....	9
<b>Figure 12</b> Geogrid used in road foundation [16].....	10
<b>Figure 13</b> Uniaxial geogrids [17]. .....	10
<b>Figure 14</b> Biaxial geogrids [18]. .....	11
<b>Figure 15</b> Triaxial geogrids [19]. .....	11
<b>Figure 16</b> Schematic representation of tire contact area [14]. .....	14
<b>Figure 17</b> Tire Contact Area Display a) Actual Tire Contact Area b) Equivalent Tire Contact Area. ....	14
<b>Figure 18</b> Modeling layers. .....	16
<b>Figure 19</b> Geogrid design that we modeled as a rectangular (A), hexagonal (B) and rhombus (C). ....	19
<b>Figure 20</b> Illustration of the model non-geogrid. ....	21
<b>Figure 21</b> Showing the mesh applied to the model non-geogrid.....	21
<b>Figure 22</b> Representation of the force applied to the model. ....	22
<b>Figure 23</b> Total deformation analysis of the normal model.....	22
<b>Figure 24</b> Stress analysis of the normal model.....	23
<b>Figure 25</b> Determination of geogrid location. ....	24
<b>Figure 26</b> Total deformation analysis of the rectangular geogrid (PA6) under 60 mm asphalt.....	25
<b>Figure 27</b> Stress analysis of the rectangular geogrid (PA6) under 60 mm asphalt. ....	25
<b>Figure 28</b> Total deformation analysis of the rectangular geogrid (PET) under 60 mm asphalt.....	26
<b>Figure 29</b> Stress analysis of the rectangular geogrid (PET) under 60 mm asphalt. ....	26
<b>Figure 30</b> Total deformation analysis of the rectangular geogrid (PP) under 60 mm asphalt. ....	27
<b>Figure 31</b> Stress analysis of the rectangular geogrid (PP) under 60 mm asphalt. ....	27
<b>Figure 32</b> Total deformation analysis of the rhombus geogrid (PA6) under 60 mm asphalt.....	28
<b>Figure 33</b> Stress analysis of the rhombus geogrid (PA6) under 60 mm asphalt. ....	29
<b>Figure 34</b> Total deformation analysis of the rhombus geogrid (PET) under 60 mm asphalt.....	29
<b>Figure 35</b> Stress analysis of the rhombus geogrid (PET) under 60 mm asphalt. ....	30
<b>Figure 36</b> Total deformation analysis of the rhombus geogrid (PP) under 60 mm asphalt. ....	30
<b>Figure 37</b> Stress analysis of the rhombus geogrid (PP) under 60 mm asphalt. ....	31
<b>Figure 38</b> Total deformation analysis of the hexagon geogrid (PA6) under 60 mm asphalt. ....	32
<b>Figure 39</b> Stress analysis of the hexagon geogrid (PA6) under 60 mm asphalt. ....	33
<b>Figure 40</b> Total deformation analysis of the hexagon geogrid (PET) under 60 mm asphalt. ....	33
<b>Figure 41</b> Stress analysis of the hexagon geogrid (PET) under 60 mm asphalt. ....	34
<b>Figure 42</b> Total deformation analysis of the hexagon geogrid (PP) under 60 mm asphalt. ....	34
<b>Figure 43</b> Stress analysis of the hexagon geogrid (PP) under 60 mm asphalt. ....	35
<b>Figure 44</b> Total deformation analysis of the rectangular geogrid (Recycled PET) under 60 mm asphalt.	36
<b>Figure 45</b> Total deformation analysis of the rectangular geogrid (Recycled PP) under 60 mm asphalt...	36
<b>Figure 46</b> Total deformation analysis of the rectangular geogrid (Recycled PA6) under 60 mm asphalt.	37
<b>Figure 47</b> Total deformation analysis of the rhombus geogrid (Recycled PET) under 60 mm asphalt....	38
<b>Figure 48</b> Total deformation analysis of the rhombus geogrid (Recycled PP) under 60 mm asphalt.....	38
<b>Figure 49</b> Total deformation analysis of the rhombus geogrid (Recycled PA6) under 60 mm asphalt....	39

<b>Figure 50</b> Total deformation analysis of the hexagonal geogrid (Recycled PET) under 60 mm asphalt.	40
<b>Figure 51</b> Total deformation analysis of the hexagonal geogrid (Recycled PET) under 60 mm asphalt.	40
<b>Figure 52</b> Total deformation analysis of the hexagonal geogrid (Recycled PA6) under 60 mm asphalt.	41
<b>Figure 53</b> Total deformation analysis of the hexagonal geogrid (PP) under 30 mm asphalt .....	43
<b>Figure 54</b> Stress analysis of the hexagonal geogrid (PP) under 30 mm asphalt. ....	43
<b>Figure 55</b> Total deformation analysis of the hexagonal geogrid (PP) under 110 mm asphalt. ....	44
<b>Figure 56</b> Stress analysis of the hexagonal geogrid (PP) under 110 mm asphalt. ....	45
<b>Figure 57</b> Total deformation analysis of the hexagon geogrid (PP) under base course. ....	46
<b>Figure 58</b> Stress analysis of the hexagonal geogrid (PP) under base course. ....	46
<b>Figure 59</b> Total deformation analysis of the hexagonal geogrid (PP) under 100 mm subgrade.....	47
<b>Figure 60</b> Total deformation analysis of the hexagonal geogrid (PP) under 200 mm subgrade.....	48
<b>Figure 61</b> Stress analysis of the hexagonal geogrid (PP) under 200 mm subgrade. ....	49
<b>Figure 62</b> Total deformation analysis of the non-geogrid model with 118.5 mm asphalt. ....	50
<b>Figure 63</b> Stress analysis of the non-geogrid model with 118.5 mm asphalt.....	51
<b>Figure 64</b> Graph of Deformation of PET and 3 different designed geogrids under 60 mm Asphalt. ....	52
<b>Figure 65</b> Graph of Deformation of PA6 and 3 different designed geogrids under 60 mm Asphalt. ....	53
<b>Figure 66</b> Graph of Deformation of PP and 3 different designed geogrids under 60 mm Asphalt. ....	54
<b>Figure 67</b> Graph in which deformations are listed from least to most. ....	56
<b>Figure 68</b> Graph of stresses obtained with three different designs and material assignments. ....	57
<b>Figure 69</b> Stress and deformation comparison. ....	59
<b>Figure 70</b> Graph of deformations of hexagon PP geogrid in various locations. ....	61
<b>Figure 71</b> Strain analysis of the hexagonal geogrid (PP) .....	63
<b>Figure 72</b> Strain analysis of the rectangular geogrid (PET).....	63
<b>Figure 73</b> Strain analysis of the model non-geogrid .....	64
<b>Figure 74</b> Graph of 110 mm non-geogrid, 118.5 mm non-geogrid and Hexagonal Geogrid - PP - Under 60 mm Asphalt deformation values. ....	66

## LIST OF TABLES

<b>Table 1</b> Materials and Properties [24]. .....	16
<b>Table 2</b> Materials and Properties [25-38]. .....	17
<b>Table 3</b> Table of materials and properties of the model non-geogrid. .....	20
<b>Table 4</b> Table of materials and properties of the rectangular geogrid under 60 mm asphalt. .....	24
<b>Table 5</b> Table of materials and geogrid properties of the rectangular geogrid under 60 mm asphalt. ....	24
<b>Table 6</b> Table of materials and properties of the rhombus geogrid under 60 mm asphalt. ....	28
<b>Table 7</b> Table of materials and geogrid properties of the rhombus geogrid under 60 mm asphalt. ....	28
<b>Table 8</b> Table of materials and properties of the hexagon geogrid under 60 mm asphalt.....	32
<b>Table 9</b> Table of materials and geogrid properties of the hexagon geogrid under 60 mm asphalt. ....	32
<b>Table 10</b> Table of materials and properties of the rectangular geogrid under 60 mm asphalt. ....	35
<b>Table 11</b> Table of materials and geogrid properties of the rectangular geogrid under 60 mm asphalt....	35
<b>Table 12</b> Table of materials and properties of the rhombus geogrid under 60 mm asphalt. ....	37
<b>Table 13</b> Table of materials and geogrid properties of the rhombus geogrid under 60 mm asphalt. ....	37
<b>Table 14</b> Table of materials and properties of the hexagonal geogrid under 60 mm asphalt.....	39
<b>Table 15</b> Table of materials and geogrid properties of the hexagonal geogrid under 60 mm asphalt. ....	39
<b>Table 16</b> Table of materials and properties of the hexagonal geogrid under 30 mm asphalt.....	42
<b>Table 17</b> Table of materials and geogrid properties of the hexagonal geogrid under 30 mm asphalt. ....	42
<b>Table 18</b> Table of materials and properties of the hexagonal geogrid under 110 mm asphalt.....	44
<b>Table 19</b> Table of materials and geogrid properties of the hexagonal geogrid under 110 mm asphalt. ....	44
<b>Table 20</b> Table of materials and properties of the hexagonal geogrid under base course.....	45
<b>Table 21</b> Table of materials and geogrid properties of the hexagon geogrid under base course. ....	45
<b>Table 22</b> Table of materials and properties of the hexagonal geogrid under 100 mm subgrade.....	47
<b>Table 23</b> Table of materials and geogrid properties of the hexagonal geogrid under 100 mm subgrade.	47
<b>Table 24</b> Table of materials and properties of the hexagonal geogrid under 200 mm subgrade.....	48
<b>Table 25</b> Table of materials and geogrid properties of the hexagonal geogrid under 200 mm subgrade.	48
<b>Table 26</b> Table of materials and properties of the non-geogrid 118.5 mm asphalt model.....	50
<b>Table 27</b> Deformation of PET and 3 different designed geogrids under 60 mm Asphalt.....	51
<b>Table 28</b> Deformation of PA6 and 3 different designed geogrids under 60 mm Asphalt.....	53
<b>Table 29</b> Deformation of PP and 3 different designed geogrids under 60 mm Asphalt.....	54
<b>Table 30</b> Results of deformations obtained with three different designs and material assignments. ....	55
<b>Table 31</b> Results of stresses obtained with three different designs and material assignments.....	57
<b>Table 32</b> Compare to find the best option. ....	59
<b>Table 33</b> Deformations of Hexagon Polypropylene Geogrid in various locations.....	61
<b>Table 34</b> 110-118.5 mm non-geogrid and Hexagonal Geogrid PP Under 60 mm Asphalt deformation values.....	66

# 1. Introduction

## 1.1 Deteriorations in Asphalt

Asphalt pavements are important in road transportation, which is one of the most preferred modes of transportation. These coatings are exposed to various effects during the day. Especially heavy vehicles are the main reasons for these deformations.

It is possible to examine the ground superstructure in 4 different ways (rigid, flexible, mixed, semi-rigid). The most preferred and common type in our country is the flexible superstructure model. As with every type of pavement, deterioration occurs in flexible pavement models. As a result, maintenance and repair costs become inevitable. Cracks may occur in these structures, water-induced peeling and decomposition may occur, and deformations may occur. Rutting, which is one of these types of deterioration and occurs in the form of deformation, is seen especially in the summer months. This type of degradation manifests itself because of summer heat and high traffic load.

Although there are many reasons for rut formation, two reasons can be highlighted. These reasons are deterioration caused by a weak sublayer and a weak asphalt layer. In addition, repeated traffic load, humidity and wear are the reasons for the formation of these ruts.



**Figure 1** Deformation on asphalt [1].

These rutting deteriorations stand out as permanent vertical deteriorations. At this point, it is important to make analyzes and increase the resistance of the hot mix asphalt pavement to minimize possible deteriorations and reduce maintenance costs.



**Figure 2** Potholes in asphalt [2].

The load caused by traffic and the resulting deformation occurs in asphalt pavements exposed to this load. This is an important factor that reduces safety and comfort.

Maintenance and construction costs for asphalt paved roads are also high. These floors may change shape within a few years and require maintenance. Research and studies are constantly ongoing in order to prevent these deteriorations. These deteriorations damage the original form of the coating and can lead to permanent changes [3].

Various methods are followed to prevent these problems. One of these solutions is the use of geogrids in asphalt structures. In this way, an increase in the resistance of asphalt to load is observed. Some studies show that the loads on asphalt are spread over a wider area with the geogrid layer and that the geogrid reduces the vertical stress on the asphalt. As a result of the observations, it was seen that a thick section without reinforcement behaves like a thin section with reinforcement.

In this study, it is envisaged to use geogrid to create asphalt layers and strengthen them with the ANSYS program. It is aimed to analyze the results by changing the shape, material and location of the geogrid structure. The general purpose of this article is to provide improvements in asphalt pavements for the continuity of road transportation, which is the most common type of transportation. It is to find the optimum asphalt soil with geogrid reinforcement that minimizes rutting. In addition, comparisons are made between reinforced and unreinforced asphalt structures. Finally, the cost analysis showed how profitable geogrid reinforcement is. During the study, recycled materials were also tested.

## **1.2 Asphalt Pavement**

Asphalt pavement is done to strengthen road surfaces, increase durability, increase driving safety and provide a more comfortable journey by adding a new layer on an existing road to carry out transportation, which is one of the basic needs of humans, in a more comfortable way. Durability is one of the most important features of asphalt pavement. They can withstand heavy loads and traffic. When the coating is done to the appropriate standard, they have a long life. Additionally, repair of asphalt pavements is fast and low-cost.

This coating is mostly made by mixing stone, gravel, sand and binding materials (bitumen). The created asphalt is laid on the surface hot and then a smooth surface is obtained by compaction. This coating is used in the construction of various surfaces such as highways, parking lots, airports and industrial areas.

The historical development of asphalt pavement dates to ancient times. However, modern asphalt paving technology was established in the 19th century.

In the mid-1800s, John Loudon McAdam laid the foundations of modern asphalt by using pebbles and binder material as mortar for road surfaces and applying it on the damaged surface [4].

Especially in the second half of the 20th century, when asphalt technology developed and high-quality mixtures were produced, the durability and life of asphalt pavement increased. Today, constantly developing technology increases the use of sustainable materials and the sustainability of asphalt pavement.

### **1.2.1 Asphalt Pavement Types and Layers**

There are many types of asphalt pavements. Hot mix asphalt is the most used type of asphalt. After increasing the fluidity of the asphalt binder by heating it, mixing it with aggregate and pouring it onto the surface, a durable road surface is obtained by compaction. The lack of air voids in hot mix asphalt greatly affects the life of the asphalt. Cold mix asphalt is practical because it is produced at ambient temperature and then the asphalt is ready for direct application. However, hot mix is not as durable as asphalt and is mostly used for temporary repairs, areas with low traffic or in cold weather.

Asphalt pavement has a structure consisting of three main layers. These layers are coating layer, base layer and subbase layer. These layers support each other and increase the stability, life and durability of the road.

The pavement layer is usually the top layer and carries the traffic load on the road to provide a smooth surface containing high-quality asphalt such as hot mix, increase skid resistance, increase driving safety and improve the aesthetics of the road. It also protects the asphalt against climatic conditions and environmental factors, prevents water from seeping into the base layer and protects the surface of the road [5].

The base layer usually contains aggregate materials including gravel, sand, crushed stone. Aggregate dimensions determine the strength of the layer. The purpose of this layer is to position it under the coating layer, support it, increase its stability and increase its carrying capacity. It also creates resistance against erosion [6].

The subbase layer contains finer aggregate materials than the base layer. It settles under the base layer and sits on the ground of the road. It provides a surface that is compatible with the ground underneath and helps level it. Corrects surface imperfections. It also increases resistance to freezing and thawing events by facilitating water drainage [5].

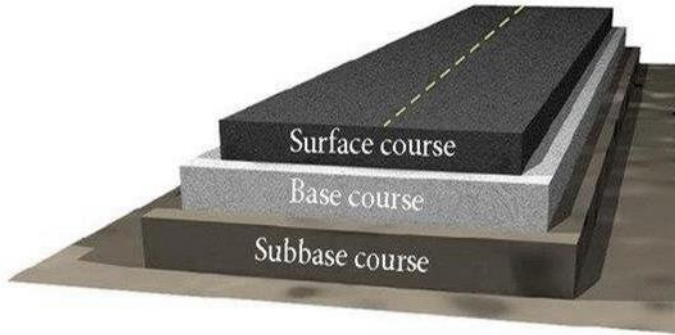


**Figure 3** Asphalt Layers [7].

These three layers work in harmony to meet the engineering and performance needs of the road. The design of asphalt layers may vary depending on the climate, traffic and ground of the region.

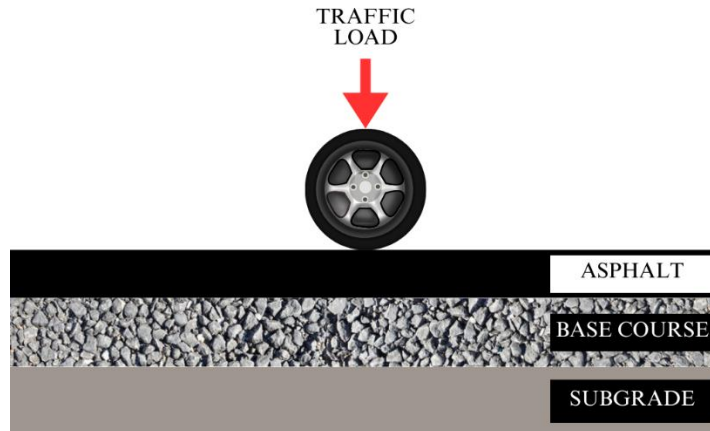


**Figure 4** Schematic view of asphalt.

### 1.3 Deformations in asphalt

#### 1.3.1 Distortions

The deformations that occur on roads can be addressed in four different ways. These are cracks, water-induced peeling, permanent shape deformations and decomposition.

#### 1.3.2 Cracks

There are many types such as edge cracks and alligator cracks. The basis of these cracks may be the continuous heavy traffic load or sudden temperature changes.



**Figure 5** Alligator Type Crack Formation [8].

### **1.3.3 Separations**

It is one of the types of deterioration that occurs due to both excessive traffic loads and climatic conditions. It can be seen in forms such as blistering, peeling, and breaking.



**Figure 6** Example of Separation Deformation [9].

### **1.3.4 Distortion by Shape Change**

This type of deterioration is due to insufficient stability of the asphalt pavement and superstructure layers. The higher the stability, the less deformation will occur. To improve stability homogeneous distribution is achieved with rough aggregates and required density. Compression is also an important factor.

In addition, high temperatures during the summer months increase the viscosity property of the coating. Higher than normal load is also the cause of such distortions. Rutting is one of this type of deterioration.



**Figure 7** Deterioration Caused by Insufficient Stability of Asphalt Pavement and Pavement Layers [10].

## 1.4 Rut Distortion

These distortions are permanent deformations. It has a negative effect in terms of both security and comfort. They are vertical and permanent deformations. One of the focuses of the research is to predict and prevent ruts. More importantly, this problem can cause increased asphalt cracking due to fatigue and the road being completely out of service.

Although related studies can be carried out experimentally, they can proceed more easily with computer-aided analysis programs. Before this modelling, it is necessary to recognize the rut.

- Ruts can be divided into 3 classes. (AASHTO 1986)
- Low: 6-13 mm
- Medium 13-25 mm
- High: 25 and above (mm)

Asphalt mixtures have high sensitivity levels. It is sensitive to the duration, amount and ambient temperature of the load placed on it. All these factors also lead to fatigue crack formation [11]. In the related study, temperature-variable rutting experiments were carried out and these were tabulated. Rut depth increases in direct proportion to temperature.



**Figure 8** Modeling the rut [12].

Additionally, due to the viscoelastic structure of asphalt, the smaller the cross section the load is on, the less deformation it will cause.

There are many reasons for rutting. When these are considered in order of effect, it has been observed that load repetition and loading speed are less effective than other parameters [13].

The effects of tire properties on deformation were observed. That is, as the tire internal pressure increases, the contact surface of the tire decreases. Therefore, pressure generally increases, and deformation increases [14].

The tire contact area is close to an oval shape and looks like Figure 10 due to the tire tread patterns.

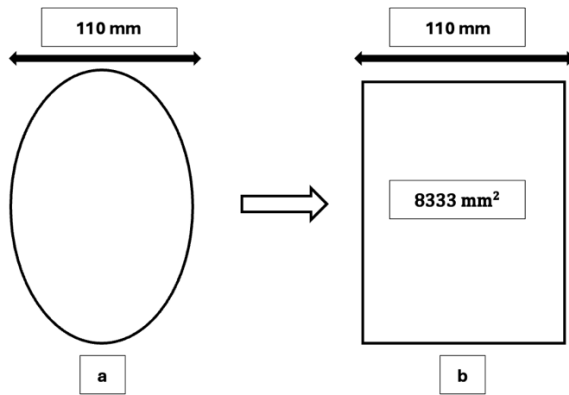


**Figure 9** Wheel pressing area.

In our experiment, the asphalt area was meshed accordingly to show the tire area in this way.

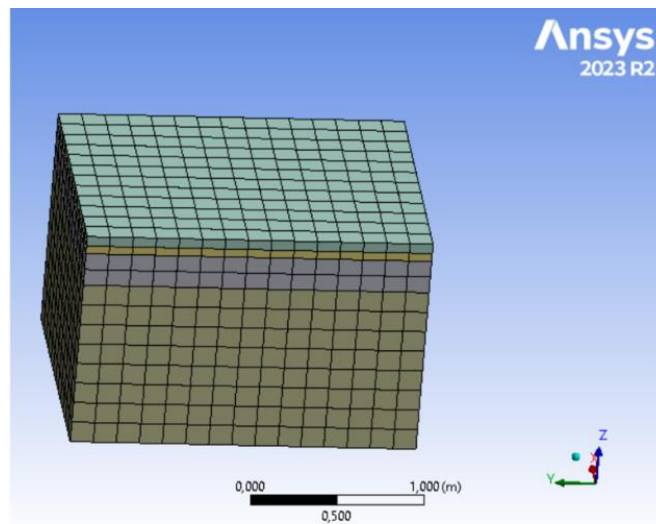


**Figure 10** Meshing of the experimental setup.

The experimental setup that was prepared has an area of 1600 mm x 2000 mm. The representation of the vertical force exerted by the wheel was also applied to the area at the middle point of this mechanism.

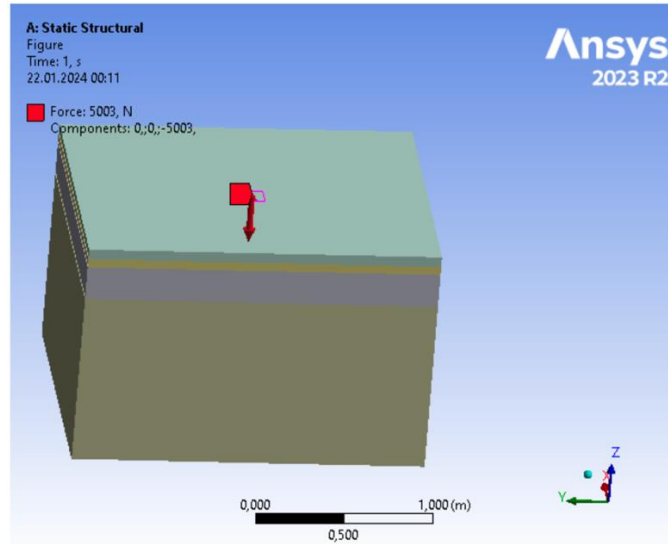


**Figure 11** Location of the wheel pressing area on the experimental setup.

In our experiment, the part where the force is applied is applied to an area of  $8333 \text{ m}^2$ , as stated in the articles we have read.

At the same time, a force of 5003 N is applied to this area. A load of 510 kg was applied based on the LCPC French rut test [15].

In a vehicle weighing 2 tons, a load of approximately 510 kg is placed on one wheel. The 510 kg load was also converted into N to be used in our analysis.  $[1 \text{ kgf} = 9.80665 \text{ N}] - [510 \text{ kgf} = 510 \text{ kgf} \times 9.80665 \text{ N} = 5003 \text{ N}]$ . Following this formula, the force to be applied to the experimental area was determined to be 5003 N and, as stated in the figure above, this force was applied to an area of  $8333 \text{ mm}^2$ .

## 1.5 Geogrids

Geogrids are a different type of geosynthetics. Geosynthetics are generally used in fields, construction industry, pavement improvement, retaining walls and similar areas.

If the places where geoinputs are generally used are considered, examples can be given such as extending the service life of the road by increasing the carrying capacity of the road foundation, preventing possible soil erosion by increasing the soil slope, strengthening soil and asphalt, and increasing the durability and strengthening of highway structures.



**Figure 12** Geogrid used in road foundation [16].

Additionally, geogrids are divided into 4 according to their raw materials. These geogrids are plastic geogrid, steel plastic geogrid, fiberglass geogrid and polyester geogrid. In this study, the geogrids to be used are plastic geogrids. Plastic geogrids are also divided into 3 according to their axes. Single axis, dual axis and 3 Axis. Uniaxial, biaxial and triaxial properties give the name to these geogrid types. It refers to the number of directions in which geogrids provide power. Uniaxial geogrids provide strength in one direction, while biaxial geogrids provide strength in two directions. Triaxial geogrids also provide strength in three directions.

Uniaxial geogrids are generally used in road works and in the construction industry as they are reinforced against construction damage.



**Figure 13** Uniaxial geogrids [17].

Biaxial geogrids are advantageous in situations such as good load capacity, long-term stability, resistance to dynamic loads and high bending stiffness. For these reasons, geogrid is the most used.

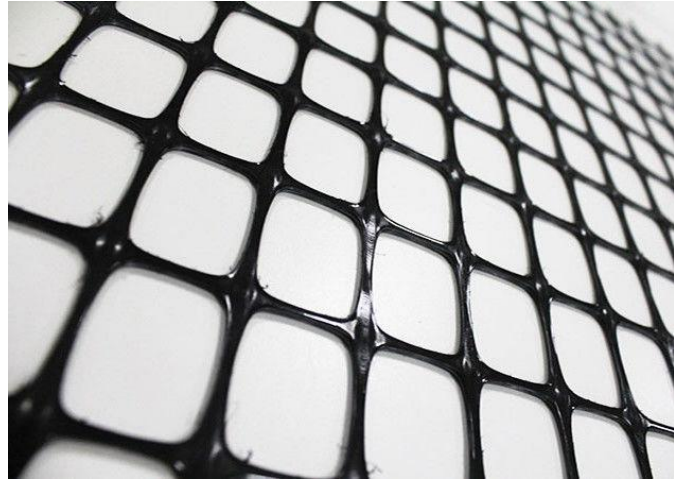


**Figure 14** Biaxial geogrids [18].

Triaxial geogrids also have good in-plane stiffness with good span stability.

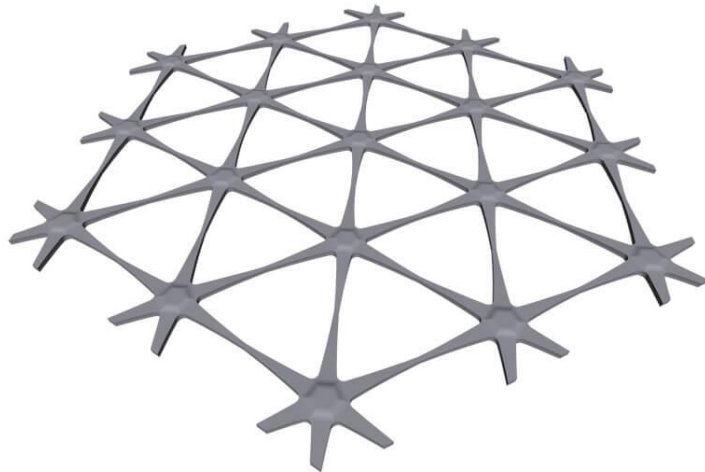


**Figure 15** Triaxial geogrids [19].

According to the conclusions drawn from what mentioned above, biaxial and triaxial geogrids will be used in asphalt in this study.

In a study, a model incorporating geogrid reinforcement in asphalt was developed, and the static tensile and repeated loading analyses under static load were conducted for this model. They demonstrated a reduction of 22% and 14%, respectively [20].

In another study, a 2D analysis was performed using the PLAXIS model. Reductions in the stress in the load area of the wheel on the asphalt and in the vertical displacement of the asphalt were observed [21].

## 2. Modelling

### 2.1 Introduction to Modeling

Geogrid reinforced asphalt is a solution developed to minimize or prevent the damage caused to the asphalt layer by excessive load and stress, vehicle traffic, weather conditions and chemical substances. Geogrid is used by integrating between a two-layer asphalt or between asphalt and the base layer. In this study, the usefulness of using geogrid in asphalt will be examined to assess its potential in increasing the lifespan of asphalt. In addition, the effect of differentiating the production materials and designs of the geogrid used on the durability of asphalt will also be investigated. The selection of rectangular, hexagonal and rhombus-shaped designs is based on the ability of these shapes to best adapt to the asphalt layer and provide the best load distribution. A closer examination of the results obtained from using the geogrid material as a recyclable material is also desired. The primary motivation behind this is to mitigate the environmental damage we inflict, which could lead to more significant issues such as climate-related problems and environmental pollution. The common benefits of the recyclable materials selected for this study include protecting natural resources, reducing waste generation, saving energy, and minimizing cost impacts. Three-dimensional finite element (FE) method was used to capture the reactions in these analyses.

The finite element method enables the design to be safer and optimized by modeling the behavior of materials under load. In addition, it provides the opportunity to easily model different loads and other conditions. Thus, using finite element analysis instead of laboratory experiments accelerates the analysis costs and the design process. In addition to analysis costs, it helps to understand the behavior of asphalt over time and plays a major role in the determination of factors such as material selection in the design process, which affects the cost greatly [22].

In the forthcoming analyses, the procedure involved initially modeling asphalt without the inclusion of geogrid material. Subsequently, the analysis was conducted by incorporating three differently shaped geogrids designed into the asphalt. Furthermore, these three different geogrids were constructed from three distinct materials. As a result, a detailed analysis was

carried out with 3 different geogrid types having 3 different materials. In addition, recycled forms of the materials were also tested. Geogrids were obtained from both normal and recycled materials. All these experiments were carried out under the same conditions.

Because of these comparisons, further experimentation was conducted on the geogrid shape-material combination that resulted in the least deformation on asphalt. In further experiments, analyses were performed at various heights to determine the location where deformation was minimized by adjusting the height of the geogrid higher or lower. After completing these analyses, the cost analysis will be done. The deformation that would occur by increasing the height of our asphalt in our model without geogrid was re-examined. During the performance of these analyses, our designs were made using SOLIDWORKS, a computer-aided 3D solid modeling and design software, and then completed these designs by performing simulations using ANSYS, a FE program that has a very important place in the market.

## 2.2 Design Traffic Loading

As mentioned above, our work is to carry out assembly tests to prevent deteriorations such as tire marks and cracks on asphalt. While analyzing these designs for this issue, it was determined our asphalting as 1600 mm \* 2000 mm. In rut analysis, it can be determined in this way so that the impact area can be viewed from a wide angle. In this way, the focus was placed on evaluating the results of our main goal without combining them. This asphalt resistant power is based on the weight of an average vehicle and its strength on a single wheel of 2 tons (500 kg). In this context, multiple sections were available for use when presenting them as power over our summarized sections. These are LCPC French Wheel Track, Hamburg Wheel Track, APA Wheel Track, British Wheel Track [15].

In order to apply the LCPC French wheel under the conditions of its realization, the load must be 510 kg and the wheel type must be a rubber wheel [23].

In this study, this feature wheel and this power to apply it are the same. For this reason, the French rutting test was conducted in our own study.

The schematic representation of an example tire contact in the literature studies on the contact scheme of the tire has been completed [14].

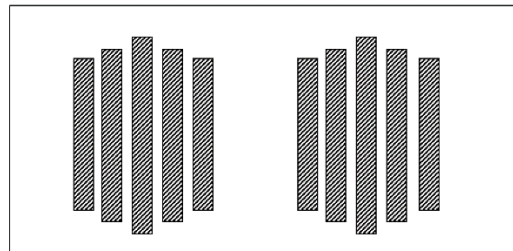


**Figure 16** Schematic representation of tire contact area [14].

In reality, the contact area resembles an oval shape, but the patterns on the tire also create a tire contact area similar to the figure above. The actual and equivalent representation of the tire contact area is shown in the figure below.

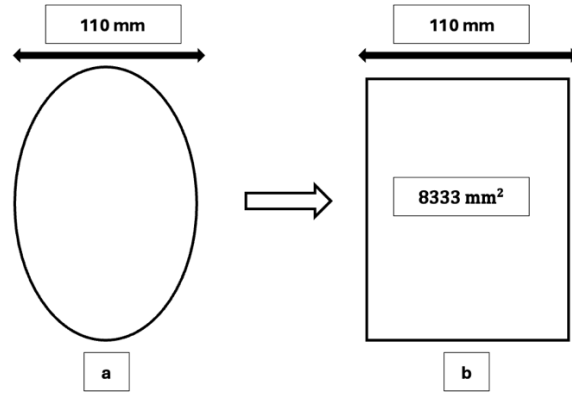


**Figure 17** Tire Contact Area Display a) Actual Tire Contact Area b) Equivalent Tire Contact Area.

### 2.3 Modeling procedures on ANSYS and SOLIDWORKS

In this work, the modeling was first designed on the SOLIDWORKS program. Then, the materials were defined by throwing these designs into the ANSYS program. Subsequently, step and mesh modules were created. After completing this part, the tire contact area was selected, and the force was applied to the calculated to this area. As a result of this force, the analysis was carried out, and the results of these analyzes will be shown with photographs in the following sections.

## **2.4 Determination of Materials**

PA6, PET and PP materials are the preferred materials in geogrids. Each material has its own advantages.

### **PA6 Geogrid:**

It has high strength. They have a long-lasting and durable structure. They are not easily affected by chemicals, and they have a flexible structure.

### **PET Geogrid:**

It has high strength. They have a long-lasting and durable structure. It also has low water absorption, which means it is suitable for use in humid environments.

### **PP Geogrid:**

It has a light structure. Thanks to its flexible structure, it adapts to movements on the ground and thus maintains balance. It also offers a more economical solution in terms of cost compared to other types of materials.

In geogrids, hexagonal and rectangular shaped geogrids are generally preferred.

### **Rectangular Geogrid:**

It can be easily combined. It is more suitable for application on flat surfaces. Provides stability.

### **Hexagon Geogrid:**

It is quite good in terms of spatial efficiency. It has less waste space. “Having less wasted space” means that a particular material or structural element is spread over less void or unused space within the space in which it is used. It is good for adapting to prone places such as curved surfaces.

### **Rhombus Geogrid:**

If spatial efficiency is a priority, it may be preferred in some special cases.

## 2.5 Geometry in simulation

The thickness, density, Poisson's ratio, and Young's modulus values for the subgrade, base course, and asphalt materials were taken as shown in the table below. The components in our study and the properties of these components are as follows.

**Table 1** Materials and Properties [24].

Material	Subgrade	Base Course	Asphalt
<b>Density</b>	2400 kg/m <sup>3</sup>	2000 kg/m <sup>3</sup>	1600 kg/m <sup>3</sup>
<b>Poisson's Ratio</b>	0.40	0.30	0.35
<b>Young's Modulus</b>	10 MPa	100 MPa	2500 MPa
<b>Constitutive Model</b>	Linear Elastic	Linear Elastic	Linear Elastic

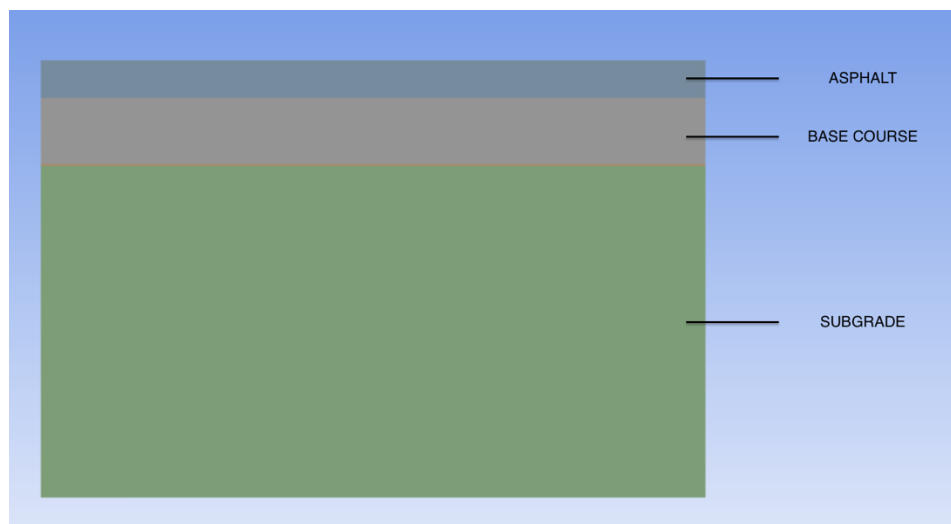


**Figure 18** Modeling layers.

This image shows the layers of a road section. The top layer is called the asphalt layer. It is the layer that the surface traffic directly contacts, and the load is distributed. It consists of bitumen and various aggregates. The asphalt layer increases resistance to traffic loads and temperature changes. It has high resistance to abrasion, slip and weather conditions.

The base course layer is located below the upper layer. It creates a bond between the superstructure and the infrastructure. Crushed stones, gravel and binding materials for stabilization are used as materials. It provides water drainage, thus helping to drain water quickly.

The subgrade layer is the bottom layer of the path. This layer must be resistant to erosion, freezing and other environmental influences.

The features of the components used are as follows. Information about their thickness will be provided in this analysis.

The information needed for entering the geogrids used in this study into material assignment on ANSYS is as shown in the table below.

**Table 2** Materials and Properties [25-38].

Material & Geogrid	Polyamide 6	PET	Polypropylene	Recycled Polyamide 6	Recycled PET	Recycled Polypropylene
<b>Density</b>	1130 kg/m <sup>3</sup>	1380 kg/m <sup>3</sup>	904 kg/m <sup>3</sup>	1220 kg/m <sup>3</sup>	1310 kg/m <sup>3</sup>	910 kg/m <sup>3</sup>
<b>Poisson's Ratio</b>	0.39	0.486	0.42	0.28	0.37	0.36
<b>Young's Modulus</b>	2.90 GPa	3.50 GPa	1.325 GPa	2.552 GPa	2 GPa	0.962 GPa

Material selection in the project is determined by considering the mechanical properties of the material, application requirements and boundary conditions of the design. Mechanical properties such as density, Poisson's ratio and Young's modulus are important factors when determining the performance of a material.

Polymer materials have many common points such as recyclability, heat resistance, wide usage areas and more. In this study, three polymer materials with different properties were identified. These polymer materials are Polyamide, PET, and Polypropylene.

In terms of density, PET has the highest density with 1350 kg/m<sup>3</sup>. Since it is a dense material, it can generally provide advantages in terms of durability and durability. It can be preferred especially in areas that require strength and durability. Likewise, Polypropylene has the lowest density with 904 kg/m<sup>3</sup>. It can provide advantages such as low density, lightness and low cost.

Looking at Young's modulus values, PET has the highest Young's modulus with 3.50 GPa. Young's modulus generally indicates the hardness and tensile strength of the material.

When looking at Poisson's ratio values, PET has the highest Poisson's ratio with 0.486. A high Poisson's ratio generally affects the elasticity and deformation properties of the material.

There are significant differences between these materials. It is an important choice which material should be used in which applications.

In this project, PP, PET, and PA6 materials chosen will be used will be used recycled versions and also virgin ones. The discussion of their test results will follow the test results of the virgin materials.

If the results of recycled materials are compared, the density of PET material, as in virgin materials, is 1310 kg/m<sup>3</sup>, which is the highest value compared to the density of other recycled materials. As mentioned above, it is predicted that advantages in terms of durability and robustness will be provided by dense materials. It can be considered advantageous in terms of lightness and cost-effectiveness that the recycled material with the lowest density measures 910 kg/m<sup>3</sup>.

When the Young's modulus values in recycled materials are examined, it is observed that the recycled version of PA6 has the highest Young's modulus with 2,552 GPa. The recycled form of PP also has the lowest Young's modulus, with 0.962 GPa. Young's modulus generally indicates the hardness and tensile strength of the material.

When the Poisson's ratio values of recycled materials are examined, it is found that recycled PET has the highest Poisson's ratio with 0.37. The recycled material with the lowest Poisson's ratio is recycled PA6 with 0.28. A high Poisson's ratio generally affects the elasticity and deformation properties of the material.

In this section, the results of the conducted experiments will be examined, and the degree to which our assumptions were realized throughout the experiments will also be evaluated.

### 3. Experiment and Analysis

In order to carry out studies to prevent the formation of deformations and cracks due to wheel marks on the asphalt over time under realistic loading conditions, the analyses will need to be conducted using a 3D finite element (FE) model. An appropriate environment for this has been established on ANSYS.

#### 3.1 Geogrid Types

Before commencing this analysis, the designed geogrids will be presented. Three different geogrid models have been designed for this project. These are rectangular, rhombus, hexagon shaped.

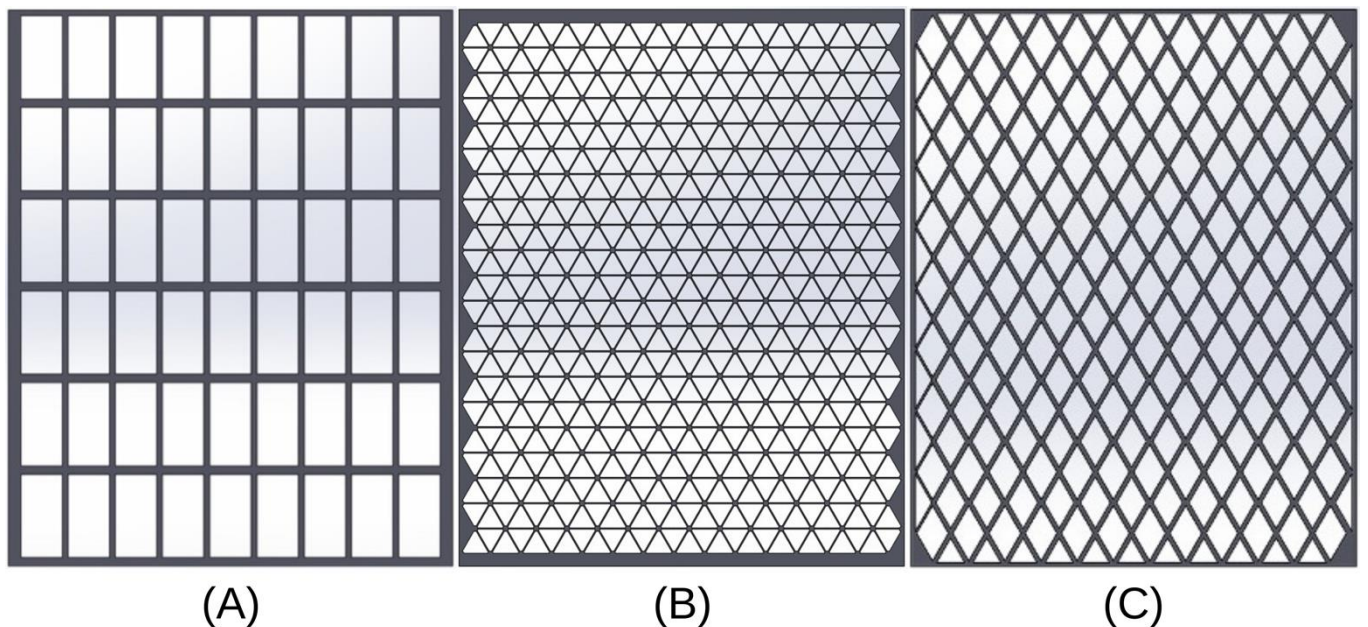


**Figure 19** Geogrid design that we modeled as a rectangular (A), hexagonal (B) and rhombus (C).

## 3.2 Model Analysis without Geogrid

### 3.2.1 Total Deformation

There are two types of deformation in Ansys Workbench. These are total deformation and directional deformation. Both deformation measures are used to find the displacement caused by stress. In directional deformation, displacement in one direction is considered. (X, Y, Z directions). In addition, total deformation is the square root of the sum of the squares of the deformations in all directions. Their formulations can be shown as follows.

$$\text{Total Deformation} = \sqrt{X^2 + Y^2 + Z^2}$$

Where X, Y, Z are directional deformation.

### 3.2.2 Von Mises Stress

Von Mises stress is a widely used measure. It shows the stress seen in the material and encountered it in finite element analysis and ANSYS. This Mises stress indicates the potential for yielding of the material under a value. This is very useful in cases where stress varies throughout the material. It combines normal and shear stress under one roof, which provides a more detailed understanding of the flow behavior of the material.

This type is also called equivalent tensile stress. It gathers all stress components under one roof. It is a special measure of stress. With this unit of measurement, the strength of the material against multi-axial loading can be understood. The formula required for this Von mises stress calculation is as follows.

$$\sigma_r = \frac{1}{\sqrt{2}} \sqrt{(\sigma_x - \sigma_y)^2 + (\sigma_y - \sigma_z)^2 + (\sigma_z - \sigma_x)^2 + 6(\tau_{xy}^2 + \tau_{yz}^2 + \tau_{zx}^2)}$$

The height of these geogrids, which have different designs, has always been 4 mm. In the analyses, both their positioning and their items were differentiated, and comparisons were made.

Our first analysis is our asphalt model non-geogrid.

**Table 3** Table of materials and properties of the model non-geogrid.

Material	Subgrade	Base Course	Asphalt
<b>Thickness</b>	1000 mm	200 mm	110 mm
<b>Density</b>	2400 kg/m3	2000 kg/m3	1600 kg/m3
<b>Poisson's Ratio</b>	0.40	0.30	0.35
<b>Young's Modulus</b>	10 MPa	100 MPa	2500 MPa
<b>Constitutive Model</b>	Linear Elastic	Linear Elastic	Linear Elastic

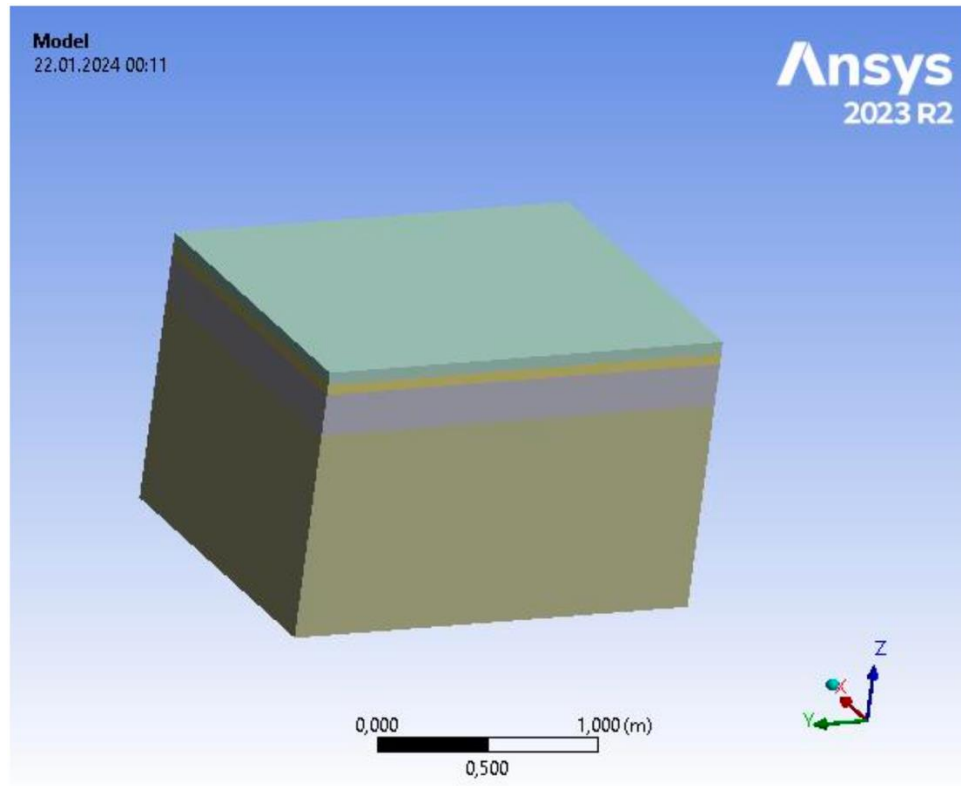


**Figure 20** Illustration of the model non-geogrid.

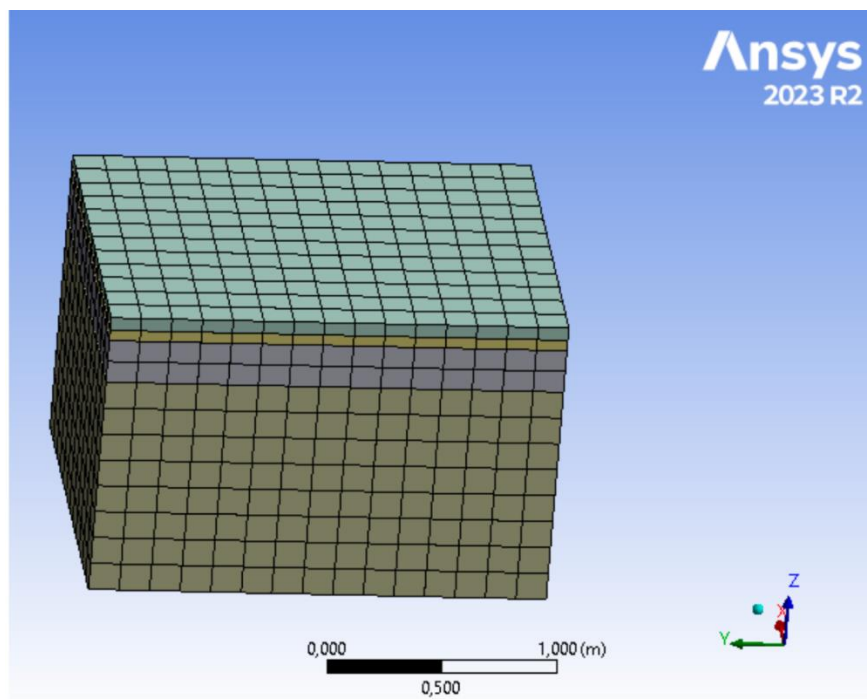


**Figure 21** Showing the mesh applied to the model non-geogrid.

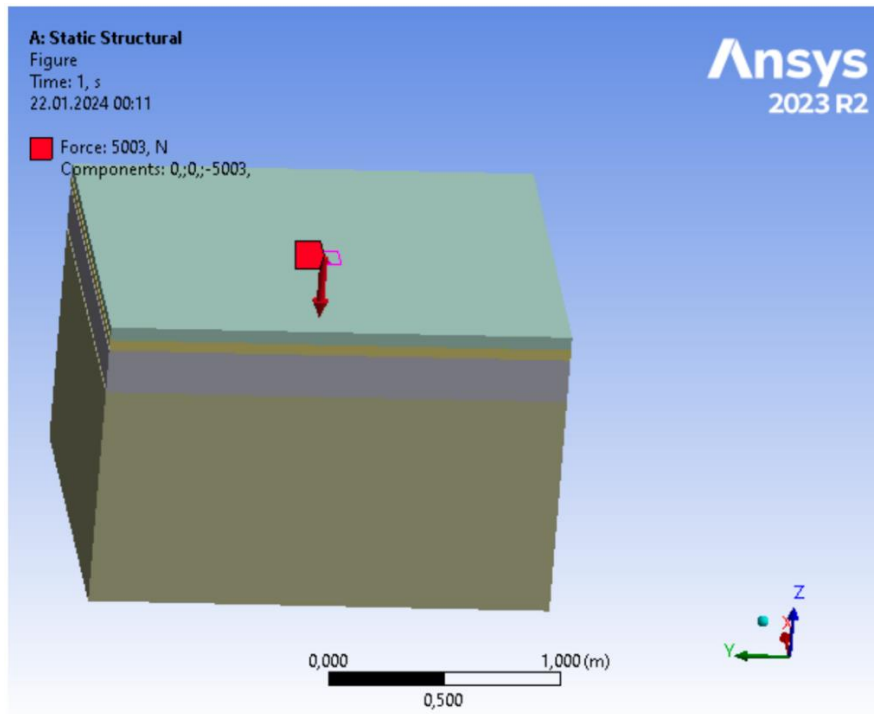


**Figure 22** Representation of the force applied to the model.

The meshing, fixed surface, and location and size of the applied force for all subsequent analyzes are as shown here. These images will not be used to avoid confusion in other analyses.

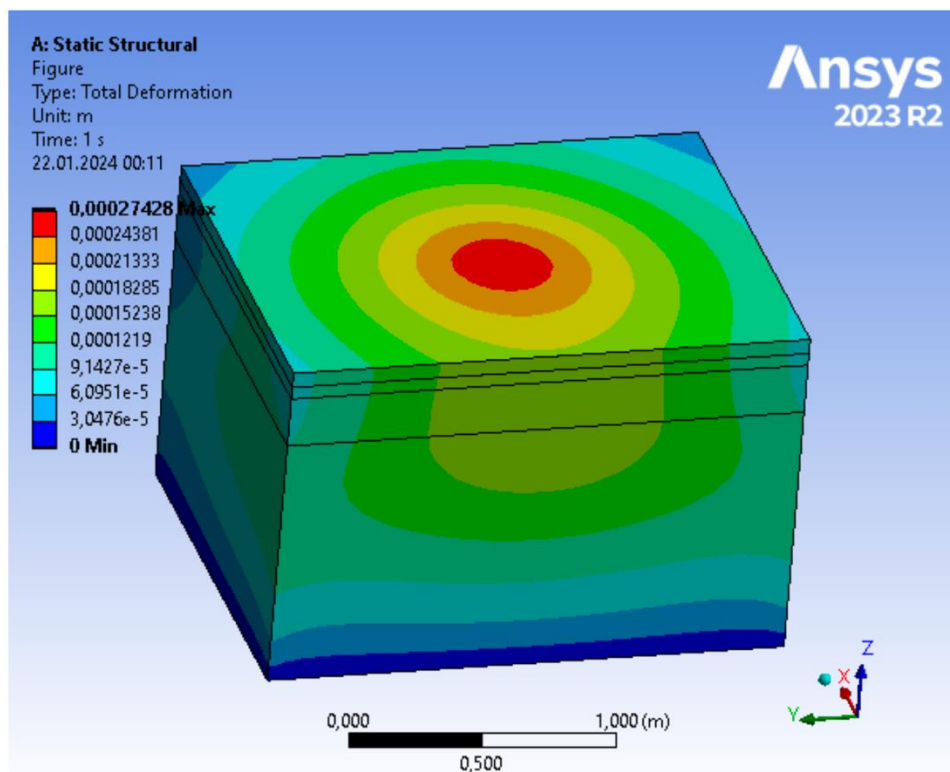


**Figure 23** Total deformation analysis of the normal model.

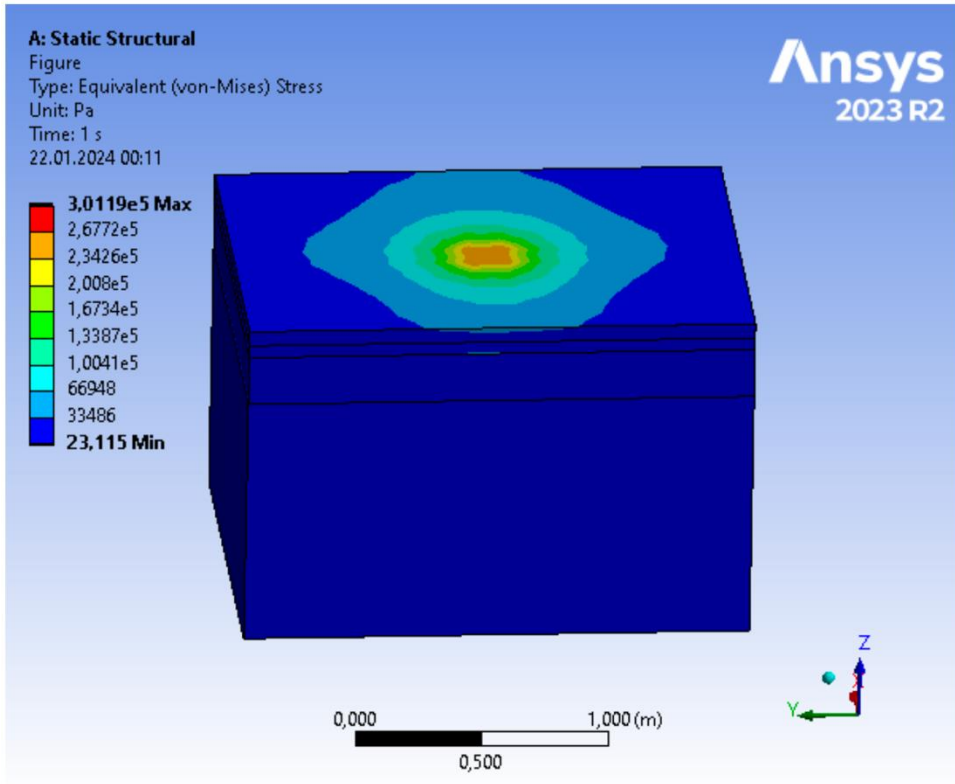


**Figure 24** Stress analysis of the normal model.

The analyses shown above belong to asphalt applications without geogrid. Now, the analyses made by adding geogrid to this model will be shown.

### 3.3 Analysis of the Rectangular Geogrid Model

The first analyzes were made by dividing the 110 mm high asphalt into 50 mm and 60 mm. In our experiment, analyses commenced by placing a geogrid under the 60 mm asphalt layer. Then, geogrid will be placed under the asphalt layer with a 30 mm difference between it and the surface, just under the asphalt layer, under the base course layer, under the 200 mm part of the subgrade layer divided into two parts as 200 mm and 800 mm, under the 100 mm part of subgrade layer divided into two parts as 100 mm and 900 mm. In addition to our material and material preferences, the benefits of altering the position of the geogrid within the asphalt will also be analyzed. According to our thoughts before the experiments, it is predicted that positioning the geogrid within half of the asphalt layer will yield effective resistance against stress and cracking in the upper asphalt layer. These aspects will be investigated in the results section of our experiments [24].

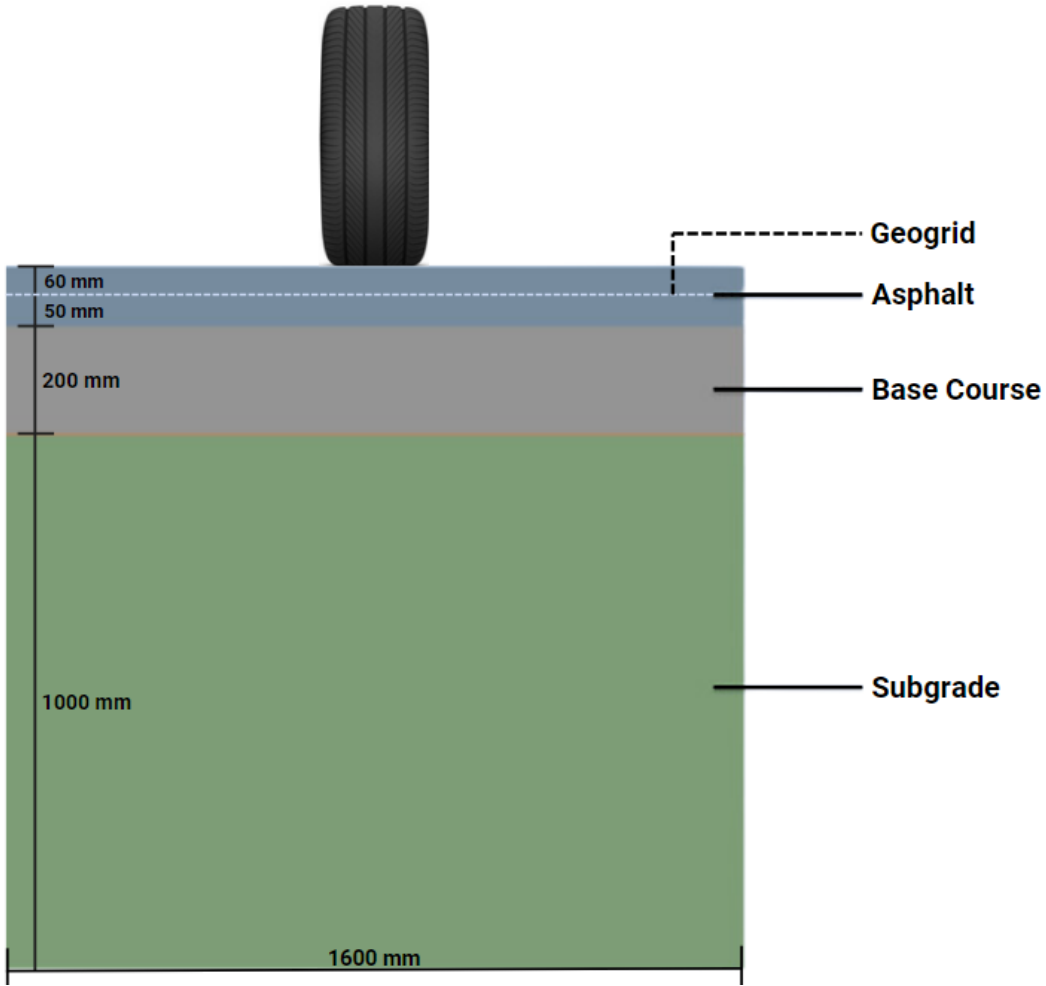


**Figure 25** Determination of geogrid location.

The first geogrid to be analyzed is a rectangular one. This geogrid was positioned between two asphalt layers, with thicknesses of 60 mm and 50 mm respectively, and was assigned three different materials. These materials are PA6, PET, and PP.

**Table 4** Table of materials and properties of the rectangular geogrid under 60 mm asphalt.

Material	Subgrade	Base Course	Bottom Asphalt	Top Asphalt
<b>Thickness</b>	1000 mm	200 mm	50 mm	60 mm
<b>Density</b>	2400 kg/m <sup>3</sup>	2000 kg/m <sup>3</sup>	1600 kg/m <sup>3</sup>	1600 kg/m <sup>3</sup>
<b>Poisson's Ratio</b>	0.40	0.30	0.35	0.35
<b>Young's Modulus</b>	10 MPa	100 MPa	2500 MPa	2500 MPa
<b>Constitutive Model</b>	Linear Elastic	Linear Elastic	Linear Elastic	Linear Elastic

**Table 5** Table of materials and geogrid properties of the rectangular geogrid under 60 mm asphalt.

Material - Geogrid	Polyamide 6	PET	Polypropylene
<b>Thickness</b>	4 mm	4 mm	4 mm
<b>Density</b>	1130 kg/m <sup>3</sup>	1380 kg/m <sup>3</sup>	904 kg/m <sup>3</sup>
<b>Poisson's Ratio</b>	0.39	0.486	0.42
<b>Young's Modulus</b>	2.90 GPa	3.50 GPa	1.325 GPa

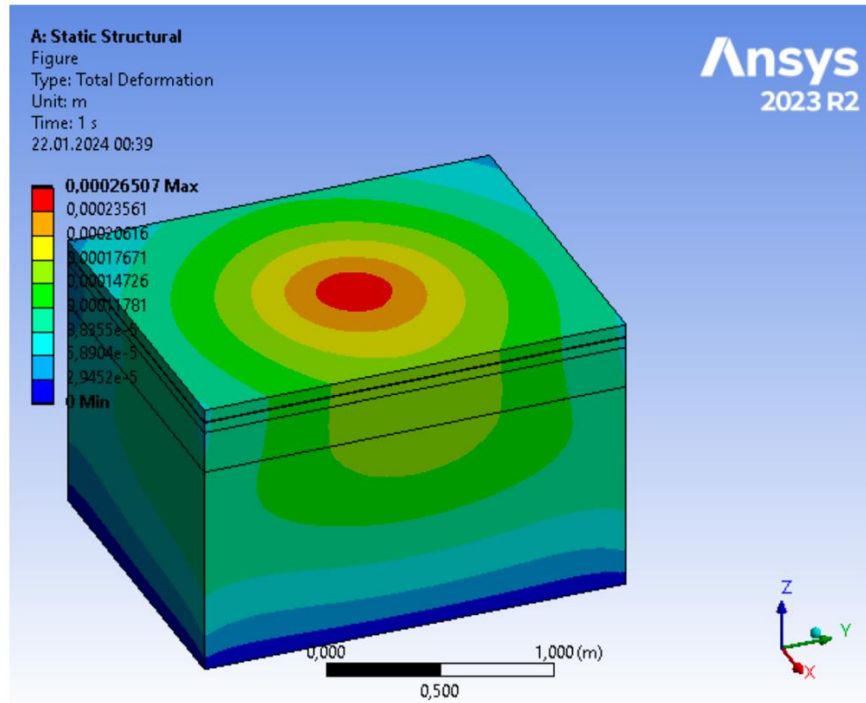


**Figure 26** Total deformation analysis of the rectangular geogrid (PA6) under 60 mm asphalt.

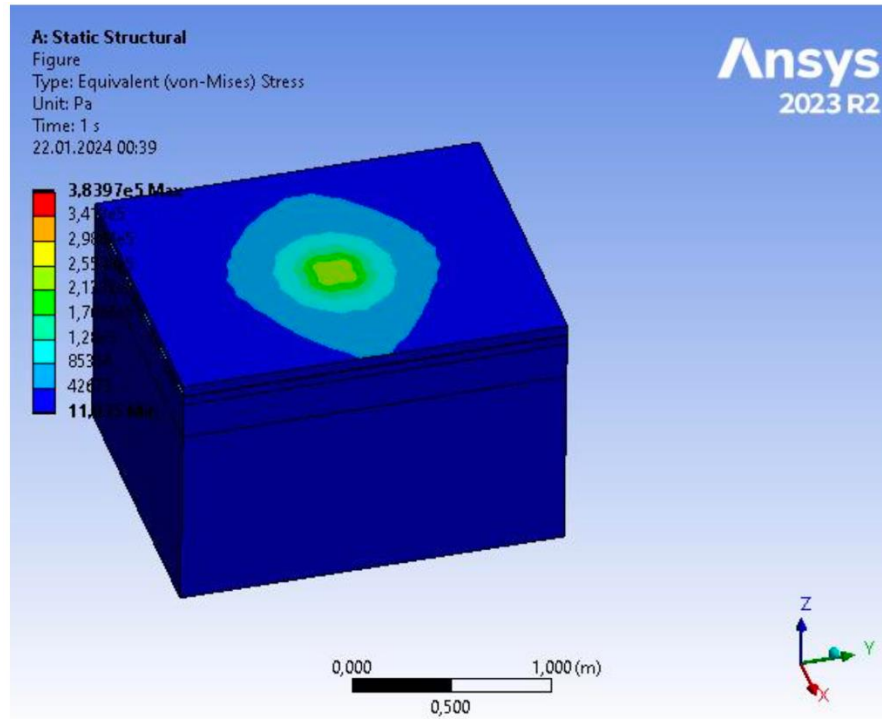


**Figure 27** Stress analysis of the rectangular geogrid (PA6) under 60 mm asphalt.

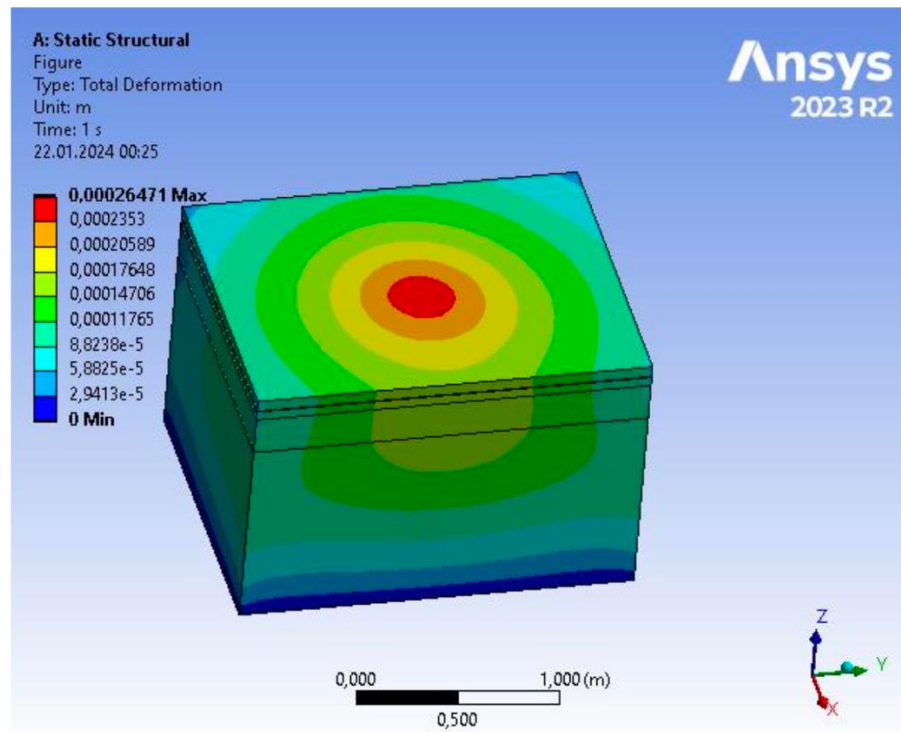


**Figure 28** Total deformation analysis of the rectangular geogrid (PET) under 60 mm asphalt.

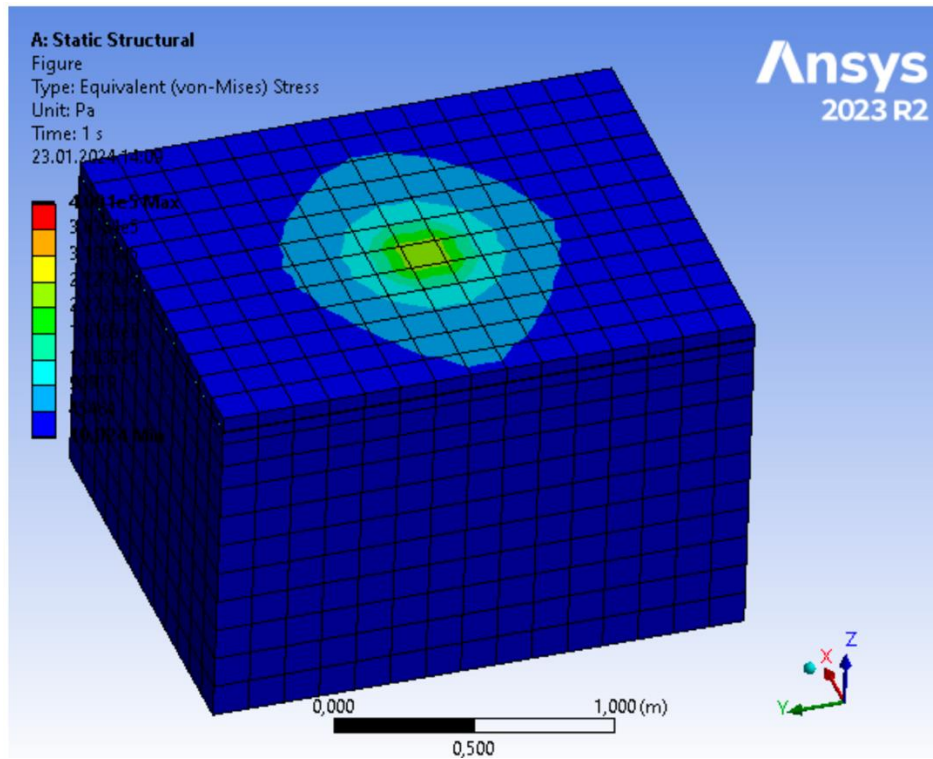


**Figure 29** Stress analysis of the rectangular geogrid (PET) under 60 mm asphalt.

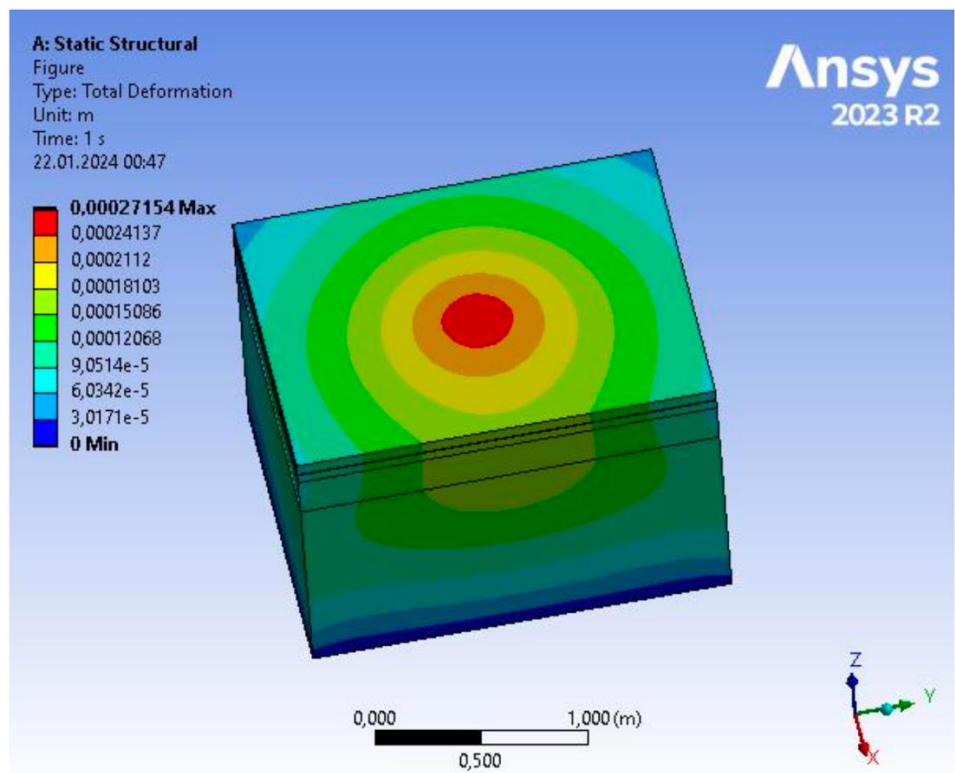


**Figure 30** Total deformation analysis of the rectangular geogrid (PP) under 60 mm asphalt.

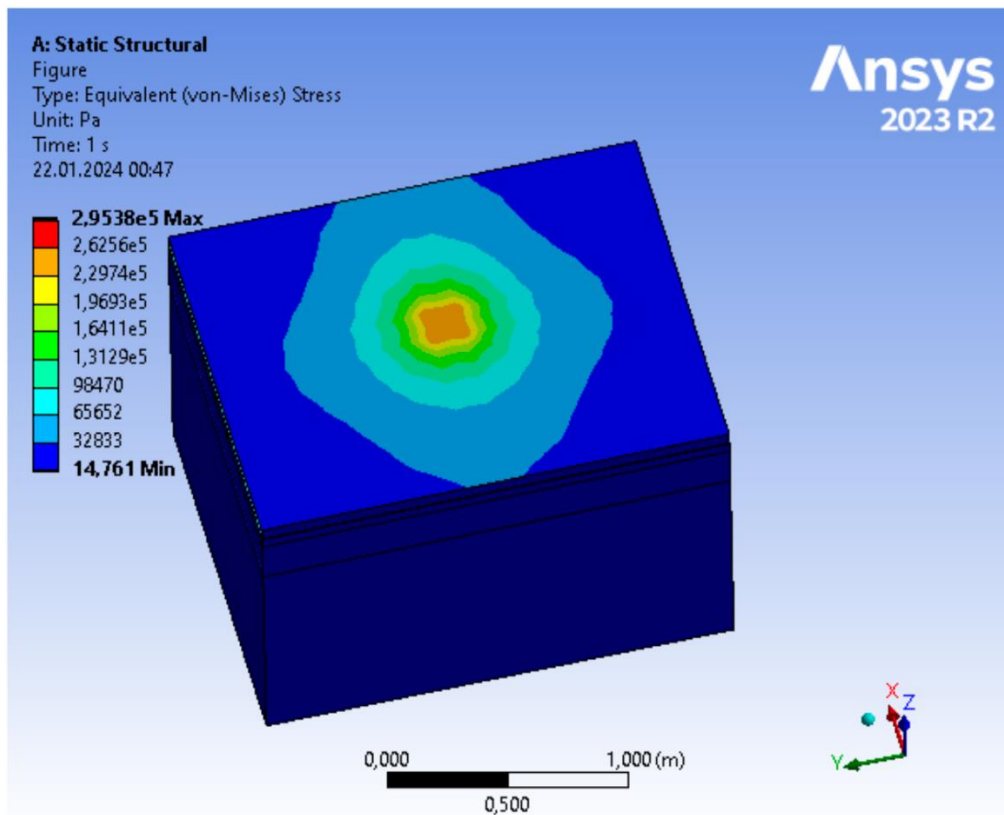


**Figure 31** Stress analysis of the rectangular geogrid (PP) under 60 mm asphalt.

### 3.4 Analysis of Rhombus Geogrid Model

Secondly, our geogrid, the analysis of which will be demonstrated, is a rhombus-shaped geogrid. This geogrid was positioned between two asphalt layers, with thicknesses of 60 mm and 50 mm respectively, and was assigned three different materials. These materials are PA6, PET, and PP.

**Table 6** Table of materials and properties of the rhombus geogrid under 60 mm asphalt.

Material	Subgrade	Base Course	Bottom Asphalt	Top Asphalt
<b>Thickness</b>	1000 mm	200 mm	50 mm	60 mm
<b>Density</b>	2400 kg/m3	2000 kg/m3	1600 kg/m3	1600 kg/m3
<b>Poisson's Ratio</b>	0.40	0.30	0.35	0.35
<b>Young's Modulus</b>	10 MPa	100 MPa	2500 MPa	2500 MPa
<b>Constitutive Model</b>	Linear Elastic	Linear Elastic	Linear Elastic	Linear Elastic

**Table 7** Table of materials and geogrid properties of the rhombus geogrid under 60 mm asphalt.

Material - Geogrid	Polyamide 6	PET	Polypropylene
<b>Thickness</b>	4 mm	4 mm	4 mm
<b>Density</b>	1130 kg/m3	1380 kg/m3	904 kg/m3
<b>Poisson's Ratio</b>	0.39	0.486	0.42
<b>Young's Modulus</b>	2.90 GPa	3.50 GPa	1.325 GPa

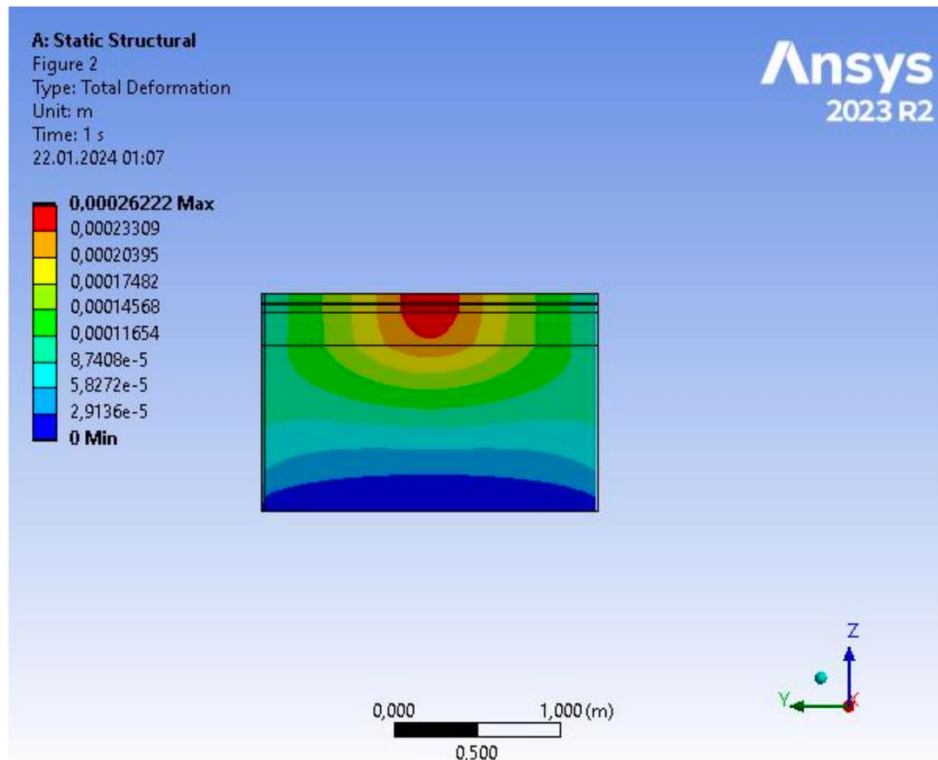


**Figure 32** Total deformation analysis of the rhombus geogrid (PA6) under 60 mm asphalt.

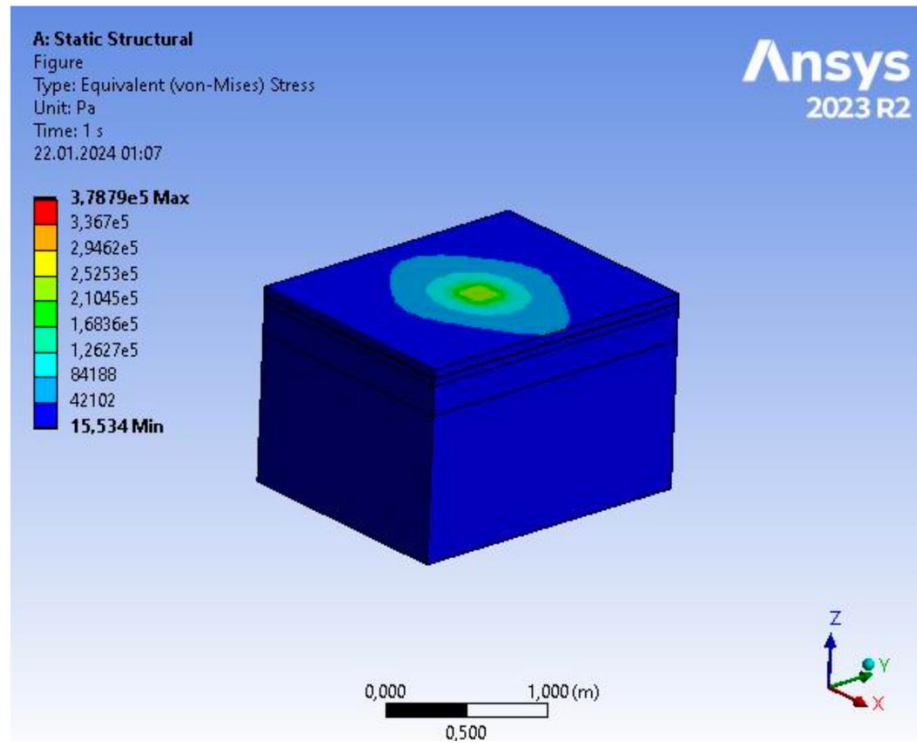


**Figure 33** Stress analysis of the rhombus geogrid (PA6) under 60 mm asphalt.

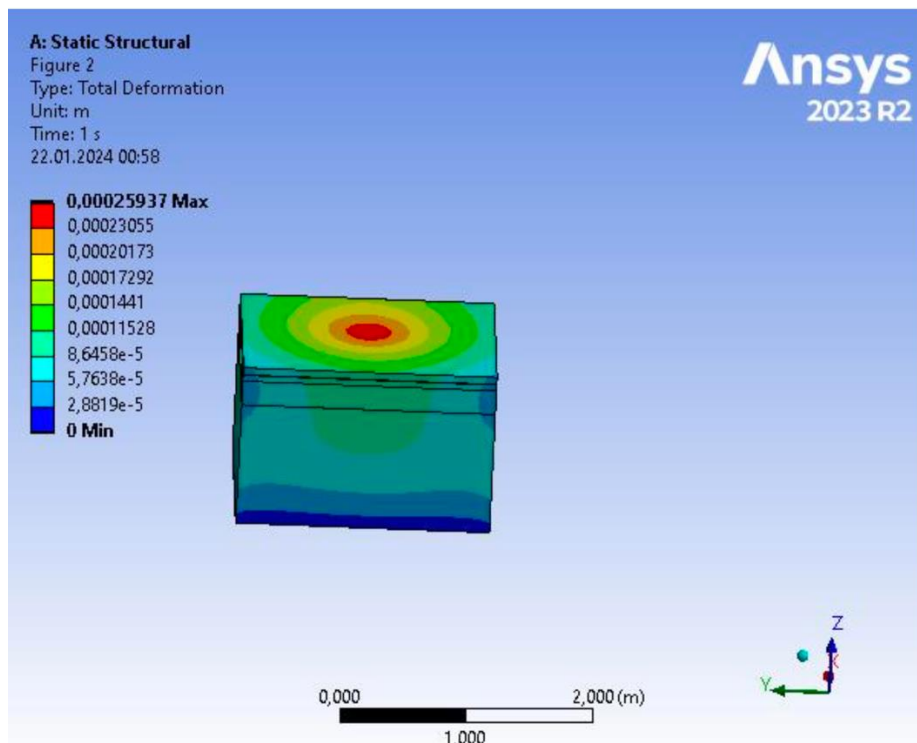


**Figure 34** Total deformation analysis of the rhombus geogrid (PET) under 60 mm asphalt.

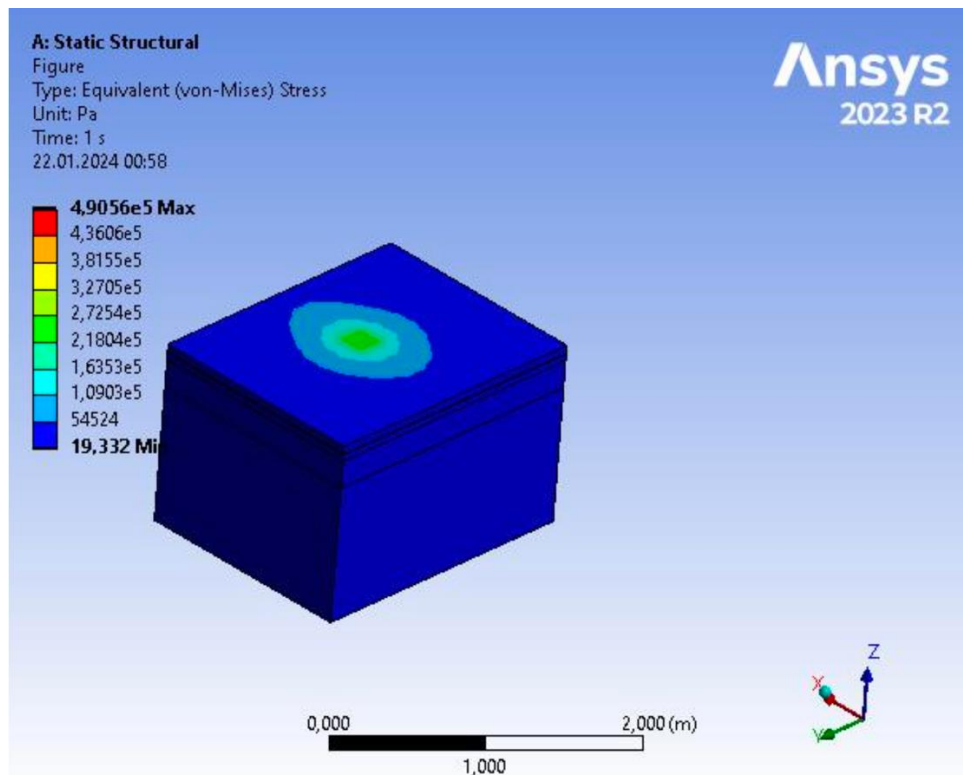


**Figure 35** Stress analysis of the rhombus geogrid (PET) under 60 mm asphalt.

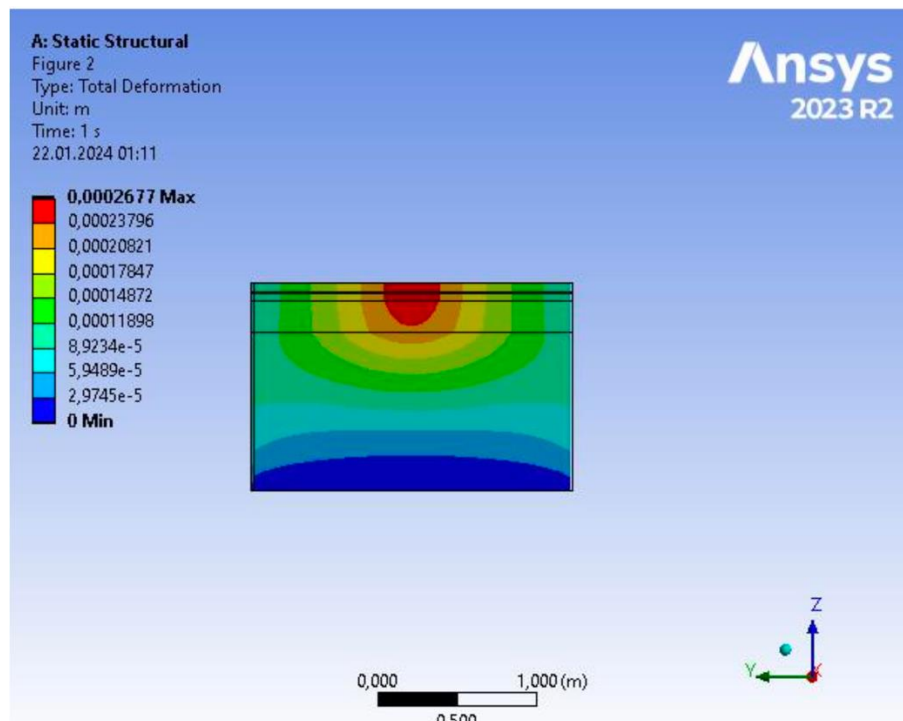


**Figure 36** Total deformation analysis of the rhombus geogrid (PP) under 60 mm asphalt.

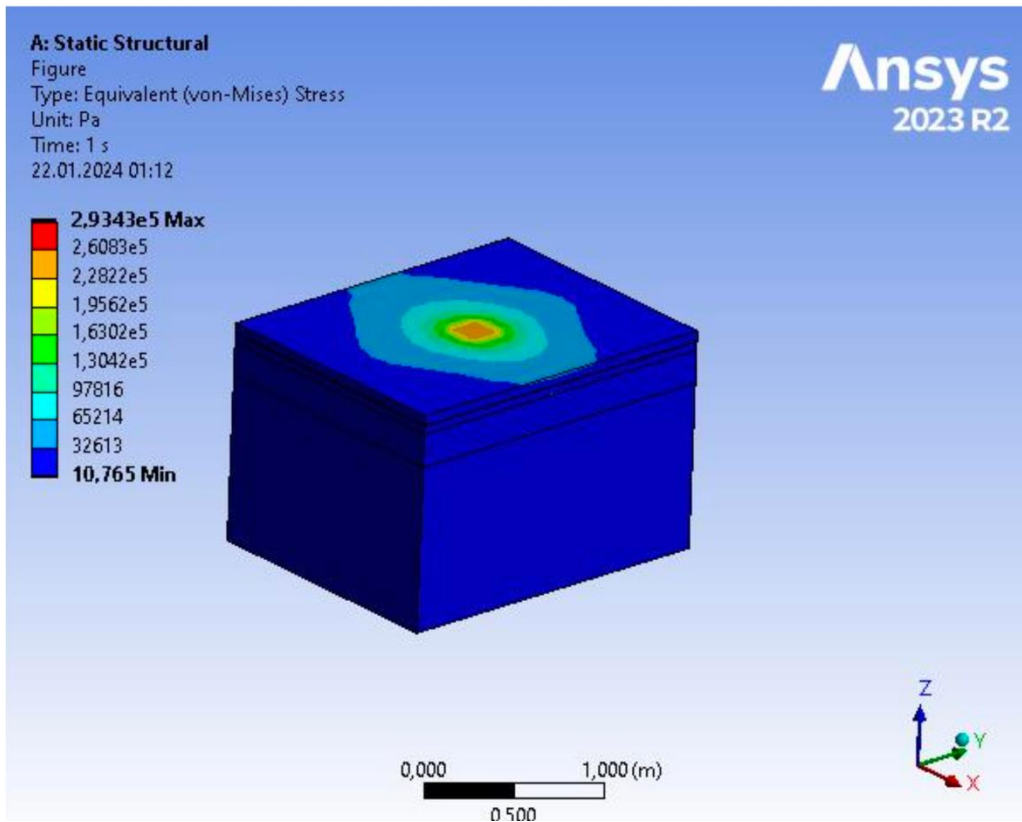


**Figure 37** Stress analysis of the rhombus geogrid (PP) under 60 mm asphalt.

### 3.5 Analysis of Hexagonal Geogrid Model

Thirdly, our geogrid, the analysis of which will be demonstrated, is a hexagonal-shaped geogrid. This geogrid was positioned between two asphalt layers, with thicknesses of 60 mm and 50 mm respectively, and was assigned three different materials. These materials are PA6, PET, and PP.

**Table 8** Table of materials and properties of the hexagon geogrid under 60 mm asphalt.

Material	Subgrade	Base Course	Bottom Asphalt	Top Asphalt
<b>Thickness</b>	1000 mm	200 mm	50 mm	60 mm
<b>Density</b>	2400 kg/m3	2000 kg/m3	1600 kg/m3	1600 kg/m3
<b>Poisson's Ratio</b>	0.40	0.30	0.35	0.35
<b>Young's Modulus</b>	10 MPa	100 MPa	2500 MPa	2500 MPa
<b>Constitutive Model</b>	Linear Elastic	Linear Elastic	Linear Elastic	Linear Elastic

**Table 9** Table of materials and geogrid properties of the hexagon geogrid under 60 mm asphalt.

Material - Geogrid	Polyamide 6	PET	Polypropylene
<b>Thickness</b>	4 mm	4 mm	4 mm
<b>Density</b>	1130 kg/m3	1380 kg/m3	904 kg/m3
<b>Poisson's Ratio</b>	0.39	0.486	0.42
<b>Young's Modulus</b>	2.90 GPa	3.50 GPa	1.325 GPa

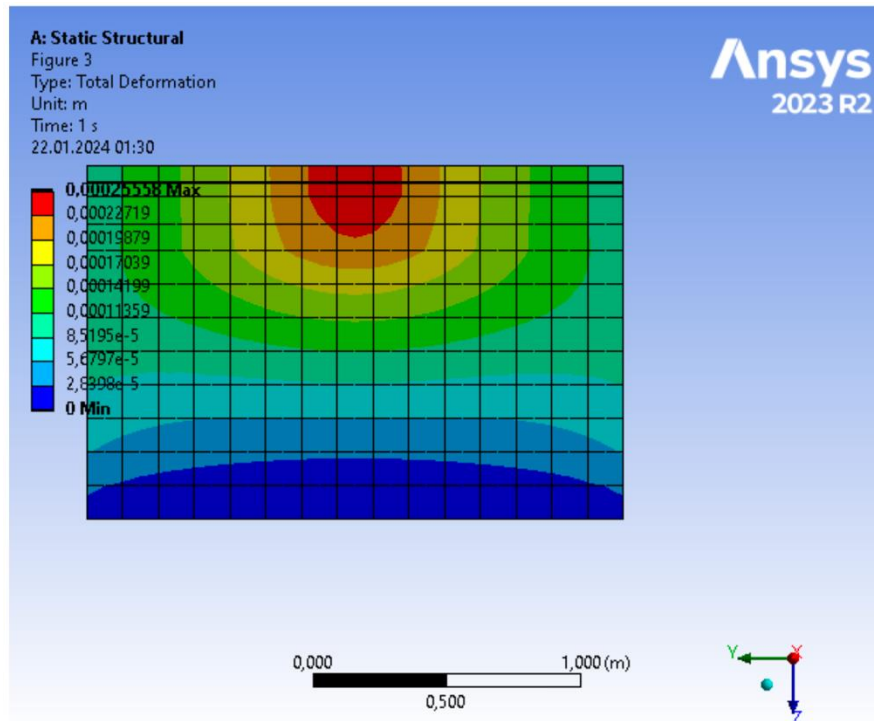


**Figure 38** Total deformation analysis of the hexagon geogrid (PA6) under 60 mm asphalt.

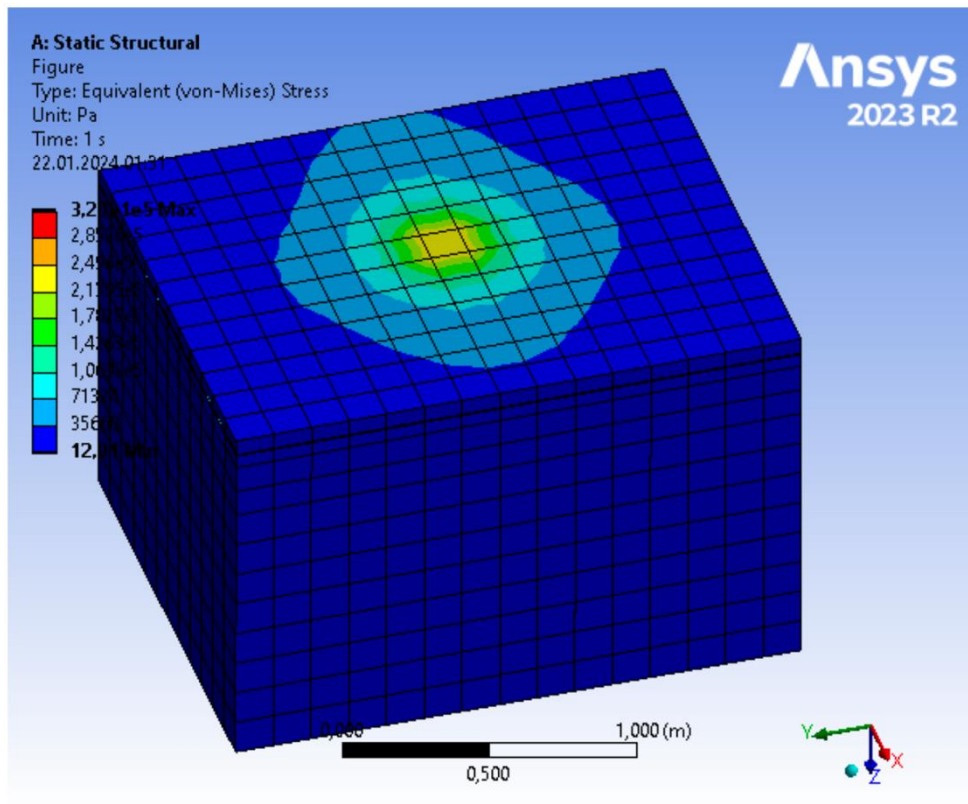


**Figure 39** Stress analysis of the hexagon geogrid (PA6) under 60 mm asphalt.

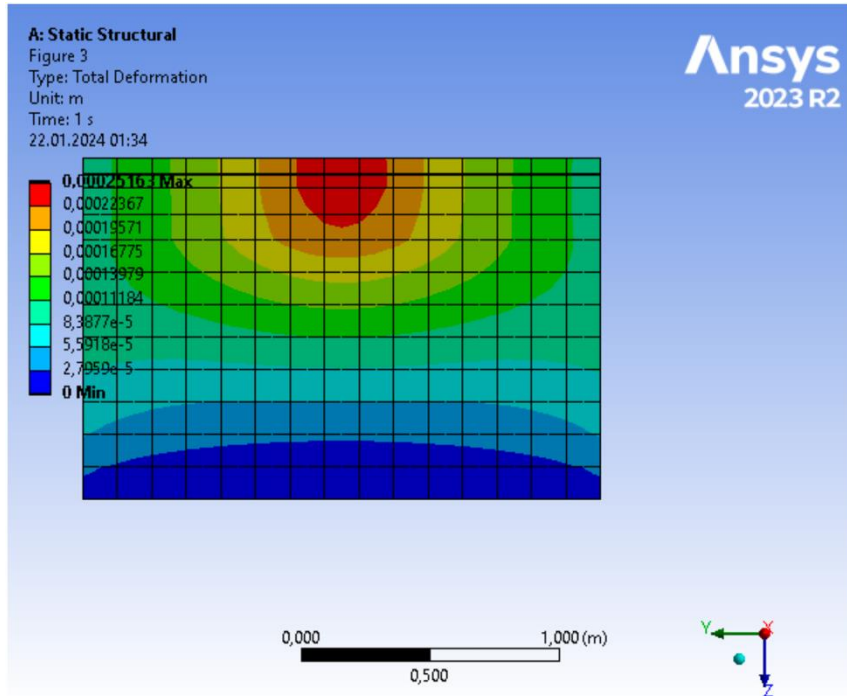


**Figure 40** Total deformation analysis of the hexagon geogrid (PET) under 60 mm asphalt.

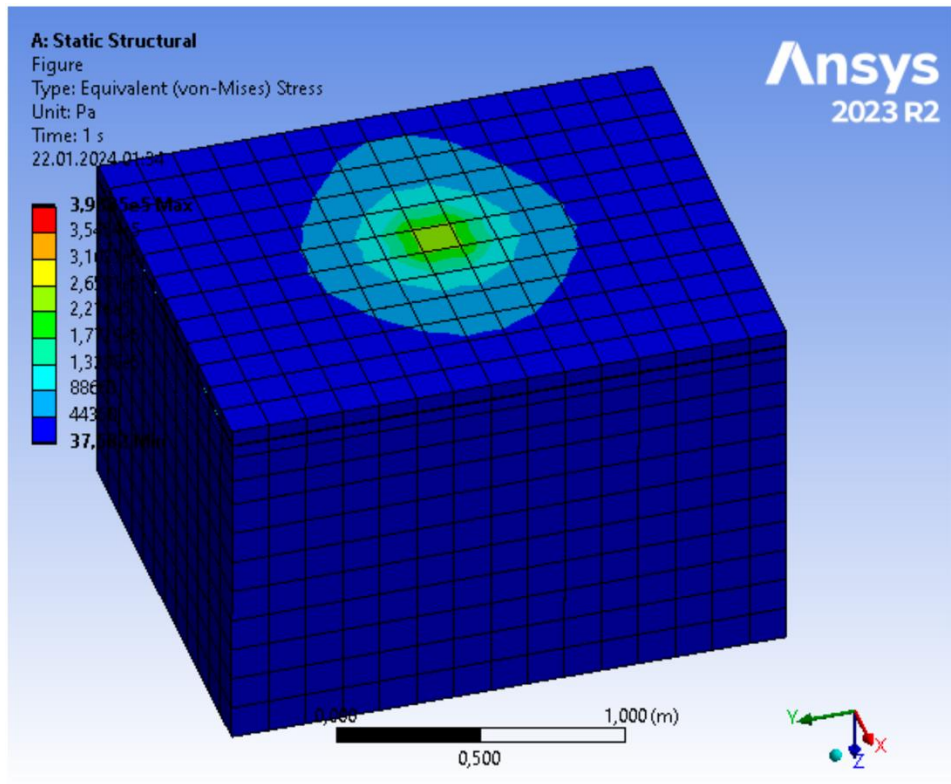


**Figure 41** Stress analysis of the hexagon geogrid (PET) under 60 mm asphalt.

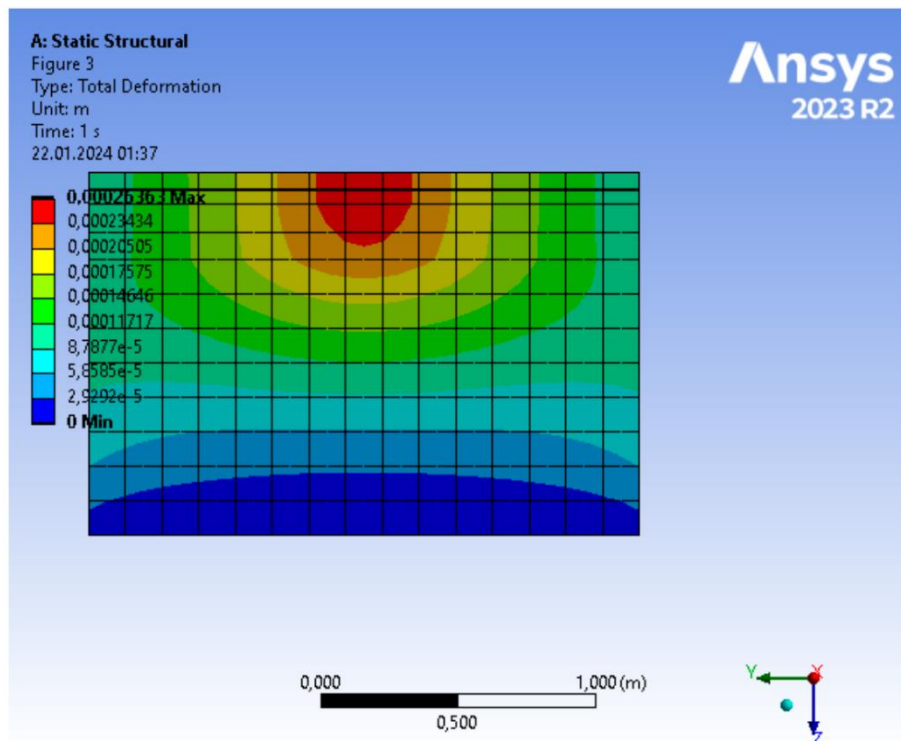


**Figure 42** Total deformation analysis of the hexagon geogrid (PP) under 60 mm asphalt.

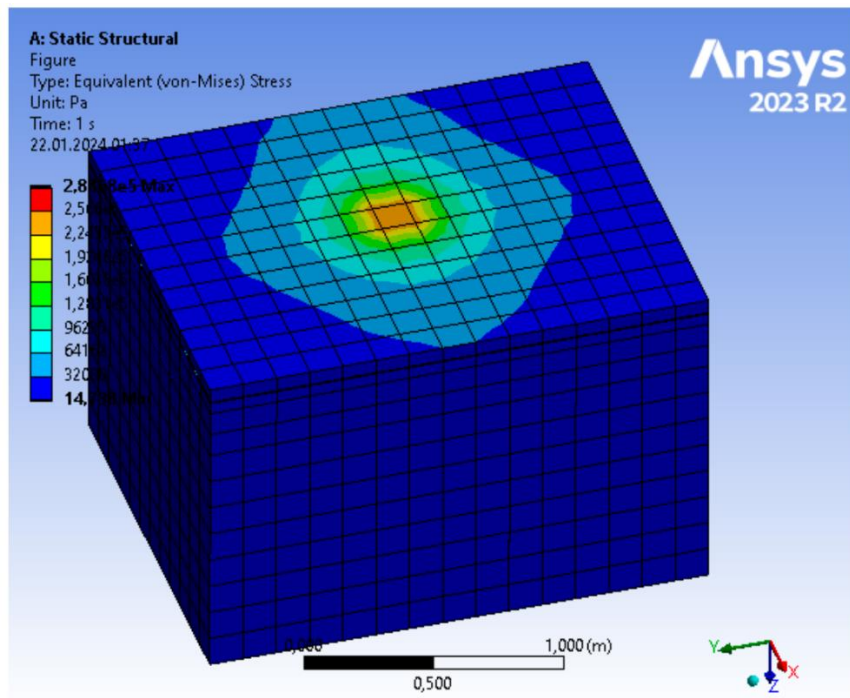


**Figure 43** Stress analysis of the hexagon geogrid (PP) under 60 mm asphalt.

### 3.6 Analysis of Rectangular Geogrid Model with Recycle Materials

Fourthly, our geogrid, the analysis of which will be demonstrated, is a rectangular-shaped geogrid. This geogrid was positioned between two asphalt layers, with thicknesses of 60 mm and 50 mm respectively, and was assigned three different materials. These materials are recycled PA6, recycled PET, and recycled PP.

**Table 10** Table of materials and properties of the rectangular geogrid under 60 mm asphalt.

Material	Subgrade	Base Course	Bottom Asphalt	Top Asphalt
<b>Thickness</b>	1000 mm	200 mm	50 mm	60 mm
<b>Density</b>	2400 kg/m <sup>3</sup>	2000 kg/m <sup>3</sup>	1600 kg/m <sup>3</sup>	1600 kg/m <sup>3</sup>
<b>Poisson's Ratio</b>	0.40	0.30	0.35	0.35
<b>Young's Modulus</b>	10 MPa	100 MPa	2500 MPa	2500 MPa
<b>Constitutive Model</b>	Linear Elastic	Linear Elastic	Linear Elastic	Linear Elastic

**Table 11** Table of materials and geogrid properties of the rectangular geogrid under 60 mm asphalt.

Material - Geogrid	Recycled Polyamide 6	Recycled PET	Recycled Polypropylene
<b>Thickness</b>	4 mm	4 mm	4 mm
<b>Density</b>	1220 kg/m <sup>3</sup>	1310 kg/m <sup>3</sup>	910 kg/m <sup>3</sup>
<b>Poisson's Ratio</b>	0.28	0.37	0.36
<b>Young's Modulus</b>	2.552 GPa	2 GPa	0.962 GPa

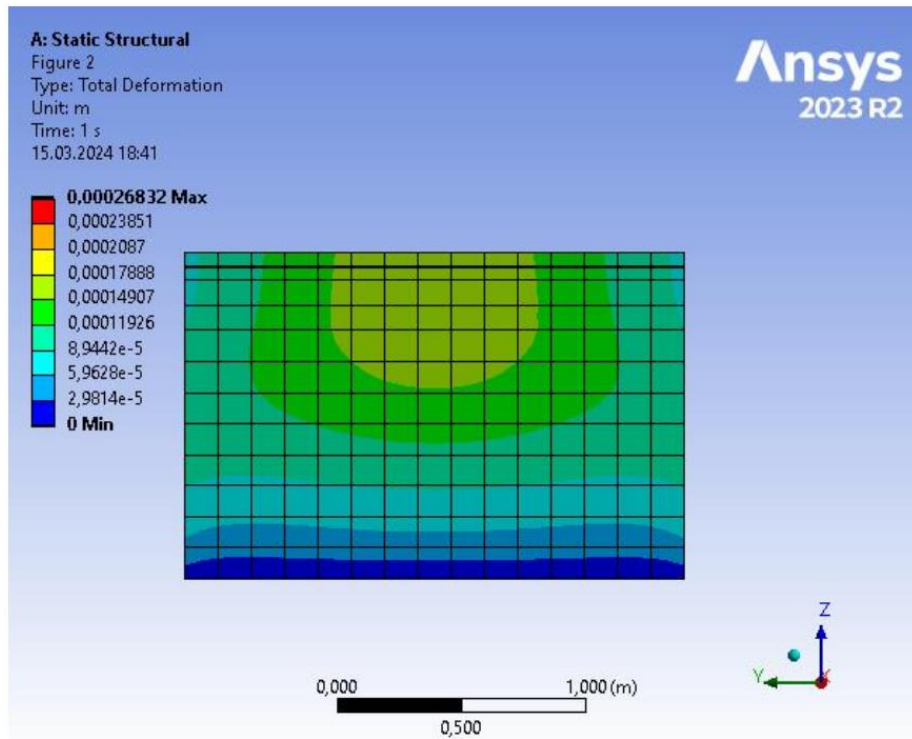


**Figure 44** Total deformation analysis of the rectangular geogrid (Recycled PET) under 60 mm asphalt.

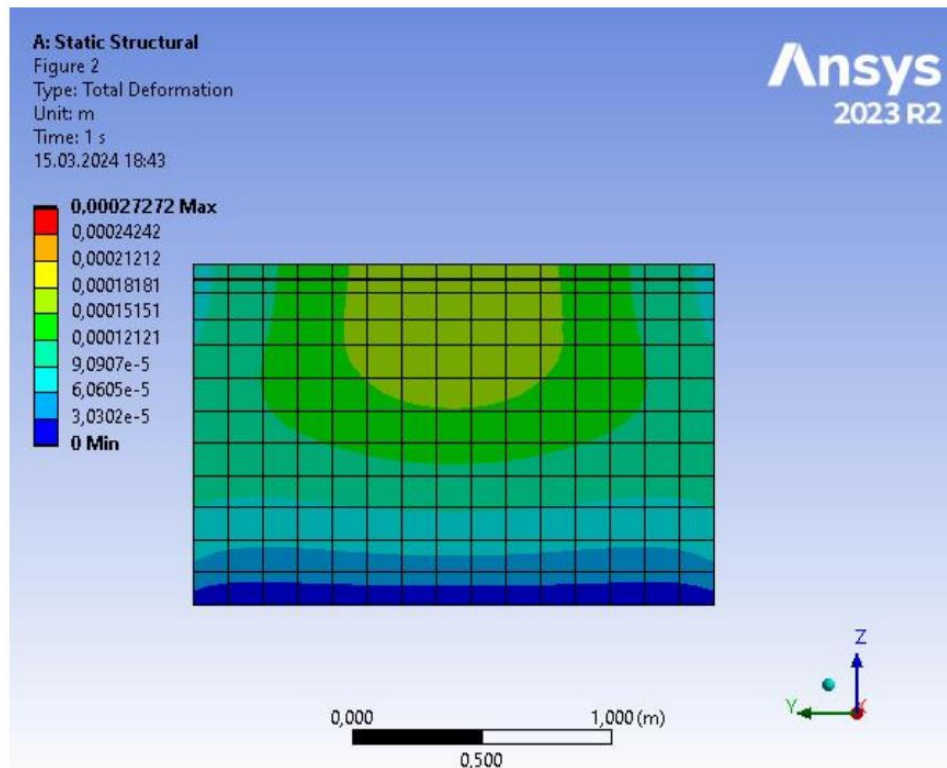


**Figure 45** Total deformation analysis of the rectangular geogrid (Recycled PP) under 60 mm asphalt.

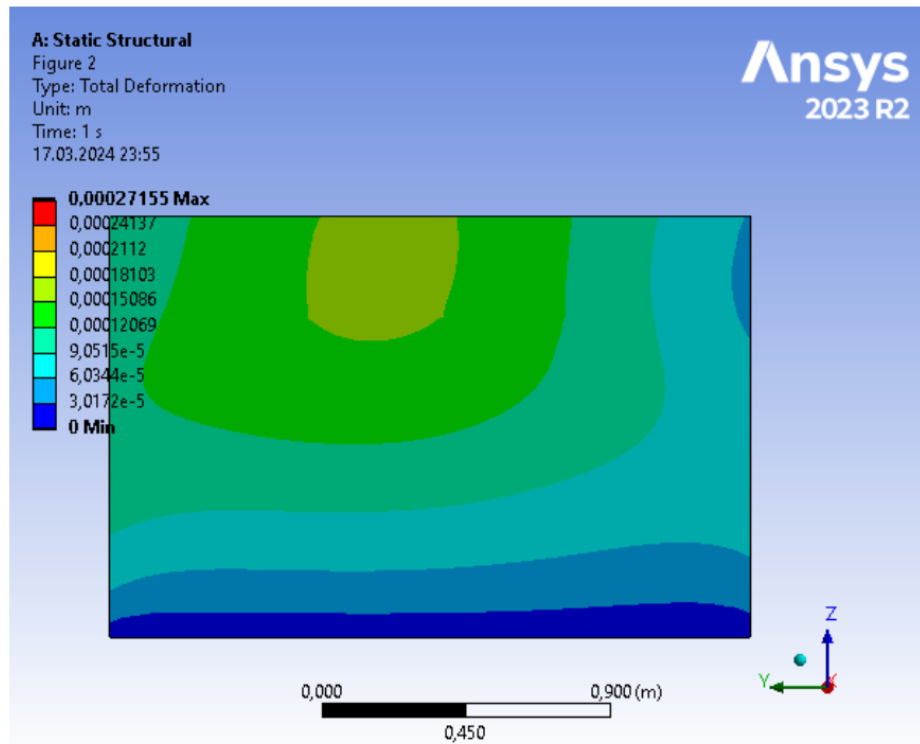


**Figure 46** Total deformation analysis of the rectangular geogrid (Recycled PA6) under 60 mm asphalt.

### 3.7 Analysis of Rhombus Geogrid Model with Recycle Materials

Fifthly, our geogrid, the analysis of which will be demonstrated, is a rhombus-shaped geogrid. This geogrid was positioned between two asphalt layers, with thicknesses of 60 mm and 50 mm respectively, and was assigned three different materials, but recycled materials were used. These materials are recycled PA6, recycled PET, and recycled PP.

**Table 12** Table of materials and properties of the rhombus geogrid under 60 mm asphalt.

Material	Subgrade	Base Course	Bottom Asphalt	Top Asphalt
<b>Thickness</b>	1000 mm	200 mm	50 mm	60 mm
<b>Density</b>	2400 kg/m3	2000 kg/m3	1600 kg/m3	1600 kg/m3
<b>Poisson's Ratio</b>	0.40	0.30	0.35	0.35
<b>Young's Modulus</b>	10 MPa	100 MPa	2500 MPa	2500 MPa
<b>Constitutive Model</b>	Linear Elastic	Linear Elastic	Linear Elastic	Linear Elastic

**Table 13** Table of materials and geogrid properties of the rhombus geogrid under 60 mm asphalt.

Material - Geogrid	Recycled Polyamide 6	Recycled PET	Recycled Polypropylene
<b>Thickness</b>	4 mm	4 mm	4 mm
<b>Density</b>	1220 kg/m3	1310 kg/m3	910 kg/m3
<b>Poisson's Ratio</b>	0.28	0.37	0.36
<b>Young's Modulus</b>	2.552 GPa	2 GPa	0.962 GPa

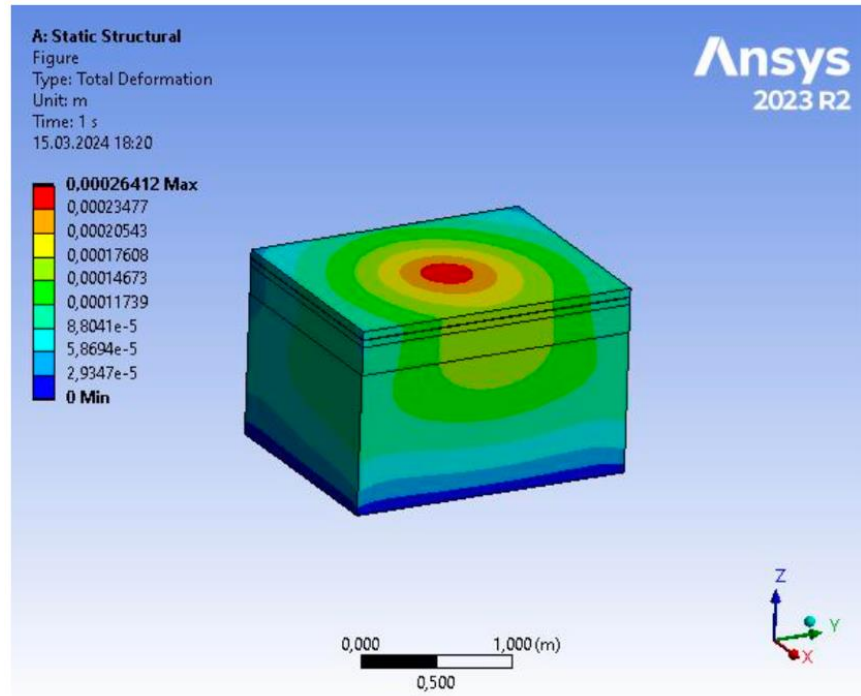


**Figure 47** Total deformation analysis of the rhombus geogrid (Recycled PET) under 60 mm asphalt.

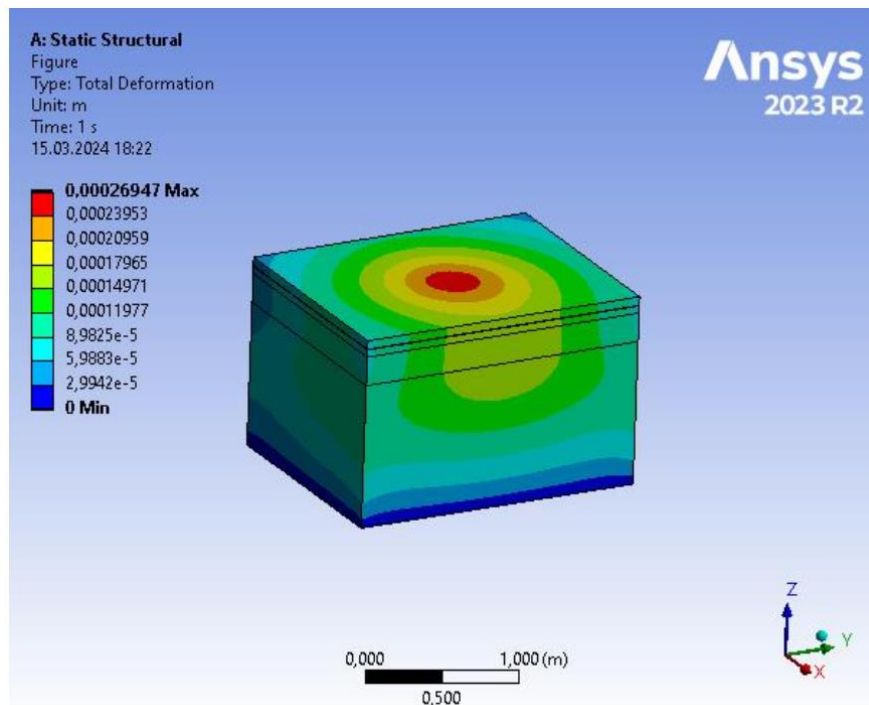


**Figure 48** Total deformation analysis of the rhombus geogrid (Recycled PP) under 60 mm asphalt.

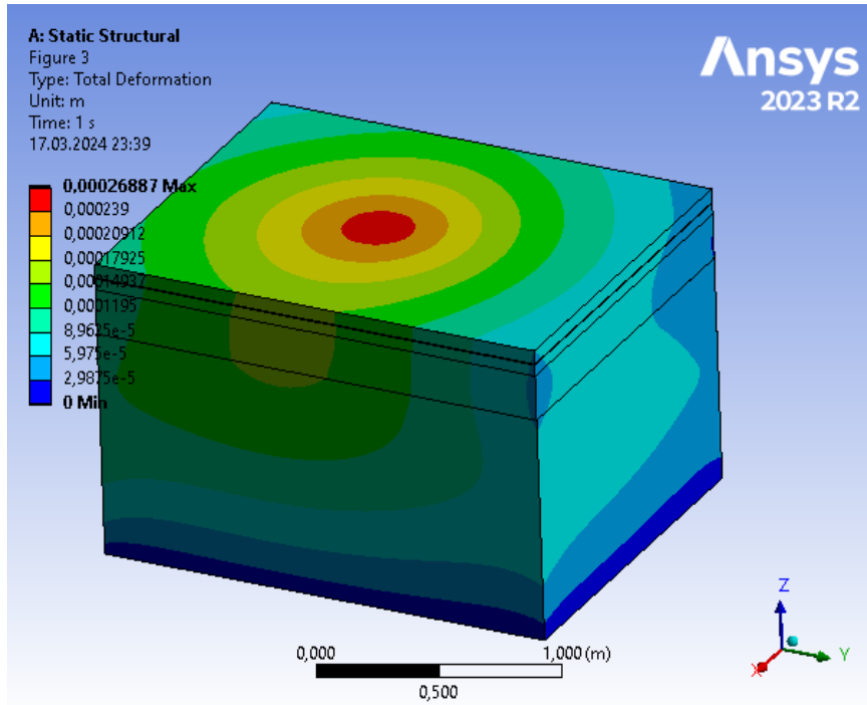


**Figure 49** Total deformation analysis of the rhombus geogrid (Recycled PA6) under 60 mm asphalt.

### 3.8 Analysis of Hexagonal Geogrid Model with Recycle Materials

Sixthly, our geogrid, the analysis of which will be demonstrated, is a hexagonal-shaped geogrid. This geogrid was positioned between two asphalt layers, with thicknesses of 60 mm and 50 mm respectively, and was assigned three different materials, but recycled materials were used. These materials are recycled PA6, recycled PET, and recycled PP.

**Table 14** Table of materials and properties of the hexagonal geogrid under 60 mm asphalt.

Material	Subgrade	Base Course	Bottom Asphalt	Top Asphalt
<b>Thickness</b>	1000 mm	200 mm	50 mm	60 mm
<b>Density</b>	2400 kg/m <sup>3</sup>	2000 kg/m <sup>3</sup>	1600 kg/m <sup>3</sup>	1600 kg/m <sup>3</sup>
<b>Poisson's Ratio</b>	0.40	0.30	0.35	0.35
<b>Young's Modulus</b>	10 MPa	100 MPa	2500 MPa	2500 MPa
<b>Constitutive Model</b>	Linear Elastic	Linear Elastic	Linear Elastic	Linear Elastic

**Table 15** Table of materials and geogrid properties of the hexagonal geogrid under 60 mm asphalt.

Material - Geogrid	Recycled Polyamide 6	Recycled PET	Recycled Polypropylene
<b>Thickness</b>	4 mm	4 mm	4 mm
<b>Density</b>	1220 kg/m <sup>3</sup>	1310 kg/m <sup>3</sup>	910 kg/m <sup>3</sup>
<b>Poisson's Ratio</b>	0.28	0.37	0.36
<b>Young's Modulus</b>	2.552 GPa	2 GPa	0.962 GPa

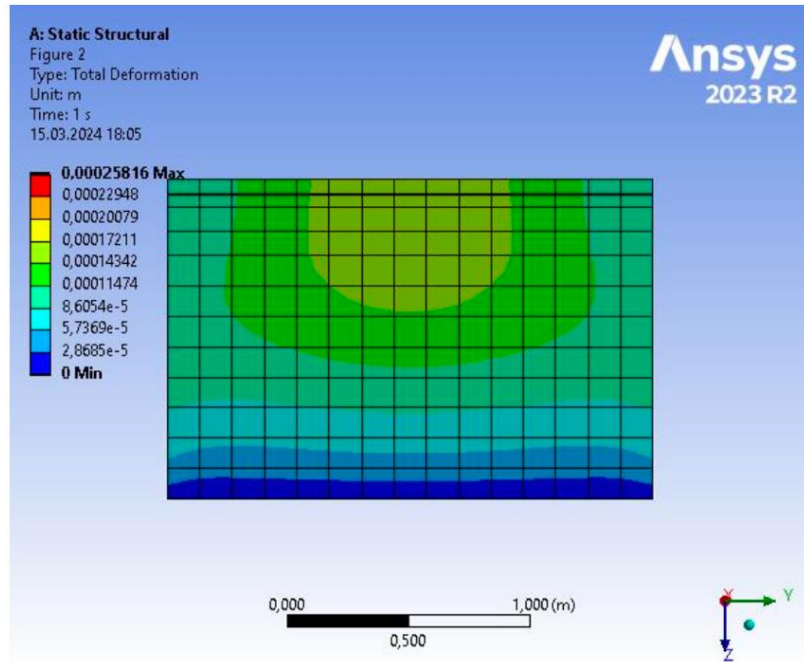


**Figure 50** Total deformation analysis of the hexagonal geogrid (Recycled PET) under 60 mm asphalt.

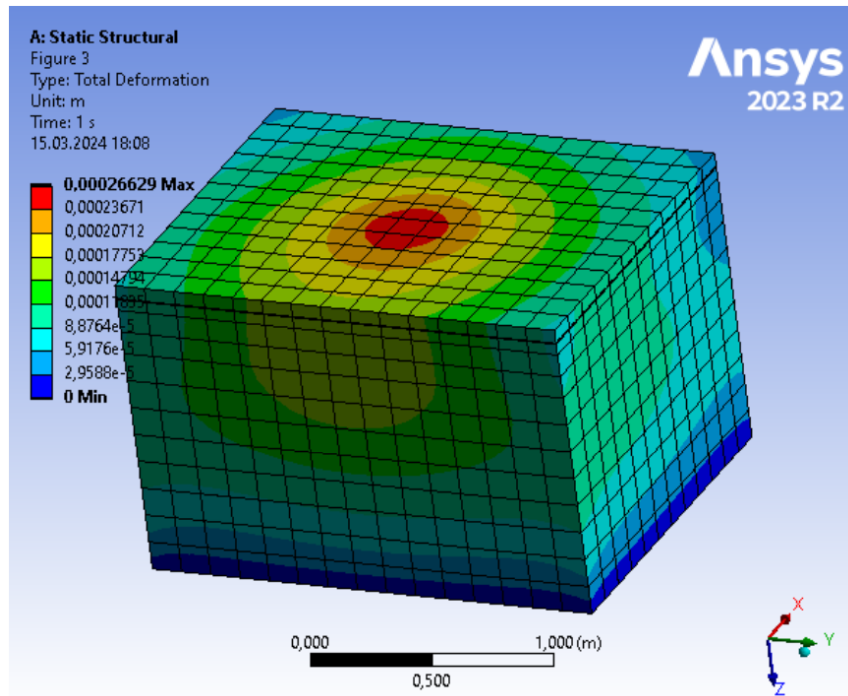


**Figure 51** Total deformation analysis of the hexagonal geogrid (Recycled PET) under 60 mm asphalt.

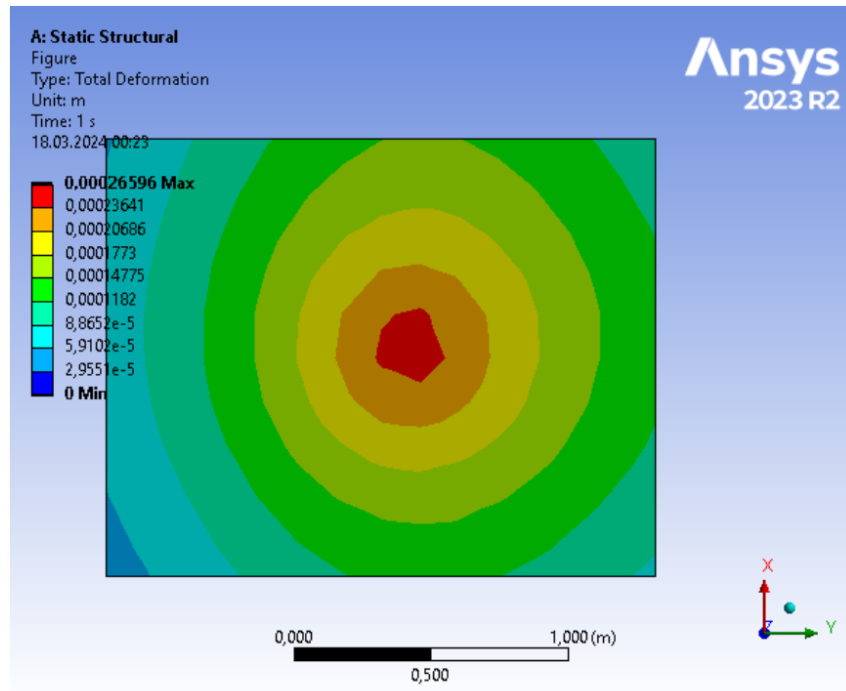


**Figure 52** Total deformation analysis of the hexagonal geogrid (Recycled PA6) under 60 mm asphalt.

### 3.9 Analyzes in which the Geogrid Changes Position

As shown in Figure 25, the experimental setup was made in this way. Our prediction for these experiments is that placing the geogrid in half of the asphalt layer will provide good resistance to stress and cracks in the upper layer of asphalt. So far in these experiments, the analyses have been completed with regarding the geogrid shape and geogrid material changes under the 60 mm asphalt layer. As a result of these, the duo of the geogrid being hexagonal and made of PP material is the most effective material when compared to the stresses and deformations of other materials.

Now, the effect on deformation by changing the position of the geogrid will be examined. As mentioned in the experiment above, our experiments will be carried out with geogrid placed under the asphalt layer, under the base course, under the 200 mm layer of the subgrade and under the 100 mm layer of the subgrade.

As a result of these tests, it was observed that the most durable modeling is achieved with hexagonal geogrid and PP material, as depicted in the images and graphics shared above.

To further enrich our experiments from a different perspective, studies were conducted to measure the effect of changing the position of the geogrid on durability by altering the position of the PP material hexagonal geogrid, which exhibits the least deformation, in the model.

The locations chosen were;

- Geogrid with 30 mm asphalt on top and 80 mm asphalt underneath,
- Geogrid located under the asphalt layer,
- Geogrid located under the base course,
- Geogrid 100 mm below the area where subgrade started,
- Geogrid 200 mm below the area where subgrade started,

Below are the results of these analyses, respectively.

First modeling, there will be 30 mm of asphalt on the hexagonal geogrid and 80 mm of asphalt underneath.

**Table 16** Table of materials and properties of the hexagonal geogrid under 30 mm asphalt.

Material	Subgrade	Base Course	Bottom Asphalt	Top Asphalt
<b>Thickness</b>	1000 mm	200 mm	80 mm	30 mm
<b>Density</b>	2400 kg/m3	2000 kg/m3	1600 kg/m3	1600 kg/m3
<b>Poisson's Ratio</b>	0.40	0.30	0.35	0.35
<b>Young's Modulus</b>	10 MPa	100 MPa	2500 MPa	2500 MPa
<b>Constitutive Model</b>	Linear Elastic	Linear Elastic	Linear Elastic	Linear Elastic

**Table 17** Table of materials and geogrid properties of the hexagonal geogrid under 30 mm asphalt.

Material - Geogrid	Polypropylene
<b>Thickness</b>	4 mm
<b>Density</b>	904 kg/m3
<b>Poisson's Ratio</b>	0.42
<b>Young's Modulus</b>	1.325 GPa

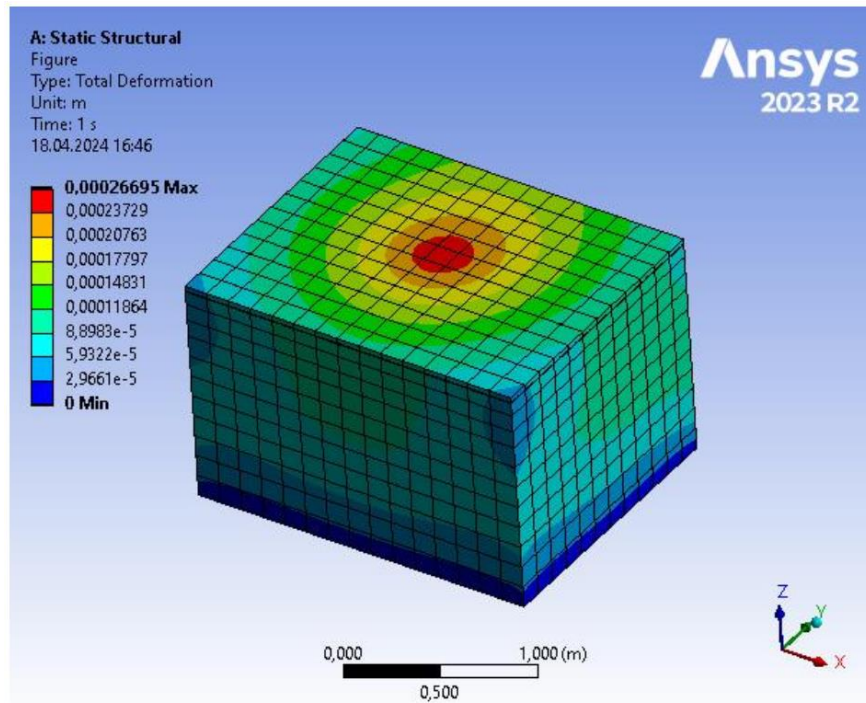


**Figure 53** Total deformation analysis of the hexagonal geogrid (PP) under 30 mm asphalt.

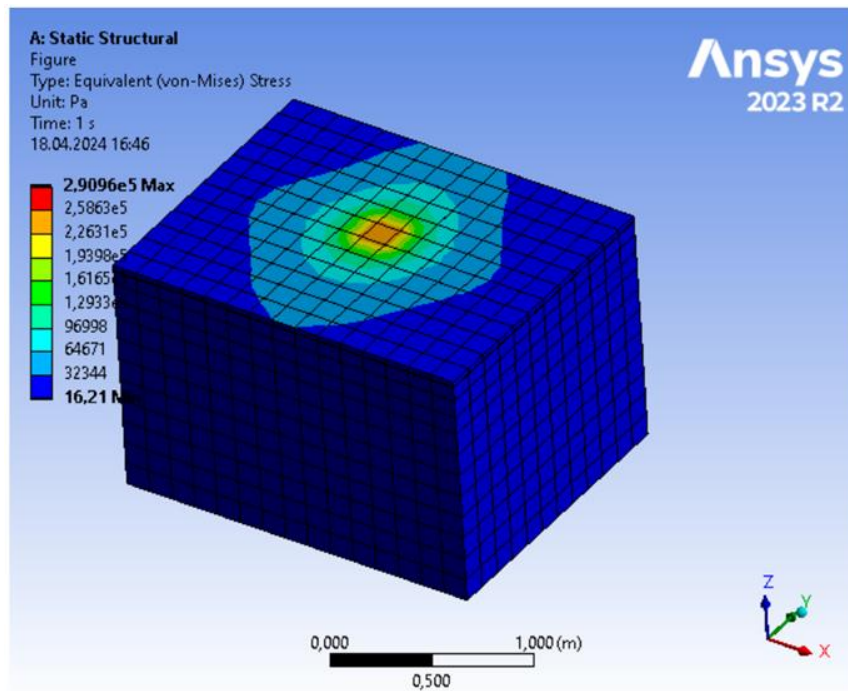


**Figure 54** Stress analysis of the hexagonal geogrid (PP) under 30 mm asphalt.

Second modelling, the hexagonal geogrid is located between the 110 mm asphalt and the base course.

**Table 18** Table of materials and properties of the hexagonal geogrid under 110 mm asphalt.

Material	Subgrade	Base Course	Asphalt
<b>Thickness</b>	1000 mm	200 mm	110 mm
<b>Density</b>	2400 kg/m3	2000 kg/m3	1600 kg/m3
<b>Poisson's Ratio</b>	0.40	0.30	0.35
<b>Young's Modulus</b>	10 MPa	100 MPa	2500 MPa
<b>Constitutive Model</b>	Linear Elastic	Linear Elastic	Linear Elastic

**Table 19** Table of materials and geogrid properties of the hexagonal geogrid under 110 mm asphalt.

Material - Geogrid	Polypropylene
<b>Thickness</b>	4 mm
<b>Density</b>	904 kg/m3
<b>Poisson's Ratio</b>	0.42
<b>Young's Modulus</b>	1.325 GPa

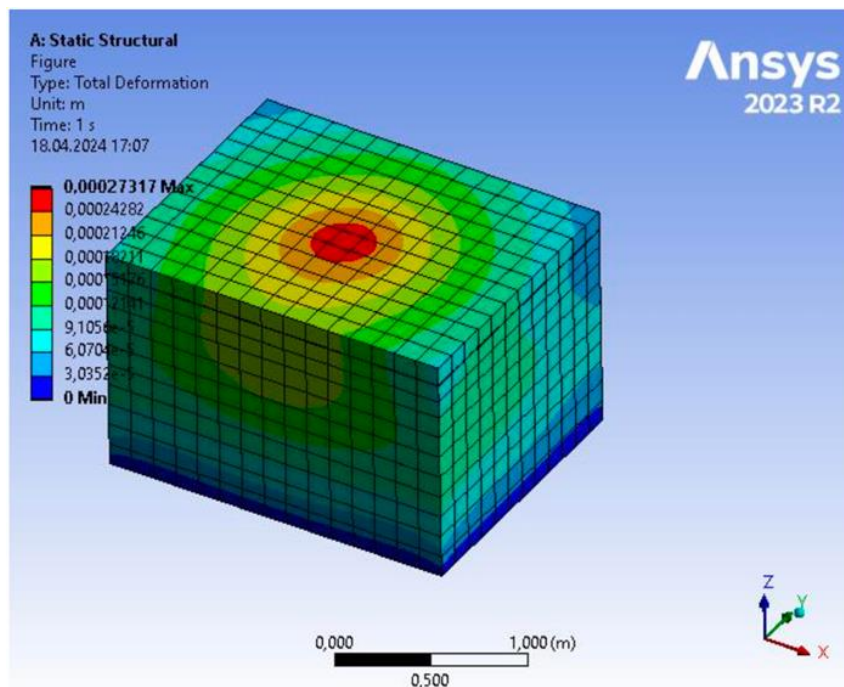


**Figure 55** Total deformation analysis of the hexagonal geogrid (PP) under 110 mm asphalt.

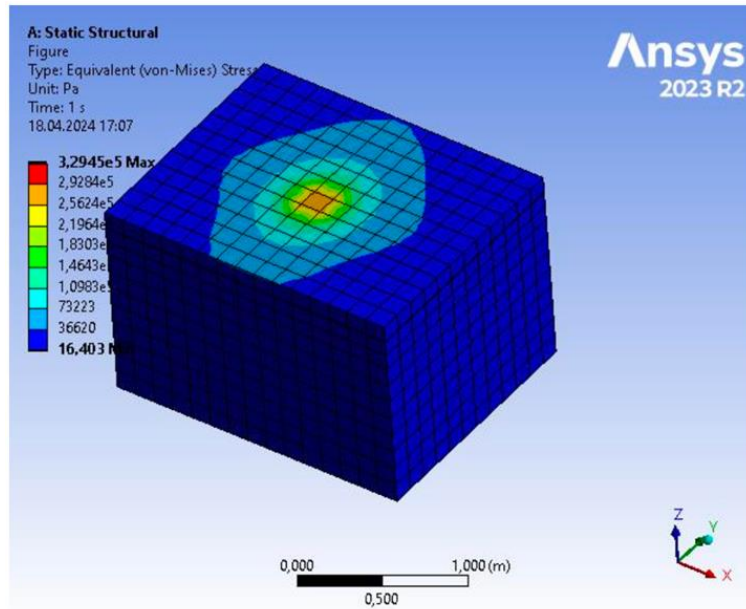


**Figure 56** Stress analysis of the hexagonal geogrid (PP) under 110 mm asphalt.

Third modeling, the hexagonal geogrid is located between the base course and subgrade.

**Table 20** Table of materials and properties of the hexagonal geogrid under base course.

Material	Subgrade	Base Course	Asphalt
<b>Thickness</b>	1000 mm	200 mm	110 mm
<b>Density</b>	2400 kg/m <sup>3</sup>	2000 kg/m <sup>3</sup>	1600 kg/m <sup>3</sup>
<b>Poisson's Ratio</b>	0.40	0.30	0.35
<b>Young's Modulus</b>	10 MPa	100 MPa	2500 MPa
<b>Constitutive Model</b>	Linear Elastic	Linear Elastic	Linear Elastic

**Table 21** Table of materials and geogrid properties of the hexagon geogrid under base course.

Material - Geogrid	Polypropylene
<b>Thickness</b>	4 mm
<b>Density</b>	904 kg/m <sup>3</sup>
<b>Poisson's Ratio</b>	0.42
<b>Young's Modulus</b>	1.325 GPa

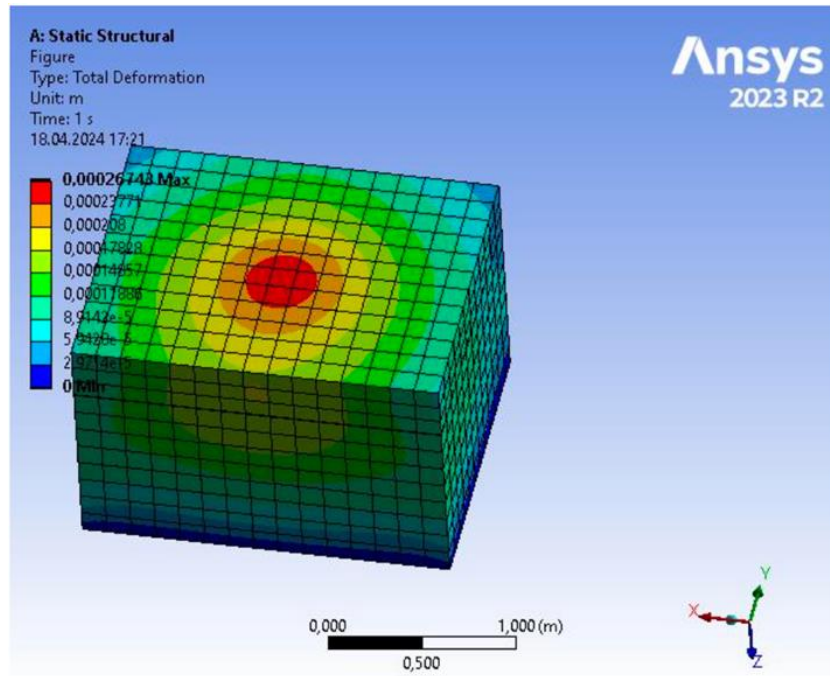


**Figure 57** Total deformation analysis of the hexagon geogrid (PP) under base course.

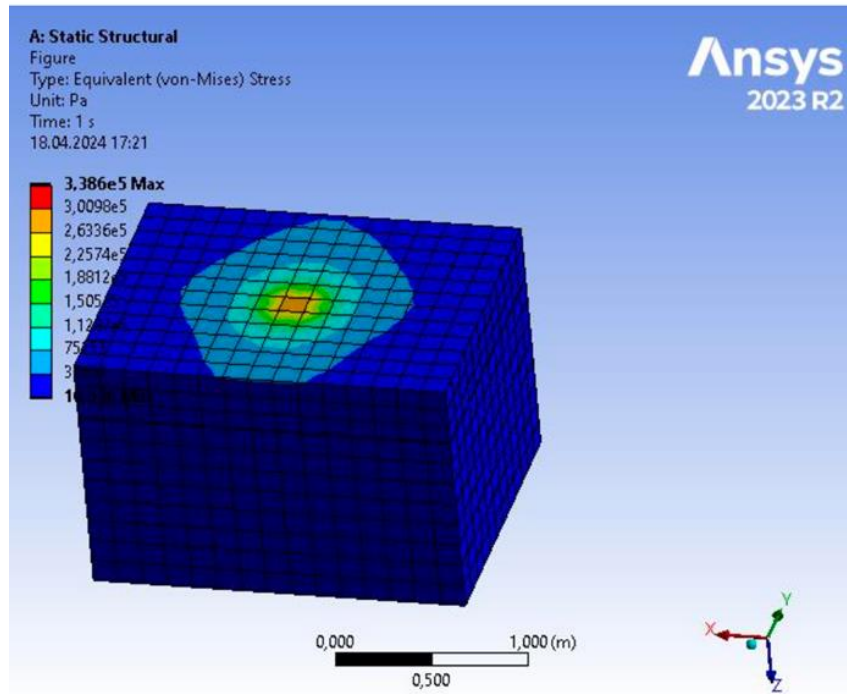


**Figure 58** Stress analysis of the hexagonal geogrid (PP) under base course.

Fourth modeling, there is a 100 mm subgrade on the hexagonal geogrid and 900 mm subgrade below it.

**Table 22** Table of materials and properties of the hexagonal geogrid under 100 mm subgrade.

Material	Bottom Subgrade	Top Subgrade	Base Course	Asphalt
<b>Thickness</b>	900 mm	100 mm	200 mm	110 mm
<b>Density</b>	2400 kg/m <sup>3</sup>	2400 kg/m <sup>3</sup>	2000 kg/m <sup>3</sup>	1600 kg/m <sup>3</sup>
<b>Poisson's Ratio</b>	0.40	0.40	0.30	0.35
<b>Young's Modulus</b>	10 MPa	10 MPa	100 MPa	2500 MPa
<b>Constitutive Model</b>	Linear Elastic	Linear Elastic	Linear Elastic	Linear Elastic

**Table 23** Table of materials and geogrid properties of the hexagonal geogrid under 100 mm subgrade.

Material - Geogrid	Polypropylene
<b>Thickness</b>	4 mm
<b>Density</b>	904 kg/m <sup>3</sup>
<b>Poisson's Ratio</b>	0.42
<b>Young's Modulus</b>	1.325 GPa

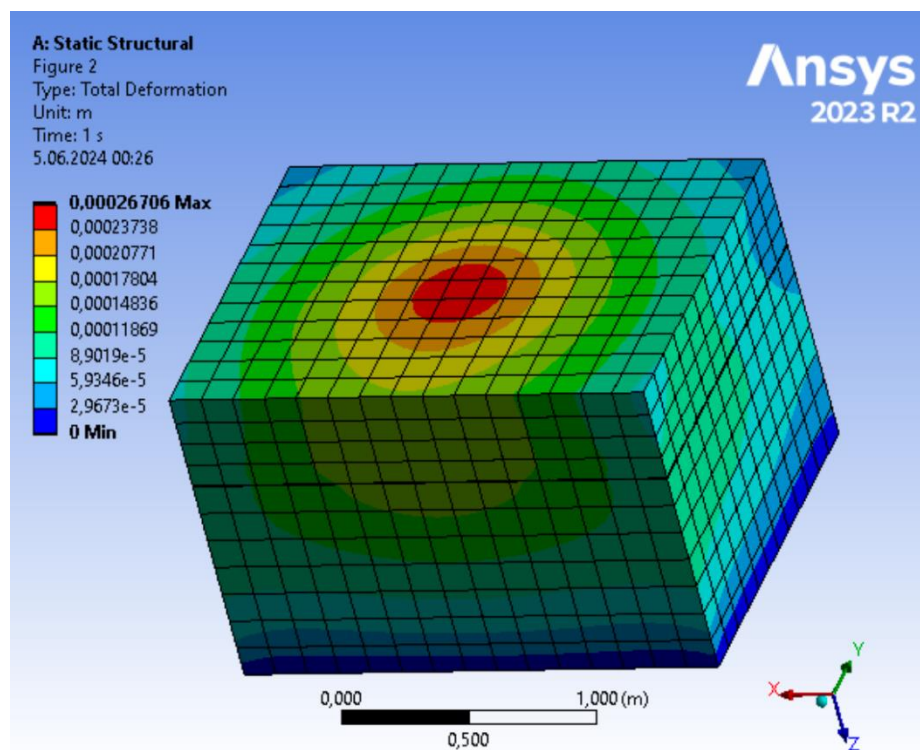


**Figure 59** Total deformation analysis of the hexagonal geogrid (PP) under 100 mm subgrade.

Fifth modeling, there is a 200 mm subgrade on the hexagonal geogrid and an 800 mm subgrade below it.

**Table 24** Table of materials and properties of the hexagonal geogrid under 200 mm subgrade.

Material	Bottom Subgrade	Top Subgrade	Base Course	Asphalt
<b>Thickness</b>	800 mm	200 mm	200 mm	110 mm
<b>Density</b>	2400 kg/m <sup>3</sup>	2400 kg/m <sup>3</sup>	2000 kg/m <sup>3</sup>	1600 kg/m <sup>3</sup>
<b>Poisson's Ratio</b>	0.40	0.40	0.30	0.35
<b>Young's Modulus</b>	10 MPa	10 MPa	100 MPa	2500 MPa
<b>Constitutive Model</b>	Linear Elastic	Linear Elastic	Linear Elastic	Linear Elastic

**Table 25** Table of materials and geogrid properties of the hexagonal geogrid under 200 mm subgrade.

Material - Geogrid	Polypropylene
<b>Thickness</b>	4 mm
<b>Density</b>	904 kg/m <sup>3</sup>
<b>Poisson's Ratio</b>	0.42
<b>Young's Modulus</b>	1.325 GPa

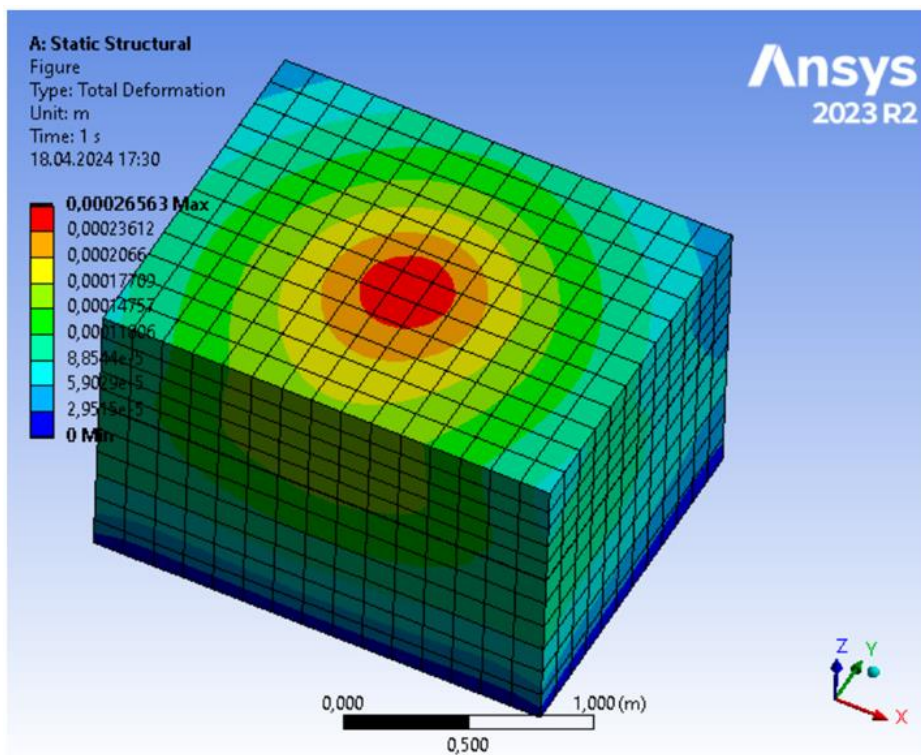


**Figure 60** Total deformation analysis of the hexagonal geogrid (PP) under 200 mm subgrade.

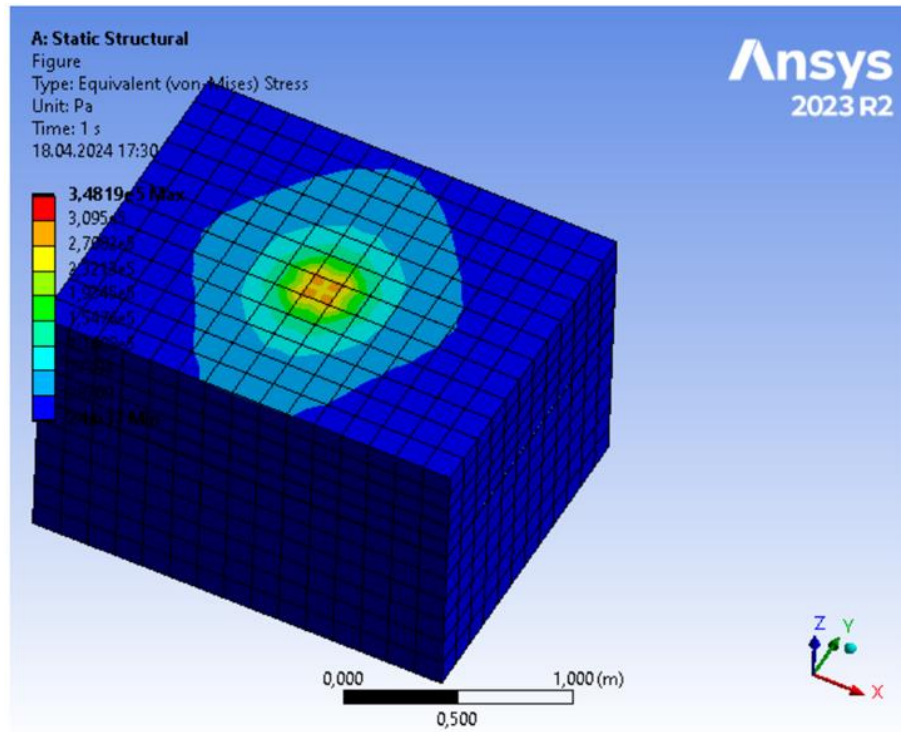


**Figure 61** Stress analysis of the hexagonal geogrid (PP) under 200 mm subgrade.

When comparing our latest tests based on changes in geogrid positions to our initial tests, it was found that the model with the least deformation is the one incorporating hexagonal geogrid with PP content. This model is positioned between a 60 mm layer of asphalt and a 50 mm layer of asphalt.

### 3.10 Model Analysis without Geogrid with Increased Asphalt

This model, which had the least deformation, suffered 5% less deformation than our model non-geogrid.

Because of the rate which received necessitated an increase in our asphalt by 7.73% (to 118.5 mm) and analysis without the addition of geogrid was also deemed necessary.

The table showing the information and results of the experiments conducted according to these features is as follows.

**Table 26** Table of materials and properties of the non-geogrid 118.5 mm asphalt model.

Material	Subgrade	Base Course	Asphalt
<b>Thickness</b>	1000 mm	200 mm	118.5 mm
<b>Density</b>	2400 kg/m <sup>3</sup>	2000 kg/m <sup>3</sup>	1600 kg/m <sup>3</sup>
<b>Poisson's Ratio</b>	0.40	0.30	0.35
<b>Young's Modulus</b>	10 MPa	100 MPa	2500 MPa
<b>Constitutive Model</b>	Linear Elastic	Linear Elastic	Linear Elastic

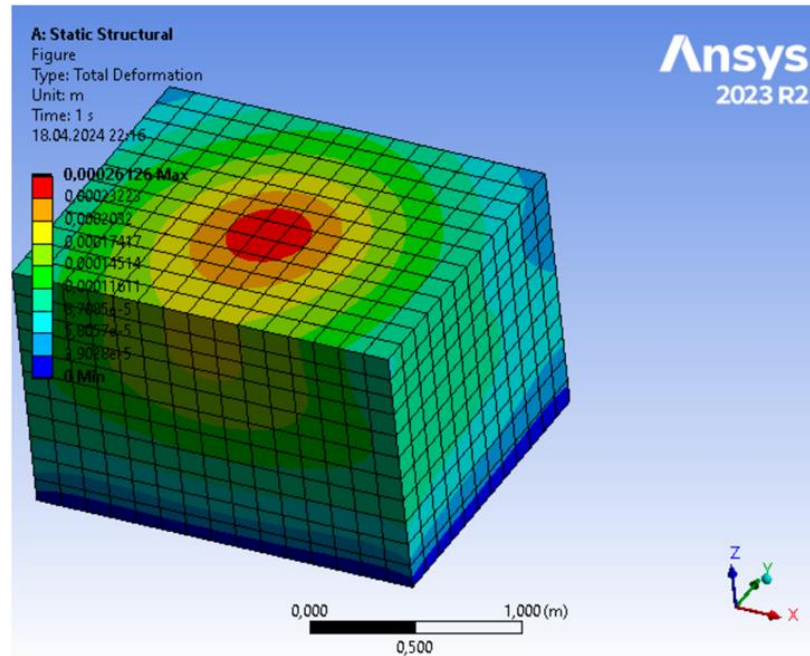


**Figure 62** Total deformation analysis of the non-geogrid model with 118.5 mm asphalt.

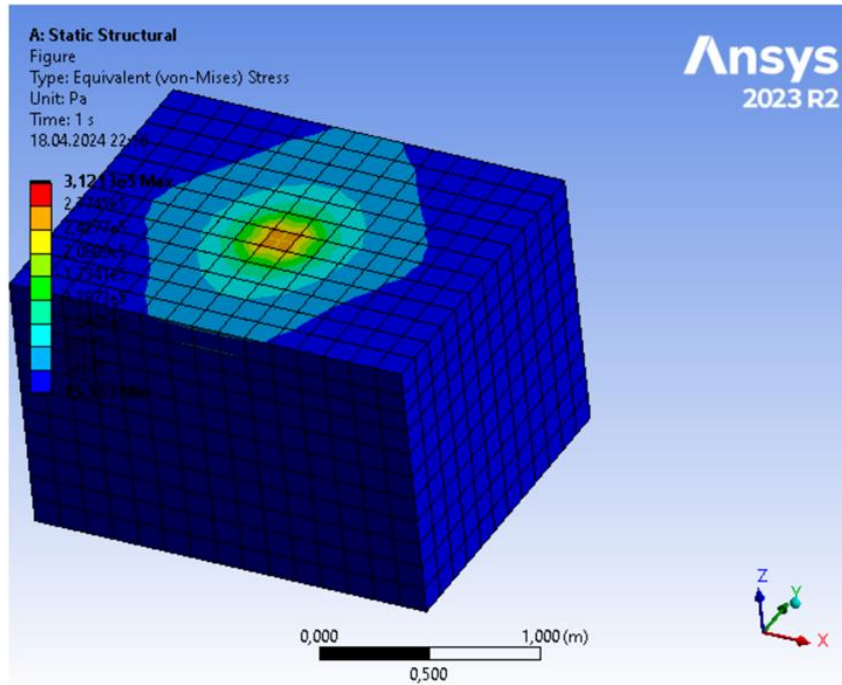


**Figure 63** Stress analysis of the non-geogrid model with 118.5 mm asphalt.

## 4. Analysis Results and Comparisons

### 4.1 Deformation of PET Geogrid Under 60 mm Asphalt

**Table 27** Deformation of PET and 3 different designed geogrids under 60 mm Asphalt.

Model	Max. Total Deformation
<b>Rectangular Geogrid - PET</b>	0,26471
<b>Rhombus Geogrid - PET</b>	0,25937
<b>Hexagonal Geogrid - PET</b>	0,25163
<b>Rectangular Geogrid - RPET</b>	0,26832
<b>Rhombus Geogrid - RPET</b>	0,26412
<b>Hexagonal Geogrid - RPET</b>	0,25816

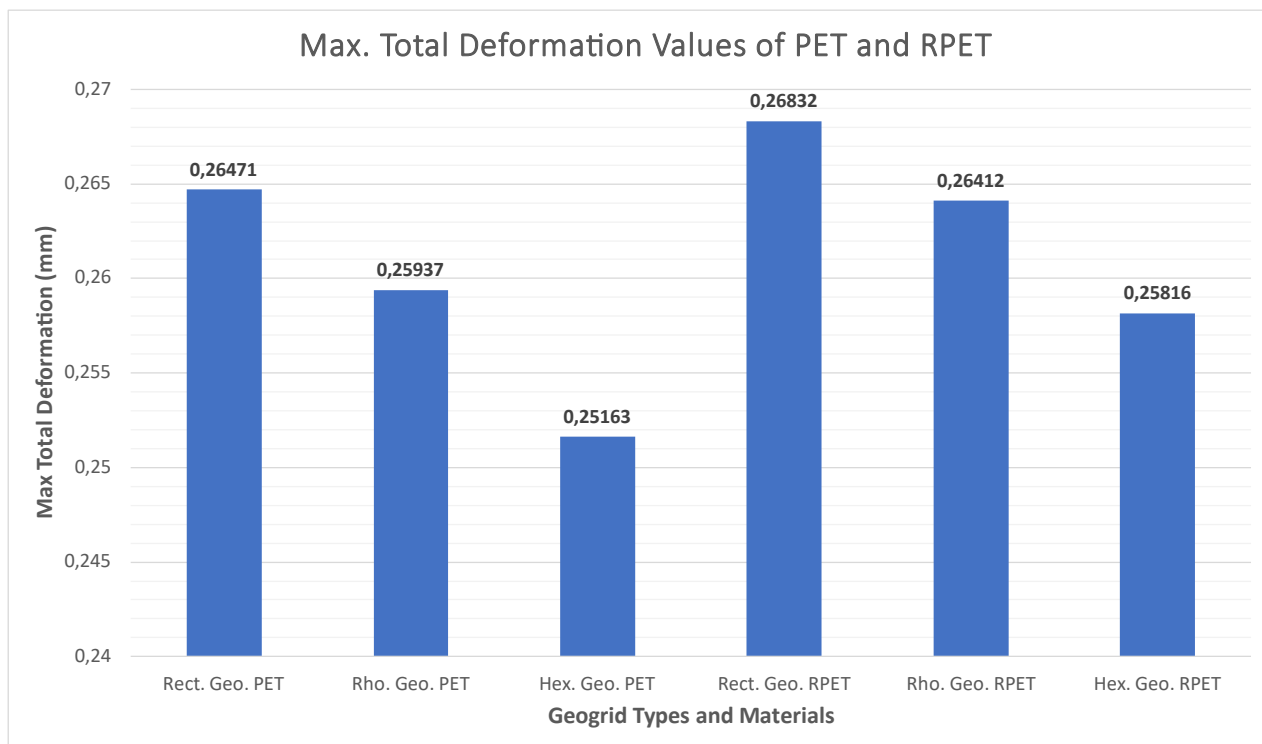


**Figure 64** Graph of Deformation of PET and 3 different designed geogrids under 60 mm Asphalt.

The data in this table and graph show the maximum total deformations of geogrids in three different shapes designed with PET material. These values show how much the geogrid deforms against the applied force. According to the graph, the geogrid with the lowest deformation is hexagonal (0.25163). This means that hexagonal geogrid is more durable and stronger than rectangular and rhombic geogrids. The geogrid with the highest deformation is rectangular (0.26471). This means that the rectangular geogrid is weaker and more flexible than the other two shapes.

When the deformation results of geogrids made with recycled materials are examined, higher deformation values were obtained compared to virgin materials. This is because when plastics are recycled, their quality decreases and therefore the deformation value increases. According to the results of increases in deformation values, hexagonal geogrid again showed the best performance.

The data in the table shows that the shape and material of the geogrid is an important factor affecting the performance of the material.

## 4.2 Deformation of PA6 Geogrid Under 60 mm Asphalt

**Table 28** Deformation of PA6 and 3 different designed geogrids under 60 mm Asphalt.

Model	Max. Total Deformation
<b>Rectangular Geogrid - PA6</b>	0,26507
<b>Rhombus Geogrid - PA6</b>	0,26222
<b>Hexagonal Geogrid - PA6</b>	0,25558
<b>Rectangular Geogrid - RPA6</b>	0,27155
<b>Rhombus Geogrid - RPA6</b>	0,26887
<b>Hexagonal Geogrid - RPA6</b>	0,26596

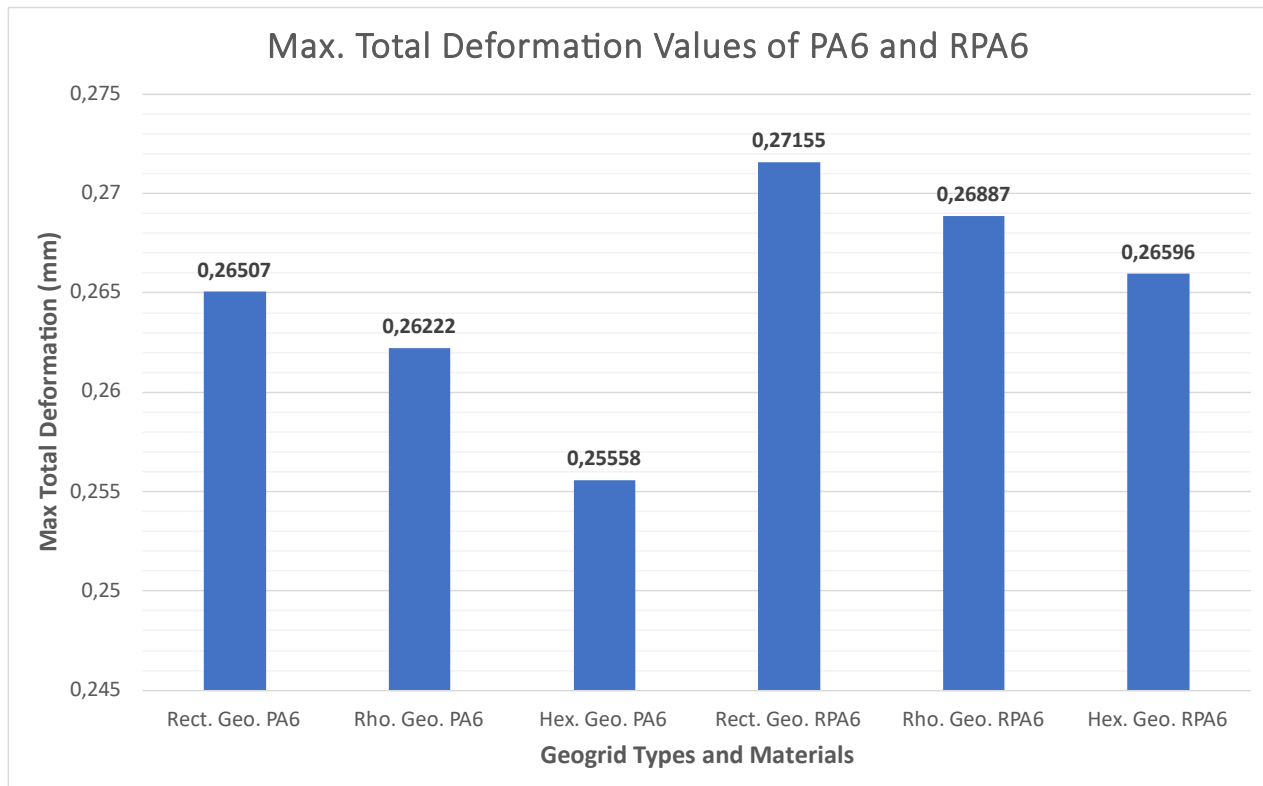


**Figure 65** Graph of Deformation of PA6 and 3 different designed geogrids under 60 mm Asphalt.

The data in the table and graph show the maximum total deformations of geogrids of three different geometries made of polyamide material. The maximum total deformations of geogrids in rectangular, rhombic and hexagonal geometries were measured as 0.26507, 0.26222 and 0.25558, respectively. Accordingly, the geogrid with the lowest deformation is hexagonal. This means that hexagonal geogrid is more durable and stronger than rectangular and rhombus geogrids. The geogrid with the highest deformation is rectangular, meaning it is less durable and flexible than the other two shapes. When looking at the analyzes of geogrids made with recycled materials, an increase in deformation was observed.

### 4.3 Deformation of PP Geogrid Under 60 mm Asphalt

**Table 29** Deformation of PP and 3 different designed geogrids under 60 mm Asphalt.

Model	Max. Total Deformation
<b>Rectangular Geogrid - PP</b>	0,27154
<b>Rhombus Geogrid - PP</b>	0,2677
<b>Hexagonal Geogrid - PP</b>	0,26363
<b>Rectangular Geogrid - RPP</b>	0,27272
<b>Rhombus Geogrid - RPP</b>	0,26947
<b>Hexagonal Geogrid - RPP</b>	0,26629

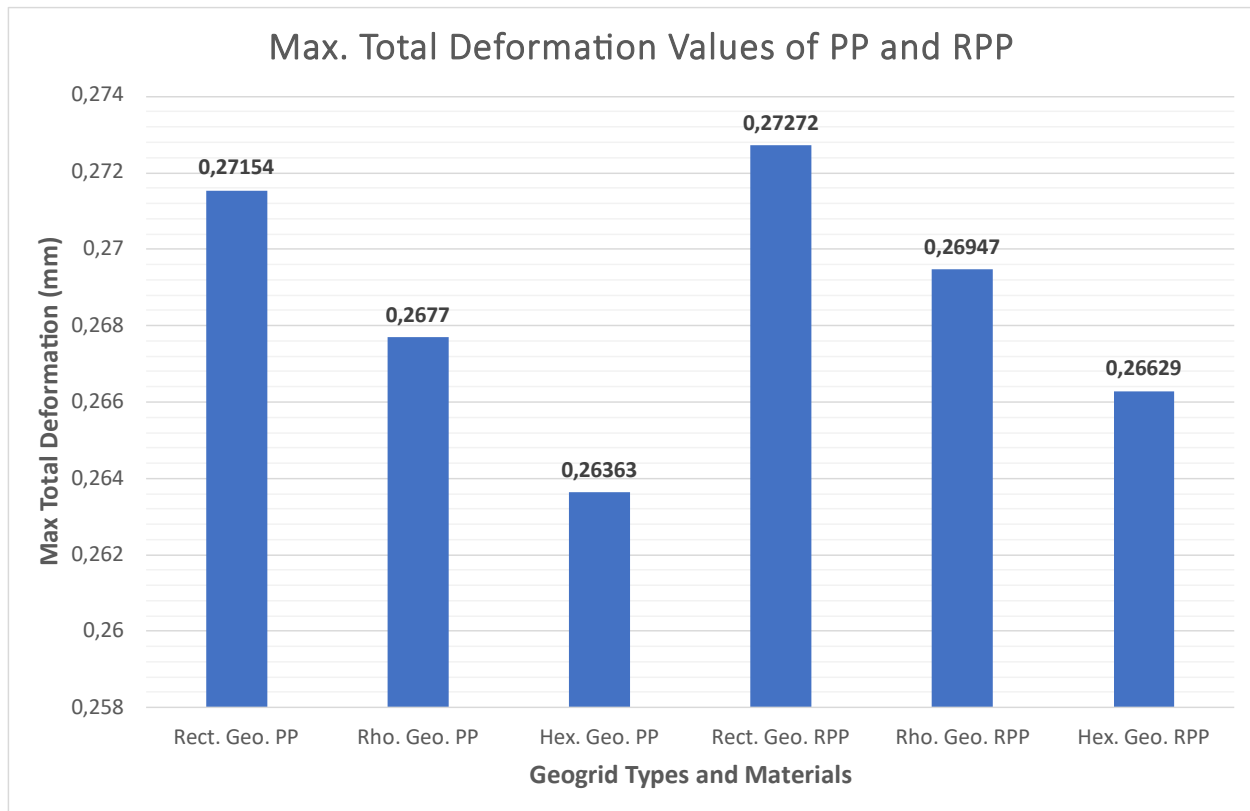


**Figure 66** Graph of Deformation of PP and 3 different designed geogrids under 60 mm Asphalt.

When the table and graph are considered, polypropylene emerged as the chosen material for the designs. The maximum total deformation values of three different geogrid models (Rectangle, Rhombus, and Hexagon) are also observed. The rectangular geogrid model has the highest deformation value (0.27154). This shows that this model is more deformed than the others. The deformation value of the rhombus geogrid model is slightly lower (0.2677).

Hexagonal Geogrid model is the model with the lowest deformation value (0.26363).

This shows that this model is less deformed than others.

An increase in deformation values was observed due to the loss of quality in recycled materials. This shows that when recycled material is used, the durability will decrease compared to virgin material, and hexagonal geogrid gives the best results.

#### 4.4 Collection and Comparison of Data

**Table 30** Results of deformations obtained with three different designs and material assignments.

<b>Model</b>	<b>Max. Total Deformation</b>
<b>Hexagonal PET</b>	0,25163
<b>Hexagonal PA6</b>	0,25558
<b>Hexagonal RPET</b>	0,25816
<b>Rhombus PET</b>	0,25937
<b>Rhombus PA6</b>	0,26222
<b>Hexagonal PP</b>	0,26363
<b>Rhombus RPET</b>	0,26412
<b>Rectangular PET</b>	0,26471
<b>Rectangular PA6</b>	0,26507
<b>Hexagonal RPA6</b>	0,26596
<b>Hexagonal RPP</b>	0,26629
<b>Rhombus PP</b>	0,2677
<b>Rectangular RPET</b>	0,26832
<b>Rhombus RPA6</b>	0,26887
<b>Rhombus RPP</b>	0,26947
<b>Rectangular PP</b>	0,27154
<b>Rectangular RPA6</b>	0,27155
<b>Rectangular RPP</b>	0,27272
<b>Normal Model</b>	0,27428

The graph of the results of the deformations obtained with three different designs and material assignments, in order from least to most, is as follows.

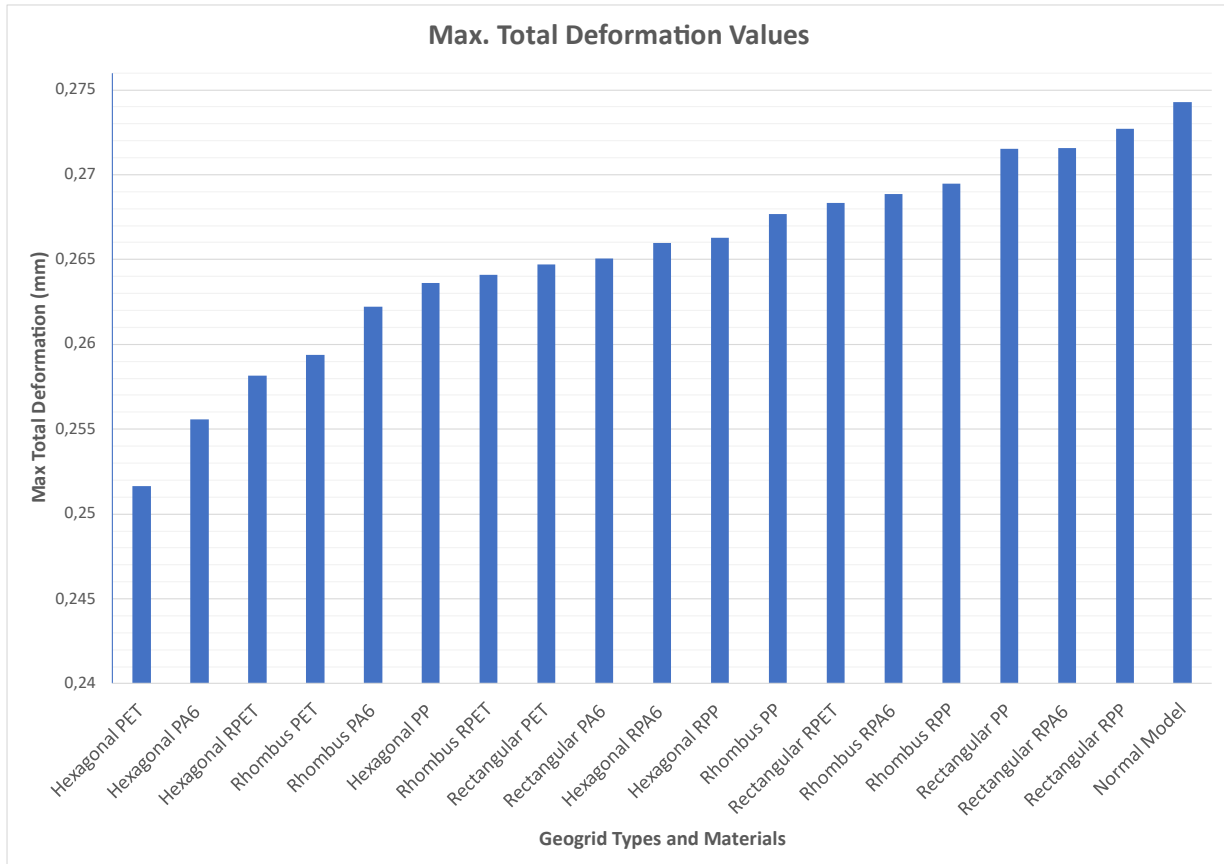


**Figure 67** Graph in which deformations are listed from least to most.

When the data obtained from the above studies with three materials and three designs are compiled, the normal model has the highest deformation value (0.27428). This shows that this model may be more deformed than others.

Among the Rectangular Geogrid models, the geogrid made of polypropylene material (0.27154) has the highest deformation value, while those made of polyamide (0.26507) and PET (0.26471) materials have lower values.

Among the Rhombus Geogrid models, the one with the highest deformation value is the one made of PP material (0.2677), and the lowest value is the one made of PET material (0.25937). This means PET is more durable and durable than PP and PA6.

The results are not much different between Hexagonal Geogrid models, and the model made of PET material (0.25163) has the lowest deformation values.

Among the recycled materials, the lowest value belongs to hexagonal RPET. This indicates that it is the most resistant material to deformation among recycled models. The highest deformation value belongs to Rectangular PP after the Normal Model.

As a result, the lowest deformation value generally indicates better performance. In this case, the Hexagonal Geogrid model with PP material performed better than the others.

#### 4.5 Collection and Comparison of Max. Equivalent Stress Data

**Table 31** Results of stresses obtained with three different designs and material assignments.

Model	Max. Equivalent Stress
Rectangular Geogrid - PA6	3,84E+05
Rectangular Geogrid - PET	4,09E+05
Rectangular Geogrid - PP	2,95E+05
Rhombus Geogrid - PA6	3,79E+05
Rhombus Geogrid - PET	4,91E+05
Rhombus Geogrid - PP	2,93E+05
Hexagonal Geogrid - PA6	3,21E+05
Hexagonal Geogrid - PET	3,99E+05
Hexagonal Geogrid - PP	2,89E+05

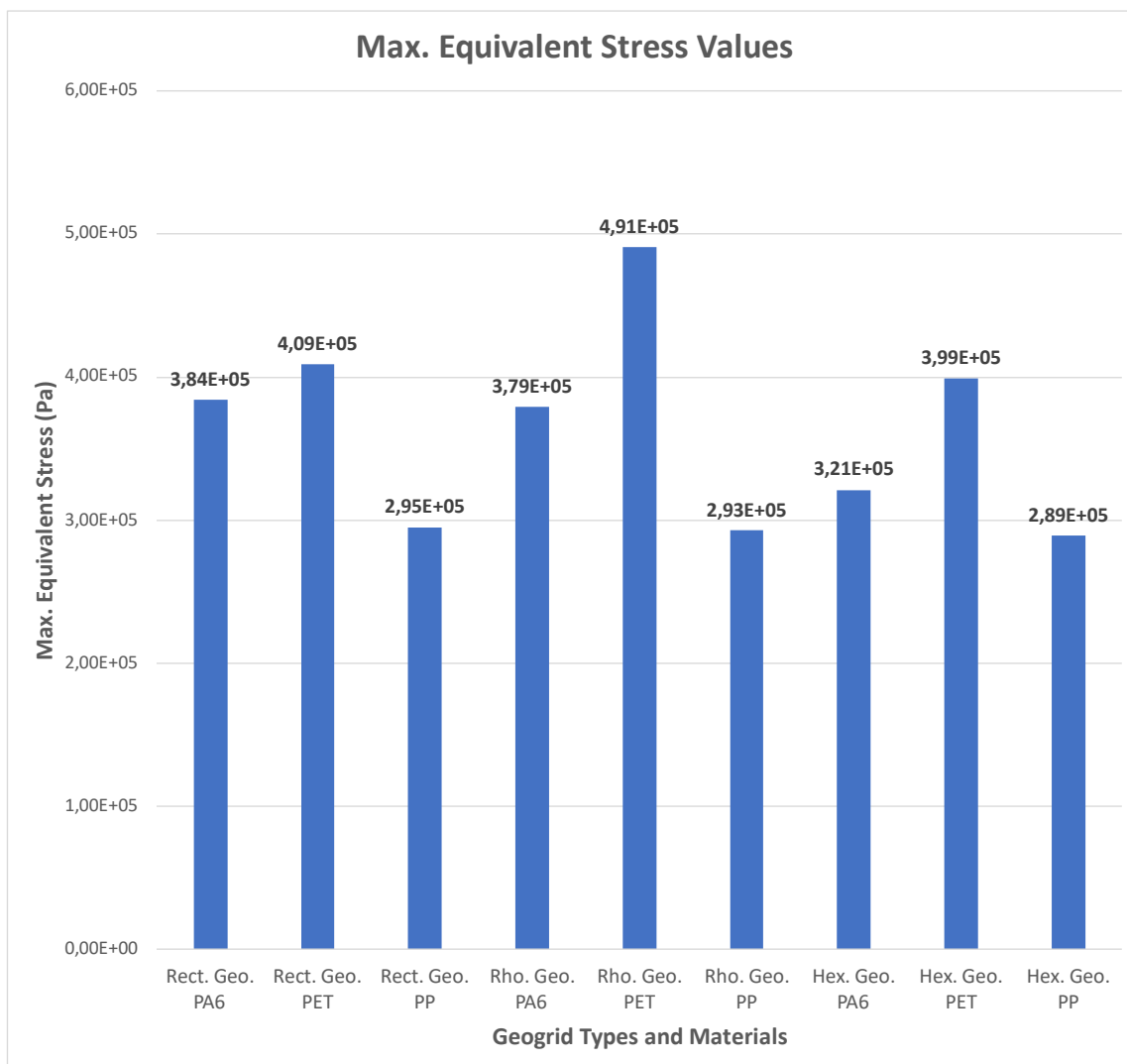


**Figure 68** Graph of stresses obtained with three different designs and material assignments.

The material with the lowest equivalent stress value will undergo less deformation, meaning it will be more durable. For this reason, when choosing a material, the most logical option can be Hexagonal Geogrid - PP with the lowest max equivalent stress value of 2.89E+05.

- Rectangular Geogrid, PP (2.95E+05) has the lowest max equivalent stress value, while PET (4.09E+05) has the largest stress value.
- Rhombus Geogrid, PP (2.93E+05) has the lowest max equivalent stress value, while PET (4.91E+05) has the highest stress value.
- Hexagonal Geogrid, PP (2.89E+05) has the lowest max equivalent stress value, while PET (3.99E+05) has the largest max equivalent stress value.

In general, PP materials have the lowest max equivalent stress values, while PET materials have the highest max equivalent stress values. This indicates that PP materials can have a lower deformation rate and therefore be more durable.

## 4.6 Geogrid Type and Material Selection

Table 32 Compare to find the best option.

	Max. Equivalent Stress	Percentage Diff. with Best Option		Max. Total Deformation (mm)	Percentage Diff. with Best Option
Rhombus PET	4,91E+05	69,93%	Rectangular PP	0,27154	7,91%
Rectangular PET	4,09E+05	41,71%	Rhombus PP	0,2677	6,39%
Hexagon PET	3,99E+05	38,16%	Rectangular PA6	0,26507	5,34%
Rectangular PA6	3,84E+05	33,01%	Rectangular PET	0,26471	5,20%
Rhombus PA6	3,79E+05	31,21%	Hexagon PP	0,26363	4,77%
Hexagon PA6	3,21E+05	11,16%	Rhombus PA6	0,26222	4,21%
Rectangular PP	2,95E+05	2,32%	Rhombus PET	0,25937	3,08%
Rhombus PP	2,93E+05	1,65%	Hexagon PA6	0,25558	1,57%
Hexagon PP	2,89E+05		Hexagon PET	0,25163	

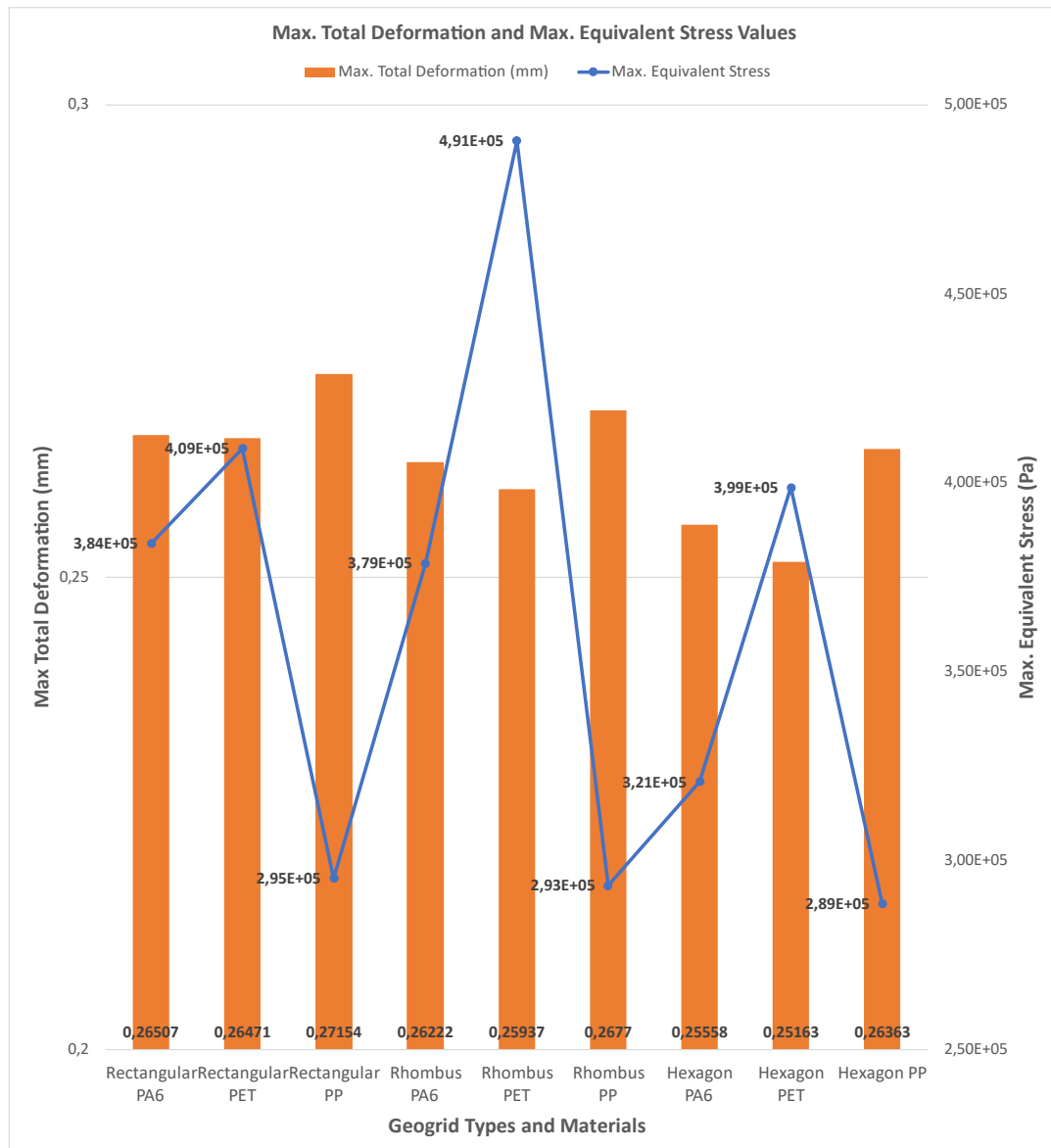


Figure 69 Stress and deformation comparison.

The graph above depicts the results of the combinations of geogrid shape and geogrid material that have been conducted thus far. While the orange columns represent deformations, the blue lines represent stress results. These values have been stated numerically in the two tables just below the graph.

As mentioned at the beginning of our report, in all analyses, the geogrid was positioned between the asphalt layer and 60 mm below the ground. Now, a geogrid type - geogrid material combination will be selected from these results, and the position of the selected combination will be altered in our report.

When this combination is selected, preference will be given to the one exhibiting the lowest deformation and stress levels. The reason for this is low stress means high durability, and low deformation value means low degradation value in the material.

After listing our values from low to high as in the tables, comparisons were made by looking at the combinations with the lowest values. Since hexagonal PET and hexagonal PP values were at the lowest levels in deformation and stress, respectively, they were compared first.

While Hexagon PET has 4.77% lower deformation than Hexagon PP, also it has a 38.16% higher stress level. That's why Hexagon PP should be chosen.

When considering a combination with both low stress levels and low deformation, hexagonal PA6 also draws our attention. Because of this, comparisons with Hexagon PP were wanted.

While Hexagon PA6 has a deformation value of 3.15% less than Hexagon PP, Hexagon PA6 has 11.16% more stress than Hexagon PP. As a result of this comparison, it is obvious that the Hexagon PP duo is a better combination.

There are no other combinations to choose from. Therefore, it has been demonstrated that our optimal combination is hexagonal PP.

## 4.7 Determining Location for Hexagonal PP Geogrid

Comparison of the deformations of 110 mm asphalt in different positions and geogrid made of hexagonal designed PP material, which was also modeled, is given in the table below. Additionally, the deformation value of asphalt without geogrid is also given.

**Table 33** Deformations of Hexagon Polypropylene Geogrid in various locations.

Model	Max. Total Deformation
<b>Non-Geogrid - 110 mm Asphalt</b>	0,27428
<b>Hexagonal Geogrid - PP - Under 110 mm Asphalt</b>	0,27317
<b>Hexagonal Geogrid - PP - Under Base Course</b>	0,26743
<b>Hexagonal Geogrid - PP - Under 100 mm Subgrade</b>	0,26707
<b>Hexagonal Geogrid - PP - Under 30 mm Asphalt</b>	0,26695
<b>Hexagonal Geogrid - PP - Under 200 mm Subgrade</b>	0,26563
<b>Hexagonal Geogrid - PP - Under 60 mm Asphalt</b>	0,26363

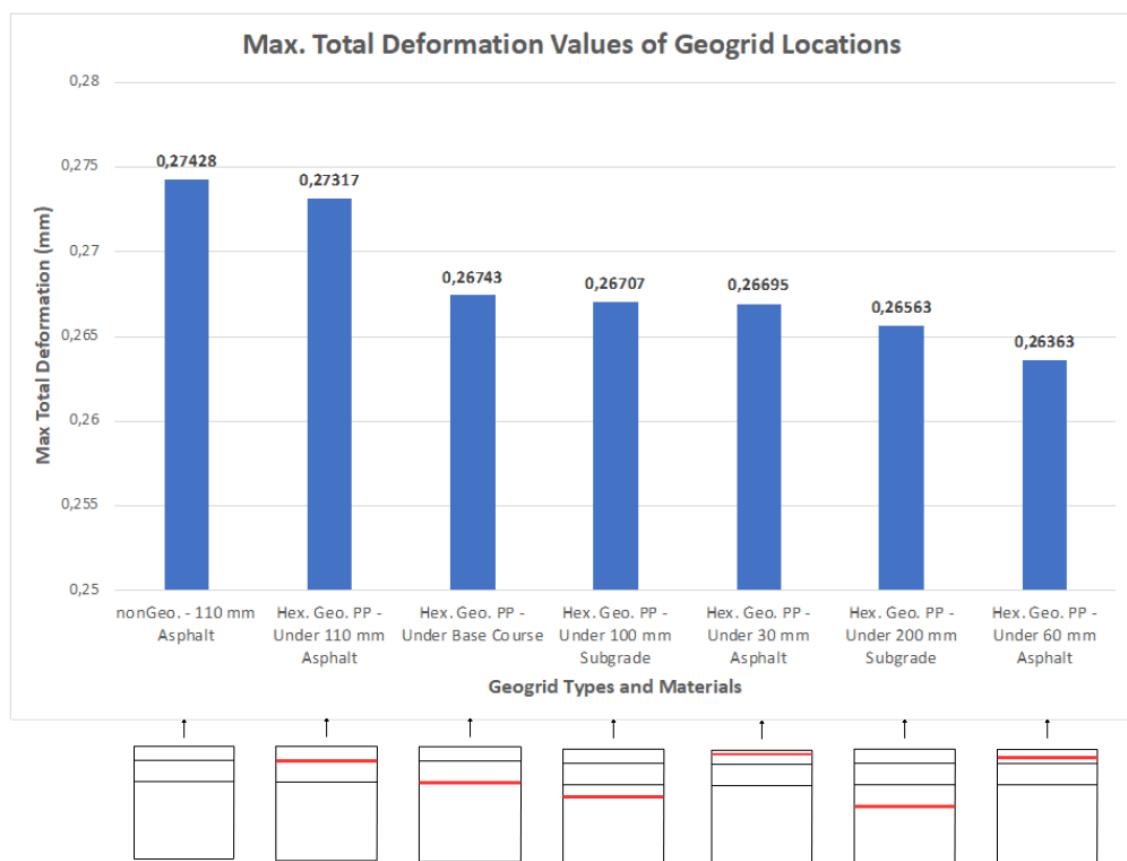


**Figure 70** Graph of deformations of hexagon PP geogrid in various locations.

As a result of the above studies, since the best geogrid design according to the maximum total deformation values is hexagonal and the best material is PP, the Hexagonal Geogrid (PP) model was chosen to determine the best position of the geogrid in the asphalt.

The graph shows the maximum total deformation values of the Hexagon Geogrid (PP) model used in different locations (under asphalt, at different heights within asphalt, under foundation, etc.). In addition, the maximum total deformation value of the asphalt model non-geogrid with 110 mm asphalt thickness is also shown. This data allows us to compare how durable the Hexagon Geogrid (PP) model is in different locations.

Non-geogrid - 110 mm asphalt case has the highest deformation value (0.27428) among all cases. This shows that an asphalt layer without geogrid can significantly reduce deformation when geogrid is used.

The lowest deformation value indicates better performance. When the situations with geogrid are examined, the hexagonal geogrid with PP model showed the best performance under 60 mm asphalt.

#### **4.8 Effect of Geogrid Reinforcement on Service Life of Road**

One of the biggest problems is the formation of pavement rutting on asphalt after long-term use. In this experiment, the asphalt was reinforced with geogrid to prevent the formation of pavement rutting. The equation below will be used to calculate how geogrid reinforcement changes the service life of asphalt [39].

$$\text{Young's Modulus} = E$$

$$E = \frac{\text{Stress}}{\text{Strain}}$$

$$N_r = 1,365 \times 10^{-9} \left[ \frac{1}{\varepsilon_c} \right]^{4.477}$$

Where,

$N_r$  = Number of load repetitions to limit rutting

$\varepsilon_c$  = Vertical compressive strains at the top of the subgrade layer

In this section, the calculations of the best pair, hexagonal PP, the rectangular PET model with the closest deformation to hexagonal PP, and the model non-geogrid will be made.

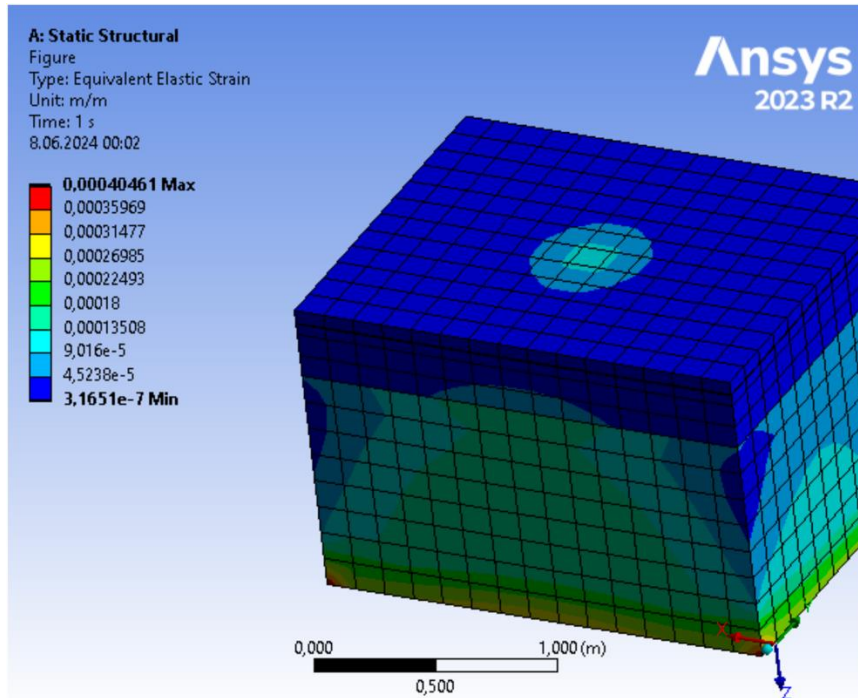


**Figure 71** Strain analysis of the hexagonal geogrid (PP)

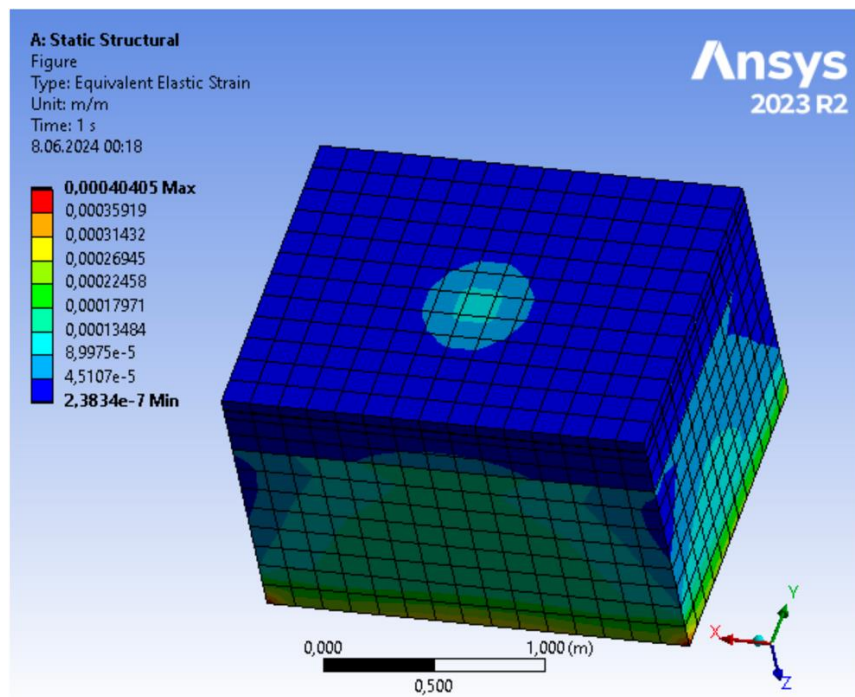


**Figure 72** Strain analysis of the rectangular geogrid (PET)

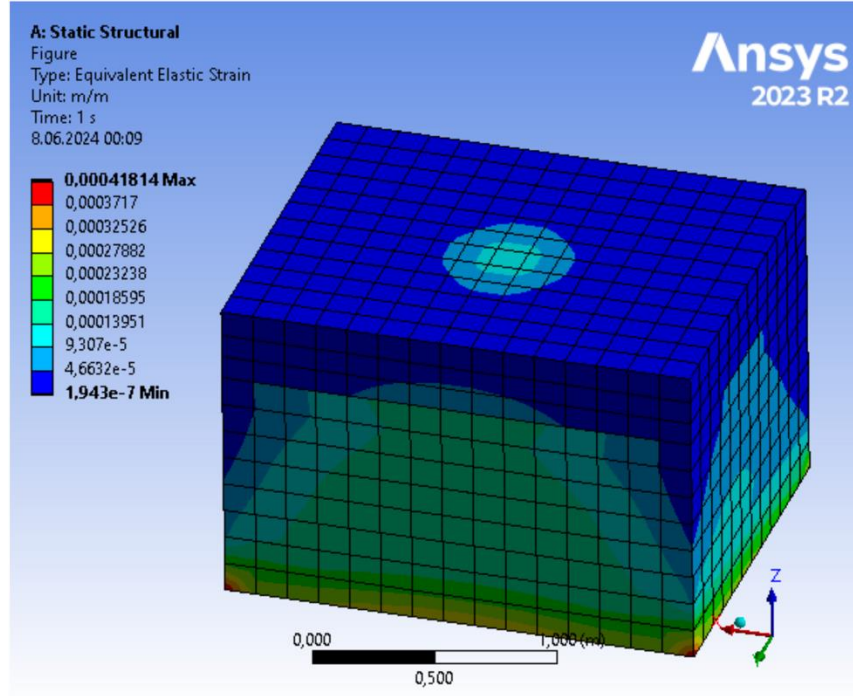


**Figure 73** Strain analysis of the model non-geogrid

According to the analysis made with ANSYS, the strain values are;

0.00013511 for hexagonal geogrid (PP)

0.00013484 for rectangular geogrid (PET)

0.00013951 for the model non-geogrid

For hexagonal PP,

$$\varepsilon_C = \text{Strain} = 0.00013511$$

$$N_{r_1} = 1,365 \times 10^{-9} \left[ \frac{1}{\varepsilon_C} \right]^{4.477} = 1,365 \times 10^{-9} \left[ \frac{1}{0.00013511} \right]^{4.477} \cong 287.107.634,38$$

For non-geogrid model,

$$\varepsilon_C = \text{Strain} = 0.00013951$$

$$N_{r_2} = 1,365 \times 10^{-9} \left[ \frac{1}{\varepsilon_C} \right]^{4.477} = 1,365 \times 10^{-9} \left[ \frac{1}{0.00013951} \right]^{4.477} \cong 248.733.654,04$$

In addition to these two analyses, a calculation was also requested for the model with the closest deformation area to the hexagonal PP model. The rectangular PET was chosen for this purpose.

For rectangular PET,

$$\varepsilon_C = \text{Strain} = 0.00013484$$

$$N_{r_3} = 1,365 \times 10^{-9} \left[ \frac{1}{\varepsilon_C} \right]^{4.477} = 1,365 \times 10^{-9} \left[ \frac{1}{0.00013484} \right]^{4.477} \cong 289.690.421,17$$

If all of these three models are compared,

$$N_{r_3} = 289.690 \times 10^3 > N_{r_1} = 287.107 \times 10^3 > N_{r_2} = 248.734 \times 10^3$$

Also;

$$\frac{N_{r_1}}{N_{r_2}} = \frac{287.107.634,38}{248.733.654,04} = 1,154$$

$$\frac{N_{r_3}}{N_{r_1}} = \frac{289.690.421,17}{287.107.634,38} = 1,008$$

$$\frac{N_{r_3}}{N_{r_2}} = \frac{289.690.421,17}{248.733.654,04} = 1,164$$

With this comparison made, it is observed that the service life of the;

- Hexagon geogrid, made of PP, is 15% longer than that of the asphalt model non-geogrid.
- Rectangular geogrid, made of PET, is 0,8% longer than that of the hexagon geogrid which made of PP
- Rectangular geogrid, made of PET, is 16% longer than that of the asphalt model non-geogrid.

As a result of these calculations, it was seen that rectangular PET was in a slightly better condition compared to hexagonal PP in terms of service life. However, it has been proven in our experiments so far, that hexagonal PP is a much better material in both deformation and stress analyses. It is also known that hexagonal PP is in a better condition in terms of water absorption rate on asphalt surfaces.

It is also very significant to pay attention to water absorption rates on asphalt surfaces and to choose materials in this regard. Low water absorption rate; It ensures the long life of the material in humid environments, rainy situations, and exposure to water. When looking at PET and PP, PP is more than 10 times more hydrophobic than PET. This shows that PP is a more durable option. PP continues to maintain its mechanical properties for longer periods of time.

## 5. Cost Analysis

**Table 34** 110-118,5 mm non-geogrid and Hexagonal Geogrid PP Under 60 mm Asphalt deformation values.

Model	Max. Total Deformation
<b>non-Geogrid - 110 mm Asphalt</b>	0,27428
<b>Hexagonal Geogrid - PP - Under 60 mm Asphalt</b>	0,26363
<b>non-Geogrid - 118,5 mm Asphalt</b>	0,26126

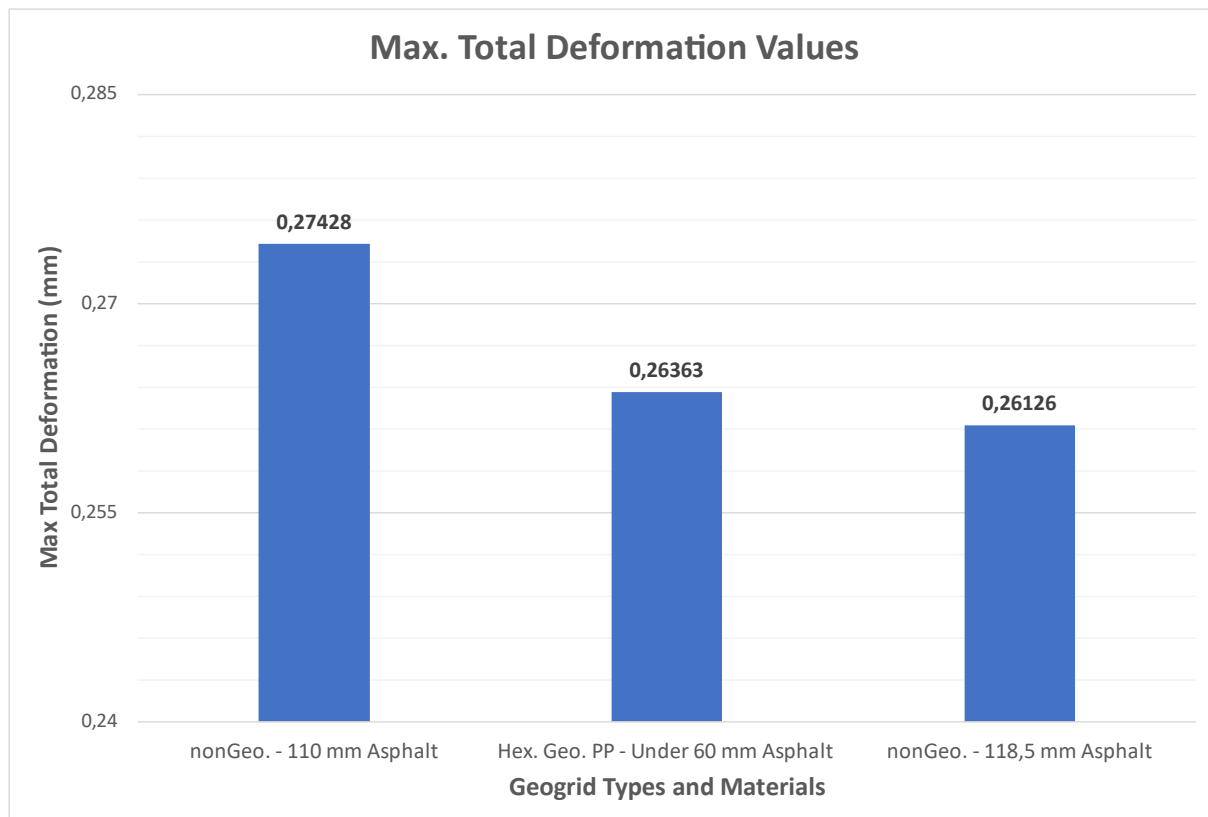


**Figure 74** Graph of 110 mm non-geogrid, 118,5 mm non-geogrid and Hexagonal Geogrid - PP - Under 60 mm Asphalt deformation values.

In our experimental setup, the thickness of the asphalt was initially determined to be 110 mm in the design non-geogrid geogrid [24].

In all our analyzes so far, three different designs were used. These different designs are hexagonal, rectangular, and rhombus along with PET, PP, PA6, and recycled versions of these materials. As a result of all these experiments, the most suitable geogrid type-geogrid material pair was Hexagonal Geogrid – PP.

While the deformation of the mechanism non-geogrid and with 110 mm asphalt thickness was 0.27428 mm, the deformation of the mechanism with hexagonal geogrid and PP material was 0.26363 mm.

In Figure 72, since the geogrid shows its best performance under 60 mm asphalt, the deformation value at this point was found during the cost analysis. Then, by increasing the asphalt thickness of 110 mm non-geogrid asphalt, the deformation value (0.27428) was increased until it approached the value (0.26363).

From here, it was observed that by increasing the asphalt thickness from 110 mm to 118.5 mm, the same durability was achieved without using geogrid.

While concluding our analysis, an investigation into the cost benefit of using geogrid in real life was also desired. To investigate this, the achievement of the deformation of the hexagonal geogrid was desired, which has PP material, by increasing the asphalt height without using any geogrid.

As a result of our experiments, it was demonstrated that when the asphalt height is increased by 8.5 mm in our non-geogrid mechanism, it will be close to the deformation of hexagonal PP geogrid.

In our next section, a comparison will be made to determine whether it would be more appropriate to increase the asphalt thickness or to apply the hexagonal PP geogrid asphalt model without increasing the asphalt thickness.

Reinforcement of asphalt can be done by increasing the thickness of the asphalt pavement layer or by adding geogrid reinforcement. There is a cost difference between these methods. For this, a cost analysis must be carried out.

According to the stress and deformation analysis values obtained because of the analyses, polypropylene hexagonal geogrid was deemed suitable for our experiment. At this point, a cost analysis was made for reinforcement on asphalt with this geogrid type. While performing the cost analysis, asphalt reinforced with asphalt and asphalt with geogrid added

were compared. They both have the same deformation value. Based on this, a general cost analysis was made. While performing the cost analysis, the TL value was calculated with the current exchange rate of May 2024.

### **Asphalt tons (EXTRA)**

$$\text{Total Weight} = \text{Area} \times \text{Height} \times \text{Density}$$

$$\text{Total Weight} = (1.6m \times 2m) \times 0.0085m \times 1.6 \frac{T}{m^3}$$

$$\text{Total Weight} = 0.04352 \text{ Ton}$$

In the upper part, the asphalt tonnage required for the required thickness increase in asphalt is calculated. Asphalt is sold by the ton. Below, the cost of the extra amount of asphalt required is calculated based on the current exchange rate [40].

$$\text{Cost of Extra Asphalt} = 0.04352 \text{ Ton} \times 17180 \frac{\text{TL}}{\text{Ton}} = 748 \text{ TL}$$

### **Polypropylene Hexagonal Geogrid**

In the lower part, the area for the required geogrid is calculated. Cost analysis was carried out on the resulting m<sup>2</sup> [41].

$$\text{Total Needed Geogrid (Area)} = (1.6m) \times (2m) = 3.2m^2$$

$$\text{Cost of Geogrid} = (3.2m^2) \times \left( \frac{1.2\$}{m^2} \right) \times \left( 32,5 \frac{\text{TL}}{\$} \right)$$

$$\text{Cost of Geogrid} = 125 \text{ TL}$$

$$\frac{748 \text{ TL}}{125 \text{ TL}} = 5.98 \text{ Ratios}$$

As a result of the Cost Analysis, asphalt reinforcement with geogrid reinforcement cost approximately 83% less. The cost analysis shows us that strengthening work on asphalt with geogrid reinforcement is much more advantageous than increasing the asphalt thickness.

## **6. Conclusion**

In this study, the strengthening of asphalt paved roads, which are frequently preferred around the world, is discussed. The effects of geogrid use on performance were examined. With this innovative approach, it was aimed to reduce asphalt maintenance costs and increase the durability of road infrastructures. Different types of geogrids are included in the study. Within the scope of the study, the necessary analyzes were carried out using the ANSYS program using the finite element analysis method. Below are the main results of the study and recommendations for future studies to improve them.

While strengthening with geogrid, the position of the geogrid in the asphalt was changed and the optimum positioning was determined. Again, studies were carried out on geogrid material type and shape. As a result, a geogrid that provides optimum results in terms of deformation and stress values and is suitable for application was preferred. It was observed that the service life of asphalt pavement reinforced with geogrid increased compared to asphalt without geogrid. In addition to all these, the performances of geogrids created with recycled materials were also observed. As a result of the study, cost analysis was performed and the advantage in cost was observed. The results are confirmed a significant increase in performance and reduced deformation. Reinforcement with geogrid reinforcement is more economically advantageous than reinforcement non-geogrid.

The aim of the study was to show the advantages of strengthening asphalt pavements with geogrid. In addition, a comparison was made between geogrids. This study is very helpful in ensuring that future research can focus more on this area. Additionally, long-term field experiments with different traffic loads in different climatic conditions may allow us to better understand this innovative technology.

## 7. References

- [1] Town of Agawam. (2018). Pavement management report. Retrieved March 4<sup>th</sup>, 2024 from: <https://www.agawam.ma.us/DocumentCenter/View/917/2018-Pavement-Management-Report?bidId=>
- [2] Wolf Paving. (n.d.). Potholes in asphalt: What causes them and how are they fixed. Retrieved March 12<sup>th</sup>, 2024 from: <https://www.wolfpaving.com/blog/potholes-in-asphalt-what-causes-them-and-how-are-they-fixed>
- [3] Özcanan, S., & Akpinar, M. V. (2014). Determination of Critical Wheel and Axle Configurations in Flexible Pavements Based on Mechanistic Analyses. Technical Journal, 25 (121).
- [4] O'Flaherty, C. A. (2002). Introduction: A historical overview of the development of the road. Highways, 1-5.
- [5] General Directorate of Highways. (2020). Surface Dressing Design Guide <https://www.kgm.gov.tr/SiteCollectionDocuments/KGMdocuments/Baskanliklar/BaskanliklarTeknikArastirma/SathiKaplamaDizaynRehberi-2020.pdf>.
- [6] Seferoğlu, A. G., Seferoğlu, M. T., Akpinar, M. V., & Çelik, M. (2020). Use and Economic Analysis of Reclaimed Asphalt Pavement (RAP) Material in the Construction of Plant-Mix Base Layer. Polytechnic Journal, 23(4), 1327-1338.
- [7] Vijaya Kumar, N. M., & Prathap Kumar, T. S. (2020). An Eco Friendly Substitute of Asphalt Binder - Review. ResearchGate. Retrieved April 3<sup>rd</sup>, 2024 from: [https://www.researchgate.net/publication/341781540\\_An\\_Eco\\_Friendly\\_Substitute\\_of\\_Asphalt\\_Binder\\_-Review](https://www.researchgate.net/publication/341781540_An_Eco_Friendly_Substitute_of_Asphalt_Binder_-Review)
- [8] Deming, New Mexico. (2017). Pavement Management Plan 2017 PDF. [https://cms5.revize.com/revize/demingnm/Document\\_Center/Government/Documents%20&%20Reports/Pavement%20Management%20Plan%202017\\_%283%29.pdf](https://cms5.revize.com/revize/demingnm/Document_Center/Government/Documents%20&%20Reports/Pavement%20Management%20Plan%202017_%283%29.pdf).
- [9] Calvarano, L. S., Palamara, R., Leonardi, G., & Moraci, N. (2017, December). 3D-FEM analysis on geogrid reinforced flexible pavement roads. In IOP conference series: earth and environmental science (Vol. 95, No. 2, p. 022024). IOP Publishing.

- [10] Yıldırım, B. (ed.) (2020). 'Stone Mastic Asphalt' Against Rutting, Steel Radar. Retrieved March 28<sup>th</sup>, 2024 from: <https://www.steelradar.com/en/tekerlek-izine-karsi-tas-mastik-asfalt-79216/>
- [11] Zhu, H., & Sun, L. (2013). A viscoelastic–viscoplastic damage constitutive model for asphalt mixtures based on thermodynamics. *International Journal of Plasticity*, 40, 81-100.
- [12] Sudarsanan, N., & Kim, Y. R. (2022). A critical review of the fatigue life prediction of asphalt mixtures and pavements. *Journal of Traffic and Transportation Engineering (English Edition)*, 9(5), 808-835.
- [13] Teng, X. Q., Li, X. Z., & Chou, K. (2008). Application of finite element analysis to access the rutting potential in asphalt pavements. In *Transportation and Development Innovative Best Practices 2008* (pp. 480-485).
- [14] Zheng, C., & Xie, S. (2003). Effects of the tirepavement contact pressure on asphalt pavement. In *Proceedings of the Eastern Asia Society for Transportation Studies* (Vol. 4, pp. 401-407).
- [15] Topçuoğlu, D. (2016). Modeling Rutting Formation Using the Finite Element Method (Master's thesis, Pamukkale University Institute of Science).
- [16] Geogrids (n.d.) GTM. Retrieved April 10<sup>th</sup>, 2024 from:  
<https://www.gtmgeo.com/tr/urunler/geogridler>
- [17] CNBM Jacky (n.d.). Reinforcement Biaxial Plastic Geogrid Uniaxial PP Geogrid. Made-in-China. Retrieved April 18<sup>th</sup>, 2024 from:  
<https://cnbmjacky.en.made-in-china.com/product/CvAEjeNoydhR/China-Reinforcement-Biaxial-Plastic-Geogrid-Uniaxial-PP-Geogrid.html> (Accessed: 25 May 2024).
- [18] Huatao Lover (n.d.). High Strength Polypropylene (PP) Biaxial Geogrid PE Geogrid Use for Road Construction. Retrieved April 25<sup>th</sup>, 2024 from:  
<https://turkish.huataolover.com/sale-12679735d-high-strength-polypropylene-pp-biaxial-geogrid-pe-geogrid-use-for-road-construction.html>
- [19] EnvTech (n.d.). Geomalla Triaxial TX130S. Retrieved May 5<sup>th</sup>, 2024 from:  
<https://envtech.com.pa/producto/geomalla-triaxial-tx130s/>

- [20] Pandey, S., Rao, K. R., & Tiwari, D. (2012, September). Effect of geogrid reinforcement on critical responses of bituminous pavements. In ARRB Conference, 25<sup>th</sup>, 2012, Perth, Western Australia, Australia.
- [21] El-Khateeb, S., & Shalaby, A. (2022). A Comparative Study on the Performance of Different Geogrid Types Used for Pavement Reinforcement. Journal of Engineering Sciences, Assiut University, 50(2), 237-251.
- [22] Zienkiewicz, O. C., & Taylor, R. L. (2005). The finite element method for solid and structural mechanics. Elsevier.
- [23] Şanlıer, İ. (2018). Stone Mastic Asphalt (SMA) Applications, Performance Comparisons, and Cost Analysis within the Scope of the Northern Marmara Motorway Project (Doctoral dissertation, Sakarya University (Turkey)).
- [24] Alharbi, F., Almoshaigeh, A., Almoshaogeh, M., Elragi, A., & Elkholly, S. (2021). Effect of geo-grid depth in roads cross-section on reducing pavement rutting. Eng, 3(1), 1-8.
- [25] Plastics, P. (n.d.). Mechanical Properties of Plastic Materials. Retrieved May 5<sup>th</sup>, 2024 from:  
<https://www.professionalplastics.com/professionalplastics/MechanicalPropertiesofPlastics.pdf>.
- [26] Designer Data. (n.d.). Polyamide 6 (PA6). Retrieved May 20<sup>th</sup>, 2024 from:  
<https://designerdata.nl/materials/plastics/thermo-plastics/polyamide-6>
- [27] Wikipedia contributors. (n.d.). Polyethylene terephthalate. Wikipedia. Retrieved May 15<sup>th</sup>, 2024 from: [https://en.wikipedia.org/wiki/Polyethylene\\_terephthalate](https://en.wikipedia.org/wiki/Polyethylene_terephthalate)
- [28] Mhanna, H. H., Hawileh, R. A., Abuzaid, W., Naser, M. Z., & Abdalla, J. A. (2020). Experimental investigation and modeling of the thermal effect on the mechanical properties of polyethylene-terephthalate FRP laminates. Journal of Materials in Civil Engineering, 32(10), 04020296.
- [29] Sonelastic. (n.d.). Tables of Materials Properties: Polymers. Retrieved May 12<sup>th</sup>, 2024 from: <https://www.sonelastic.com/en/fundamentals/tables-of-materials-properties/polymers.html>
- [30] PP (n.d.). Designerdata. Retrieved May 23<sup>rd</sup>, 2024 from:  
[https://designerdata.nl/materials/plastics/thermo-plastics/polypropylene-\(cop.\)](https://designerdata.nl/materials/plastics/thermo-plastics/polypropylene-(cop.))

- [31] INEOS Olefins & Polymers USA. (n.d.). Engineering Properties of Polypropylene (PP). Retrieved May 19<sup>th</sup>, 2024 from: <https://www.ineos.com/globalassets/ineos-group/businesses/ineos-olefins-and-polymers-usa/products/technical-information--patents/ineos-engineering-properties-of-pp.pdf>
- [32] Recycled - PA6 and PA66 compounds (2023) Nursel Engineering Polymers. Retrieved May 25<sup>th</sup>, 2024 from: <https://nurel.com/wp-content/uploads/2023/04/RECOMYDE-CATALOGUE.pdf>
- [33] Maspoch, M. L., Ferrando, H. E., & Velasco, J. I. (2003, April). Characterisation of filled and recycled PA6. In Macromolecular Symposia (Vol. 194, No. 1, pp. 295-304). Weinheim: WILEY-VCH Verlag.
- [34] Quintero, Y. G., Figueroa, D. R., Gil, H., & Zuleta, A. A. (2019). Physical and mechanical properties of recycled PET composites. Stavební obzor-Civil Engineering Journal, 28(4).
- [35] Heidari-Rarani, M., Asdollah-Tabar, M., & Mirkhalaf, M. (2023). Experimental investigation and micromechanics-based damage modeling of tensile failure of polymer concrete reinforced with recycled PET bottles. Engineering Failure Analysis, 148, 107197.
- [36] Islam, M. R., Beg, M. D., & Gupta, A. (2013). Characterization of laccase-treated kenaf fibre reinforced recycled polypropylene composites. BioResources, 8(3), 3753-3770.
- [37] Al-Maadeed, M. A., Shabana, Y. M., & Khanam, P. N. (2014). Processing, characterization and modeling of recycled polypropylene/glass fibre/wood flour composites. Materials & Design, 58, 374-380.
- [38] Satya, S. K., & Sreekanth, P. R. (2020). An experimental study on recycled polypropylene and high-density polyethylene and evaluation of their mechanical properties. Materials Today: Proceedings, 27, 920-924.
- [39] Alkaissi, Z. A., & Al-Soud, M. S. (2021, September). Effect of geogrid reinforcement on behavior of unpaved roads. In IOP Conference Series: Earth and Environmental Science (Vol. 856, No. 1, p. 012007). IOP Publishing.
- [40] TÜPRAŞ. (n.d.). Bitumen Prices. Retrieved May 25<sup>th</sup>, 2024 from: <https://www.tupras.com.tr/tr/bitum-fiyatlari>

[41] PP Hexagonal Triaxial Geogrid of Triangle (no date) Made-in-China. Retrieved May 25<sup>th</sup>, 2024 from: <https://hongxiangshare.en.made-in-china.com/product/XKCnlBbECfpM/China-PP-Hexagonal-Triaxial-Geogrid-of-Triangle.html> (Accessed: 25 May 2024)